DRIVERS OF INTERTIDAL OYSTER REEF AND TIDAL CREEK ACCRETION OVER THE LAST CENTURY

Molly Chapin Bost

A dissertation submitted to the faculty at the University of North Carolina at Chapel Hill in partial fulfillment of the requirements for the degree of Doctor of Philosophy in the Department of Marine Sciences

Chapel Hill
2022

Approved by:

Antonio Rodriguez

Brent McKee

Michael Piehler

Justin Ridge

Emily Eidam

ABSTRACT

Molly Chapin Bost: Drivers of intertidal oyster reef and tidal creek accretion over the last century
(Under the direction of Antonio B. Rodriguez)

Salt marshes and intertidal oyster reefs provide valuable ecosystem services but are being lost or altered due to human modifications at the coast. Restoration projects intend to recover ecosystem services, but little is known about the conditions that promote longevity in restoration projects which requires vertical accretion to keep pace with sea-level rise. Furthermore, while there is documentation of the impacts of land-use change on sediment loads in large river systems and sedimentation in estuaries, small coastal tidal creeks have been largely ignored. To address these issues, this work 1. Quantified intertidal oyster reef growth and identified optimal restoration settings across tidal ranges, atmospheric temperatures, and landscape settings, 2. Evaluated land-use change since 1950 CE and associated impacts on tidal creek sedimentation, and 3. Determined how land-use changes affected sediment and carbon accumulation rates of saltmarshes. Chapter one compared the growth of 12 natural intertidal oyster reefs of varying age across two tidal ranges and landscape settings in coastal North Carolina. Peak growth rates were similar among landscape and tidal settings, but flow baffling associated with fringing reefs and higher summer air temperatures contributed to a lower position of the optimal growth zone in the tidal frame. Chapters 2 and 3 were addressed by comparing sediment accumulation rates before and after a land-use change in 12 tidal creeks across two distinct regions in North Carolina, one region of low relief tidal-creek watersheds where land-use change was dominated by fluctuations

in forest, silviculture, and agriculture, and another region of high relief tidal-creek watersheds where land-use change was dominated by suburban development. While accumulation rates accelerated within the creek bottom and adjacent fringing marsh sites after a land-use change, the magnitude of the acceleration differed depending on the morphology of the creek basin. There was faster acceleration in accumulation rates at creek sites within coastal prism incised valleys, but slower acceleration for their adjacent fringing salt marshes. Results from this work will provide guidance for oyster reef restoration and coastal watershed management for sedimentation in tidal creeks and salt marshes.

ACKNOWLEDGEMENTS

I must express my sincerest gratitude to my advisor and friend, Tony Rodriguez. He has been nothing but supportive, patient, accessible, and fun to work with. His enthusiasm for my work and unwavering support was crucial to my positive experience and success throughout my dissertation work. I cannot imagine a better advisor and look forward to continued collaborations in the future. Thank you to my committee members, Brent, Mike, Justin, and Emily who helped balance my research through their perspectives and expertise and for their consistent friendly support throughout my time at UNC. Dr. Joel Fodrie, a co-PI on the Coastal Recreational Fishing License Grants that funded most of my work, was an invaluable wealth of knowledge and collaborator. I must acknowledge all members of the Rodriguez Lab past and present for their help in the field and lab especially Charlie Deaton, Rich Mahoney, and Carson Miller.

TABLE OF CONTENTS

LIST OF TABLES

LIST OF FIGURES

LIST OF ABBREVIATIONS

SLR	Sea-level rise
OGZ	Optimal Growth Zone
BS	Back Sound
SRE	Shallotte River Estuary
DEM	Digital Elevation Model
MMGR	Maximum Median Growth Rate
Tmax	Maximum daily atmospheric temperature
RSLR	Relative Sea-Level Rise
CC	Carteret County
NHC	New Hanover County
LUC	Land-Use Change
DEM	Digital Elevation Models
LOI	Loss on Ignition
CF	Constant Flux
MAR	Mass Accumulation Rate
SAR	Sediment Accumulation Rate
CAR	Carbon Accumulation Rate
MLCC	Major Land-Cover Change

CHAPTER 1 NATURAL INTERTIDAL OYSTER REEF GROWH ACROSS TWO LANDSCAPE SETTINGS AND TIDAL RANGES

Introduction

Oysters are a keystone species because they highly influence the structure of their community (Pomeroy et al. 2006; Raj 2008); however, populations are severely degraded mostly due to exploitation and have experienced a 64 and 88% decline in extent and biomass, respectively, since 1900 (Kirby 2004; zu Ermgassen et al. 2012). In addition to lost fishery revenue from fewer oysters, this decline has contributed to reduced commercially important finfish and crustacean habitat (Harding and Mann 2001; Lenihan et al. 2001), degradation of estuarine water quality (Newell 1988), reduced capacity for estuaries to bury carbon (Fodrie et al. 2017), and diminished shoreline stabilization (Meyer et al. 1997). To mitigate these losses, efforts to restore oyster populations began in the 1950s, mainly aimed at recovering the oyster as a fishery (Beck et al. 2011), but more recently the goals of restoration have included reestablishing other lost ecosystem services (Grabowski et al. 2012).

The value of the various ecosystem services provided by intertidal oyster-reef restoration depends, in part, on the landscape setting. Intertidal oyster reefs form patch reefs in the middle of tidal flats and fringing reefs, often along the margins of saltmarsh (Bahr and Lanier 1981). Grabowski et al. (2005) found that restored intertidal patch reefs had higher juvenile fish abundances than restored saltmarsh fringing reefs. Erosion resistant fringing reefs, in a landscape lacking alternative hard substrate, are shoreline stabilizers (Piazza et al. 2005; Scyphers et al.

2011) that reduce saltmarsh erosion by decreasing wave and current energy from storms and boat wakes (Manis et al. 2015).

Living shoreline projects are increasingly including restored intertidal oyster reefs as a design element to build more storm-resistant and resilient coastal communities (Meyer et al. 1997; Scyphers et al. 2011; Temmerman et al. 2013; Bilkovic et al. 2016). Unlike bulkheads and revetments that require frequent maintenance and reconstruction (Narayan et al. 2016; Reguero et al. 2018), living shorelines can adapt organically to environmental challenges including storms and sea-level rise (Spalding et al. 2014; Morris et al.2020). Living oyster reefs can accrete vertically (SLR; Morris et al. 2002; Rodriguez et al. 2014) and grow horizontally, transgressing landward (Ridge et al. 2017b). Reefs exhibit an ability for rapid recovery after storms (Livingston et al. 1999) and conditionally can provide protection from shoreline erosion (Ridge et al. 2015; Morris et al. 2018). Installing breakwaters or sills adjacent to saltmarsh-restoration projects comes with the expectation that oysters will colonize that substrate, accrete vertically via shell growth to maintain their position in the intertidal realm with rising sea level, and contribute to the ecological benefits of the restoration project (Wong et al. 2011; Ridge et al. 2015; Walles et al. 2016; Morris et al. 2018). Successful restoration of intertidal reefs that create viable living shorelines entails identifying the conditions that will facilitate oyster reef growth, but limited information about the specific conditions that optimize reef growth among estuaries exists.

Intertidal oysters find refuge from biofouling, predation, and disease by exploiting the environmental niche of aerial exposure (White et al., 1996, Bishop and Peterson 2006; Powers et al. 2009). To maintain their elevation in the tidal frame, intertidal oyster reefs accrete vertically via skeletal shell growth, biodeposition, and accumulation of allogenic sediment (from resuspension, erosion, or riverine discharge). Reef growth processes are confined to about the

upper 15 cm of intertidal reef thickness in the taphonomically active zone (Davies et al. 1989; Rodriguez et al. 2014). The elevation threshold between success or failure of a restored intertidal reef, defined as the presence of a vertically accreting taphonomically active zone or buried shell, respectively, spans only 10–15 cm for reefs in Back Sound, North Carolina (Fodrie et al. 2014). Restored intertidal patch reefs in Back Sound have a well-defined pattern of growth across the range of tidal elevations (Ridge et al. 2015; Figure 1.1). The base of a reef is generally at or below the critical exposure boundary where the duration of aerial exposure is short and reef growth rates are low. Moving up the reef to higher elevations and longer periods of aerial exposure, growth rates increase to a maximum (up to 7 cm y^{-1}; Ridge et al. 2017a) within the optimal growth zone (OGZ). The OGZ was empirically defined to encompass elevations where oysters are exposed 20–40% of the time (Ridge et al. 2015). Reef growth rates rapidly decline from the OGZ to the top of the reef, which is the growth ceiling and approximates mean sea level. The growth ceiling encompasses elevations where oysters experience stress from aerial exposure and growth is largely modulated by the rate of sea-level rise and short term (yearly) fluctuations in sea level (~55%; Ridge et al. 2017a). This Ridge et al. (2015) intertidal oyster reef growth model (Figure 1.1) highlights growth zonation across the lower half of the tidal frame; however, it was developed mainly from examining restored intertidal patch reefs in Back Sound where the tidal range is 0.94 m. Water flow across oysters is necessary for food delivery and flow likely differs between patch and fringing reefs, furthermore, the duration of aerial exposure at specific elevations varies with tidal range. It is unknown how transferable the Ridge et al., (2015) model is to restored and natural reefs in other landscape and tidal settings.

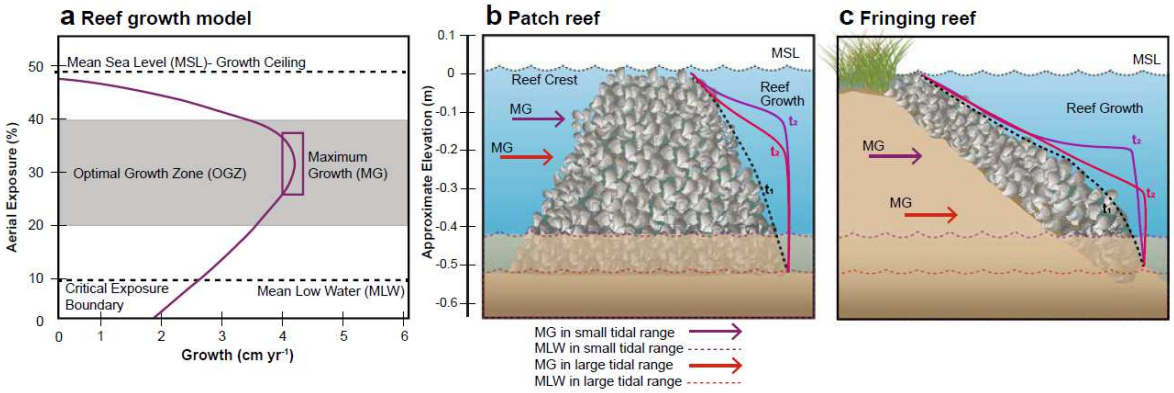

Figure 1.1 Conceptual oyster-reef growth model modified after Ridge et al. (2015). (a) Growth model applied to natural patch (b) and fringing (c) reefs with two different tidal ranges across a time step (same vertical scale). Initial topographic profile (t1) is shown as dashed black line and a subsequent hypothetical topographic profile (t2) is shown in purple for small tidal range and red for large tidal range.

This study tests the applicability of the Ridge et al. (2015) intertidal oyster reef growth model to natural patch and fringing oyster reefs within two tidal ranges. Byers et al. (2015) recognized higher accumulation of oyster biomass and heightened reef structure in areas of higher tidal energy across the U.S. South Atlantic Bight, suggesting that tidal range influences reef growth. We hypothesize that the general model showing low growth at the reef top and base, with the highest growth rates along the upper edge of intertidal reefs is widely transferable, but the specific elevations of the OGZ will be lower in areas with a larger tidal range and lower for fringing reefs than patch reefs (Figure 1.1). In addition, high growth rates previously reported for restored intertidal reefs may not be representative of natural intertidal reefs because reef morphology changes through time as the reef fills the intertidal space that is available for growth (accommodation). Few studies have focused on spatial variations in natural reef growth rates. The new growth-rate measurements presented here across the elevations of replicate natural patch and fringing reefs further allow the prediction of the performance of oyster-reef restoration projects across tidal ranges and landscape settings as they age and equilibrate with mean sea level.

Methods

Site Selection

The estuaries of North Carolina are microtidal with intertidal oyster reefs dominated by *Crassostrea virginica* (the eastern oyster). Tides in Pamlico Sound in the north are dominantly wind-driven and there are few intertidal oyster reefs in that large estuary. The lunar tidal range and the proportion of intertidal oyster reef area to overall estuarine area increases south of Cape Lookout. We chose Back Sound (BS) and the Shallotte River Estuary (SRE) as study sites (Figure 1.2) for three main reasons: 1) the sites have semidiurnal tides but are end-members across the tidal gradient of North Carolina south of Cape Lookout with tidal ranges in BS and the SRE of 0.94 m and 1.51 m, respectively (NOAA Tides & Currents); 2) both study locations are characterized by channelized sand and mud flats with marsh islands dominated by *Spartina alterniflora*; and 3) the growth rates of intertidal restored patch reefs have been extensively studied in BS, providing data for comparison to our results of natural reef growth. Salinity in both BS and the SRE was measured every two months at the same stations from March 2011–September 2015 in the SRE and from May 2010–April 2017 in BS. Average salinities during these periods were similar between sites (33.16 ± 2.54 in BS, 32.37 ± 2.76 in the SRE; Appendix 1.1).

In each estuary, three natural patch and three natural saltmarsh-fringing reefs were chosen (12 reefs in total; Figure 1.2). The patch reefs were isolated on mud or sand flats while fringing reefs occupied the perimeter of a saltmarsh island. In BS, we selected three patch and two fringing reefs near Shackleford Banks (<400 m apart) and a third fringing reef near Carrot Island ~5.5 km from the other reefs (Figures 1.2 and 1.3). Reefs in the SRE are close to the middle of the estuary, ~3.5 km landward from the tidal inlet. We selected clusters of patch and

fringing reefs, 500 m apart, with individual reefs in each cluster <70 m apart (Figures 1.2 and 1.3).

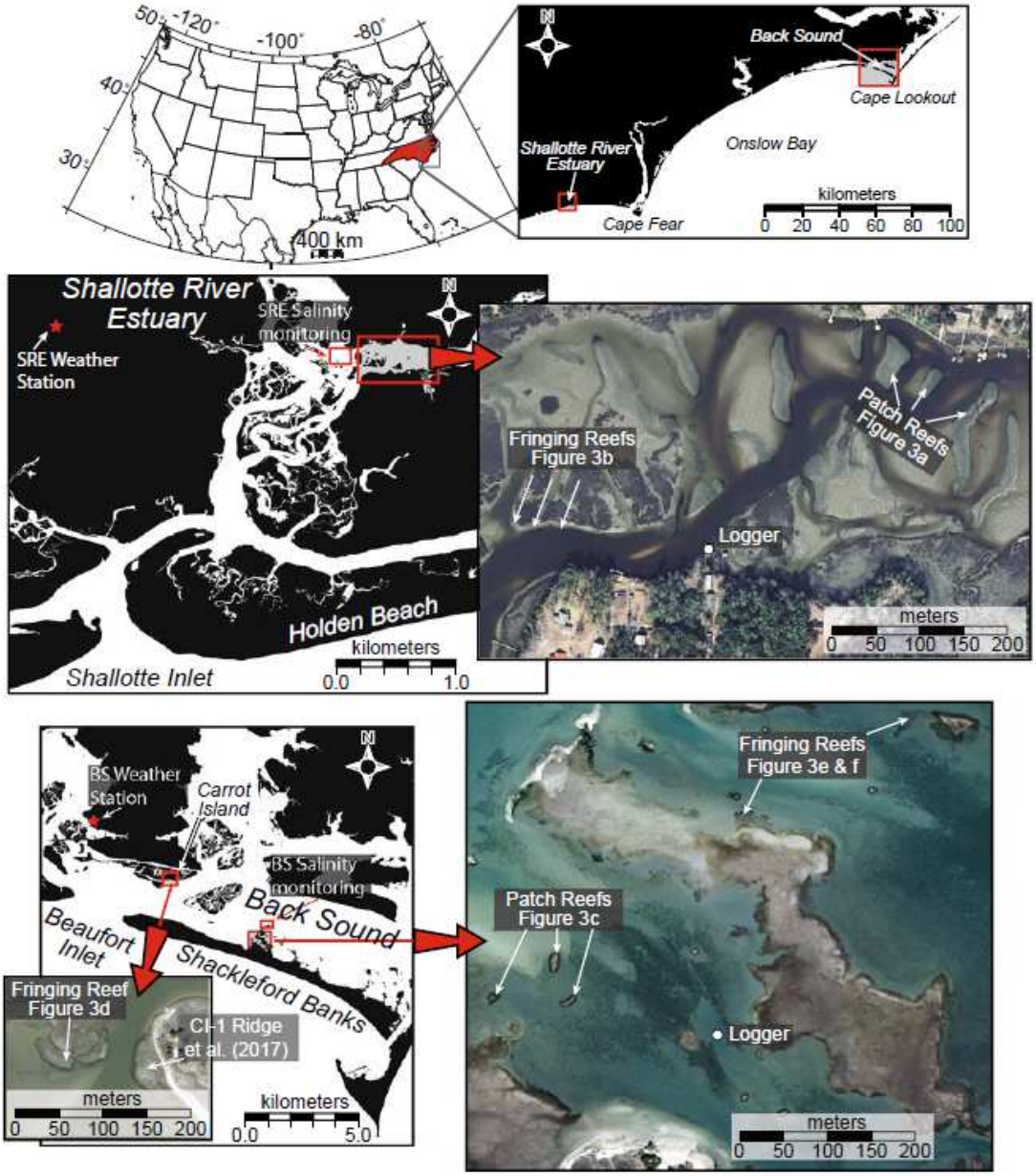

Figure 1.2 Study area map. Map showing locations of patch and fringing reefs examined in Back Sound and the Shallotte River Estuary. Locations of weather stations used for atmospheric temperature are shown on expanded maps as red stars and general areas where salinity was measured are boxed in red. Water level loggers are indicated on aerial photographs as white circles. Imagery in Shallotte from North Carolina Statewide Orthoimagery Program. Imagery in Back Sound from NOAA Digital Coast Data Access Viewer.

Reef Growth

We measured oyster reef growth rates directly from changes in surface elevation. A Riegl LMSZ210ii terrestrial laser scanner mounted on a tripod was used to map reef elevations. The scanner was set to emit 2 million laser beams, with ~500,000 being reflected by the reef and returned as relevant x, y, and z data points per scan. The reefs were scanned from 3–7 different locations (depending on reef size) and scanner positions were <15 m apart. Data points were referenced to a global coordinate system (Universal Transverse Mercator) and the geometric control datums NAD 83 and NAVD88 using nine surveyed and leveled reflectors distributed around the area of each scan position. The reflectors were surveyed to <1 cm horizontal and 1.5 cm vertical accuracy using a Trimble R8s GPS receiver with corrections provided by the North Carolina Global Navigation Satellite System Real Time Network. Scanning was limited to ~45 min before and after low spring tide when the reefs and adjacent tidal flats were exposed (the scanner cannot image through water). Considering GPS vertical accuracy is at the cm scale, we chose a time-step of ~2-y over which to measure reef growth to ensure elevation change would be resolved. Due to the time-consuming nature of the scanning process, reefs were scanned on different days, but most of the reefs were scanned in 2016 and 2018 with the average time between scans being 2.43 years (Appendix 1.2). For larger reefs, particularly patch reefs in the SRE, only part of the reef was scanned due to time constraints associated with low tide (Figure 1.3). For these partially sampled reefs, scans always included the entire range of reef elevations from the reef crest to the adjacent tidal flat, and the scanned section of the reef was kept consistent.

Following methods outlined in Ridge et al. (2017a and b), the Merrick Advanced Remote Sensing (MARS 8) software package was used to extract ground points from the point cloud, which were then gridded (5-cm grid spacing) in Surfer 15 (Golden Software) using the kriging algorithm to create digital elevation models (DEMs; Figure 1.3). Successive DEMs were subtracted, and the resulting elevation change (± 0.034 m; Rodriguez et al. 2014) of each grid cell was paired with its corresponding grid-cell elevation from the initial DEM. Those linked data, including columns of x, y, initial scan elevation, and elevation change across the time step, were sorted into 2-cm elevation bins of the initial scan. The median vertical elevation change was calculated for each elevation bin ± 95% confidence interval (McGill et al. 1978). To calculate growth rates, we divided the vertical elevation changes by the time between scans. Elevation bins were disregarded that encompassed <0.1% of total reef area because those bins were only capturing microtopography on top of the reefs from individual oyster clusters. The peak of the OGZ was defined for each reef as the range of elevations where the median growth rate was at a maximum (the maximum median growth rate or MMGR) ± 95% confidence interval, closest to the top of the reef.

To compare reef growth and the position of reefs in the tidal frame among estuaries (tidal ranges - fixed) and landscape settings (reef types - fixed) we used a factorial, rank-based test. In our analysis, we preferred to use an aligned rank transformation ANOVA procedure because of the small number of replicates (n=3) within each cell our two-way design, the presence of some outliers in our data, and the relative ease in estimating effect sizes (p-values and partial eta-squared, presented in Appendices 1.3 and 1.4) using this approach. All tests were conducted using the ARTool package in R (Feys 2016; Kay and Wobbrock 2020).

Water level and atmospheric temperature

To capture fluctuations in sea level over the periods of reef growth, we deployed a water-level logger (HOBO pressure sensor U20-001-04) in a settling well in each estuary (Figure 1.2, Appendix 1.2). The loggers were installed 200–300 m from the three patch reefs and two of the fringing reefs in BS. The third fringing reef in BS, adjacent to Carrot Island, was ~5.7 km from the logger. In the SRE, the loggers were deployed ~300 m away from both the fringing and patch reefs. To limit vertical displacement, the logger in the SRE was attached to a dock piling and in BS was attached to rebar driven into the bay floor to the point of refusal with a sledgehammer. Loggers sampled every 6 min. A barometer was deployed within 100 m of each settling well to correct water-level data for variations in atmospheric pressure. The loggers were deployed for 2–3 years (Appendix 1.2) and maintained every 3 months. Water level data spanned most of the periods over which reef growth was measured, but storms and logistical constraints prevented complete coverage during the entire period. Pressure was converted to water depth using HOBOware Pro software. Water level was measured relative to NAVD88, ± 0.03 m, by surveying the logger using a Trimble R8 GPS receiver during initial deployment and the logger was resurveyed during subsequent maintenance visits to account for minor vertical displacement (<5 cm). Water-level data from the SRE and BS were converted to aerial exposure, the percent of time intertidal elevations are exposed to the atmosphere, by binning the records into 2-cm intervals and calculating the percent of water-level observations below each bin.

Atmospheric temperature data from NOAA Climate Data Online was used to estimate potential differences in desiccation stress between the two study sites. The SRE weather station is ~3.2 km from our study reefs and the BS weather station is ~3.7–9 km from our study reefs (Figure 2). Using the time series of maximum daily atmospheric temperature (Tmax) for the

study period and both estuaries, we defined the warm season as the earliest and latest calendar day ≥ 28 °C (May 27–October 5). The threshold is based on experiments showing increased stress of *C. virginica* when subjected to temperatures above 28 °C (Chapman et al. 2011). We calculated the potential heat stress each reef experienced during the period over which growth was measured by summing the number of degrees Tmax > 28 °C.

Reef Age

To constrain the age of each reef, we radiocarbon-dated a basal oyster shell and examined historical aerial photos. Sediment cores were taken from each reef by driving a 10 cm diameter aluminum tube through the center of the reef crest with a gas-powered jackhammer. Cores were sectioned into 5-cm subsamples, shells were separated and washed, and we defined the base of the reef as the deepest subsample that contained articulated oysters. For each reef, the umbo of the deepest articulated oyster was filed off and sent to the National Ocean Sciences Accelerator Mass Spectrometry Facility at the Woods Hole Oceanographic Institution for radiocarbon analysis. Dates were calibrated to calendar years at the 95% confidence interval (2 sigma) using CALIB 7.1 (Stuiver and Reimer 1993; Reimer et al. 2013). Samples that returned dates younger than 1950 CE were calibrated using CALIBomb (Reimer et al. 2004). Those recent dates were verified using USGS historical aerial photography obtained from earthexplorer.usgs.gov noting date of initial reef presence (Table 1.1).

Core name	Sample interval/reef base (cm from top of core)	Fraction modern (FM) ± error	Radiocarbon age (y BP) ± Error	Calibrated date range (CE)	Certainty (2 sigma)	Median date (CE)
Patch SRE-1	110–115/120	0.8566 ±0.0018	1240 ± 15	1089–1233	1	1161
Patch SRE-2	165–170/175	0.8015 ±0.0020	1780 ± 20	574–677	1	625.5
Patch SRE-3	135–140/140	0.858 ±0.0022	1230 ± 20	1095–1253	1	1174
Fringe SRE-1	187–192/197	0.8693 ±0.0018	1130 ± 15	1229–1306	1	1267.5
[illegible]	[illegible]	[illegible]	[illegible]	[illegible]	1	1893
[illegible]	[illegible]	[illegible]	[illegible]	[illegible]	1	1752
Patch BS-1	70–75/85	0.9441 ±0.0022	460 ± 20	1821–1950	1	1885.5
		1.1178 ±0.0023	> Modern	1957.9–1958.4	0.066*	1958.1
Patch BS-3	40–45/55	0.9429 ±0.0018	470 ± 15	1816–1950	1	1883
Fringe BS-1	40–45/45	1.1069 ±0.0022	> Modern	1957.8–1958.2	0.034*	1958
Fringe BS-2	20–25/30	1.0382 ±0.0021	> Modern	1956.1–1956.7	0.921*	1956.5
Fringe BS-3	90–95/100	1.1533 ±0.0023	> Modern	1958.2–1958.9	0.09*	1958.6

*Low certainty of chosen age range confirmed via historical aerial photography

Table 1.1 Reef Radiocarbon. Radiocarbon dates of shell material from the base of each reef. Locations provided in Appendix 1. Table S2.

Results

Reef morphology

Intertidal reef morphology differed across sites and landscape settings. Patch reefs had an elongated mound shape with their long axis oriented perpendicular to the long axis of the estuary (Figs. 3 and 4) and are located on sandflats in BS and mudflats in the SRE (Figure 1.2). Reefs in the SRE (*n*=6) extended to a lower elevation than reefs in BS (*n*=6, -0.87 (±0.06) m, -0.52 (±0.04) m, respectively; P= 0.0009; Table 1.2; Appendices 1.3 and 1.4) and fringing reefs (*n*=6) extended to a lower elevation than patch reefs (*n*=6, -0.75 (±0.10) m, -0.71 (±0.07) m, respectively; P= 0.029; Table 1.2; Appendices 1.3 and 1.4). Mean reef crest elevations in the SRE (-0.07 (±0.04) m) were lower than in BS (0.08 (±0.02) m; P=0.001) and were lower for fringing reefs (-0.04 (±0.05) m) than patch reefs (0.06 (±0.03) m; P=0.005; Table 1.2; Appendices 1.3 and 1.4).

Fringing reefs had their long axis oriented parallel with the saltmarsh shoreline and elevations were generally highest at the saltmarsh edge and decreased towards the adjacent tidal

flat (Figures 1.3 and 1.4). The exception is Fringe BS-2 whose long axis was perpendicular to the saltmarsh shoreline, which is not an uncommon morphology for a fringing reef (Grave 1901; Figure 1.3). Fringing reefs in the SRE showed a ramp morphology with the highest elevation positioned <1 m away from or directly adjacent to the saltmarsh edge (Figure 1.4). In BS, fringing-reef morphology was more mounded than in the SRE, with the maximum elevation of Fringe BS-1 and Fringe BS-3 positioned ~5 m away from the saltmarsh edge (Figure 1.4). The crest of Fringe BS-2 was positioned >20 m away from the saltmarsh edge which is the product of its groin-like morphology relative to the fringing saltmarsh (Figure 1.4).

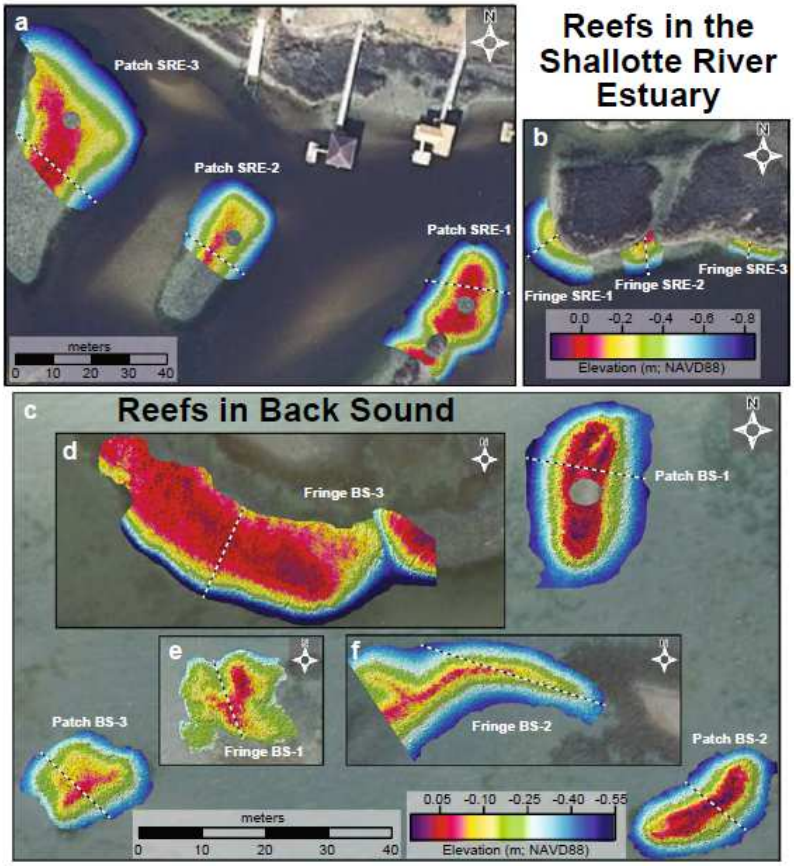

Figure 1.3 Digital elevation models of the 12 reefs. In the SRE, three patch reefs (a) and three fringing reefs (b) were examined within 1 km of each other. In BS, three patch reefs (c) and two fringing reefs (e, f) were examined adjacent to Shackleford Banks and one fringing reef was examined adjacent to Carrot Island (d). Note different elevation color scales applied to DEMs in the SRE (b) and BS (c). Dashed lines indicate locations of topographic profiles shown in Figure 4. Imagery from NOAA Digital Coast Data Access Viewer

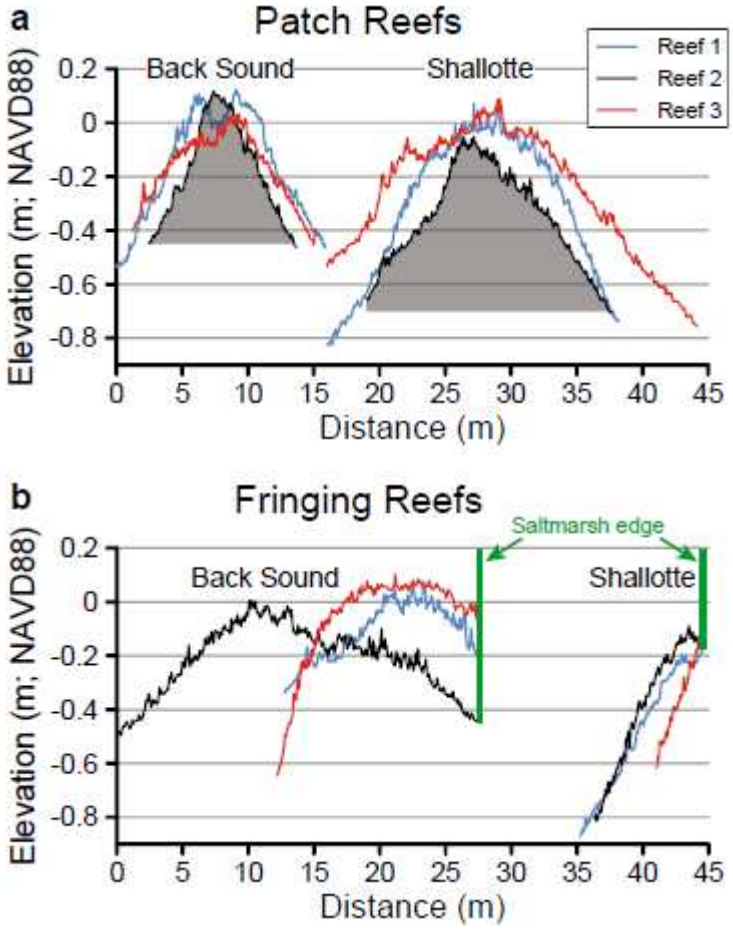

Figure 1.4 Elevation profiles extracted from DEMs across patch reefs (a) and fringing reefs (b). The x-axis should be treated as a horizontal scale bar and placement of the profiles were chosen to facilitate comparison

Growth Rates and Elevation

Intertidal reef growth varied across elevations parabolically with growth rates increasing from the top of the reef to the OGZ positioned along the upper reef flank and then decreasing towards the base of the reefs (Figure 1.5). The OGZ typically spanned a 2–6 cm range of elevations. The exception was Fringe SRE-3 where the OGZ extended across a 12-cm elevation range (Figure 1.5).

Growth at the reef crest and along the reef flank are important to constrain because these areas are where growth is limited and at a maximum, respectively. The average median growth rate of the reef crests was 0.75 cm y^{-1} ranging from -0.11–.92 cm y^{-1}, which included three reefs where rates were indistinguishable from 0 cm y^{-1} (Figure 1.5). Along the flanks of the reefs, the average MMGR was 2.21 cm y^{-1} ranging from 1.3 to 4.8 cm y^{-1}. Average reef growth rates at the crests and along the flanks, where the OGZ was identified, were similar among estuaries (SRE: 0.76 (±0.31) cm y^{-1}, BS: 0.74 (±0.28) cm y^{-1}, P= 0.788; SRE: 2.0 (±0.25) cm y^{-1}, BS: 2.42 (±0.51) cm y^{-1}, P= 0.582; Table 1.2; Appendix 1.3 and 1.4) and landscape settings (Fringe: 0.90 (±0.93) cm y^{-1}, Patch: 0.60 (±0.12) cm y^{-1}, P=0.688, Fringe: 2.68 (±0.49) cm y^{-1}, Patch: 1.74 (±0.13) cm y^{-1}, P=0.109; Table 1.2, Appendix 1.3 and 1.4).

The elevation of the OGZ varied between both estuary and reef types. In the SRE, the average elevation of the OGZ was lower than in BS (-0.14 (±0.030) m, 0.003 (±0.022) m, respectively; P=0.0062; Table 1.2) and, overall, the elevation of the OGZ was lower on fringing reefs than patch reefs (-0.12 (±0.05) m, -0.02 (0.03) m, respectively; P=0.033; Table 1.2).

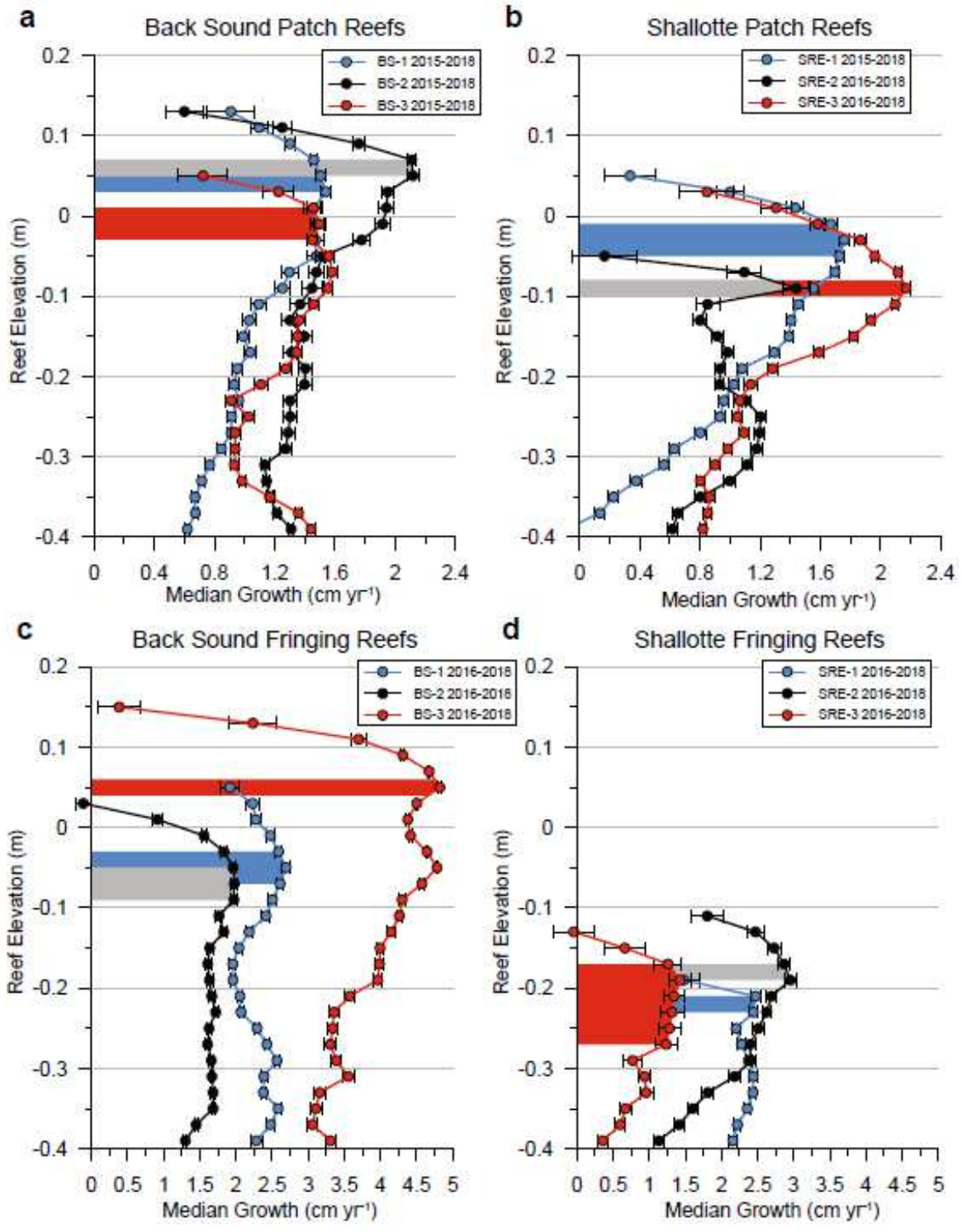

Figure 1.5 Reef growth profiles. OGZs are indicated by colored polygons extending from the curves to the y-axis. See text for OGZ identifying criteria. Color identifies the reef that OGZ is associated with and gray is associated with black-filled circles. **a** Back sound patch reefs. **b** Shallotte patch reefs. **c** Back sound fringing reefs. **d** Shallotte fringing reefs.

Reef name	MMGR (cm year^{-1})	MMGR elevation (m; NAVD88*)	MMGR aerial exposure (%)	Crest elevation (m; NAVD88*)	Crest aerial exposure (%)	Reef base elevation (m; NAVD 88*)
Patch SRE-1	1.73	−0.05	43.7	0.05	49.1	−0.65
Patch SRE-2	1.44	−0.09	41.5	−0.05	43.7	−0.75
Patch SRE-3	2.17	−0.09	41.5	0.03	48.0	−0.91
Fringe SRE-1	2.46	−0.22	34.3	−0.19	36.0	−0.99
Fringe SRE-2	2.91	−0.18	36.6	−0.11	40.4	−0.99
Fringe SRE-3	1.30	−0.22	34.3	−0.13	39.3	−0.91
Patch BS-1	1.53	0.04	54.0	0.13	64.1	−0.49
Patch BS-2	2.12	0.06	56.2	0.13	64.1	−0.53
Patch BS-3	1.46	−0.01	48.3	0.05	55.1	−0.47
Fringe BS-1	2.61	−0.05	43.9	0.05	55.1	−0.43
Fringe BS-2	1.97	−0.07	41.6	0.03	52.8	−0.49
Fringe BS-3	4.82	0.05	55.1	0.15	61.9	−0.71

*NAVD88 refers to the North American vertical datum of 1988

Table 1.2 Reef growth metrics. Reef metrics of growth, elevation, and exposure used in analysis (MMGR maximum median growth rate).

Growth and Aerial Exposure

The intertidal zone, defined broadly as elevations exposed 99.7–0.3% (3 SD from the mean water level) of the time over the study period, extended to higher and lower elevations in the SRE (-1.13–1.13 m NAVD88) than in BS (range = -0.59–0.89 m NAVD88; Figure 1.6). The range of elevations exposed in the SRE was 52% greater than BS. Intertidal reef desiccation stress is related to aerial exposure and atmospheric temperature (Figure 1.7). The reefs in the SRE experienced more potential heat stress, on average, during the study period than BS (SRE: 599 (±6) °C; BS 476 (±41) °C; Appendix 1.2). The amount of actual heat stress a reef

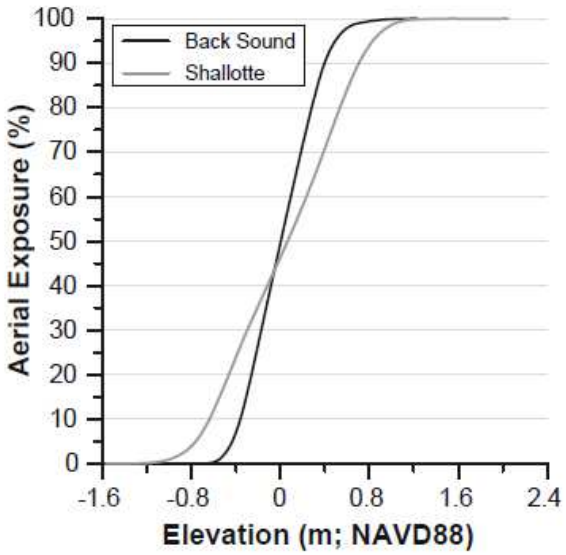

Figure 1.6 Intertidal exposure. Percent of time various intertidal elevations are exposed to atmosphere in the SRE and BS. See Figure. 2 for locations of water-level loggers.

experienced is tied to the time it spent exposed at low tide, so it was necessary to consider aerial exposures across intertidal reef elevations to assess this.

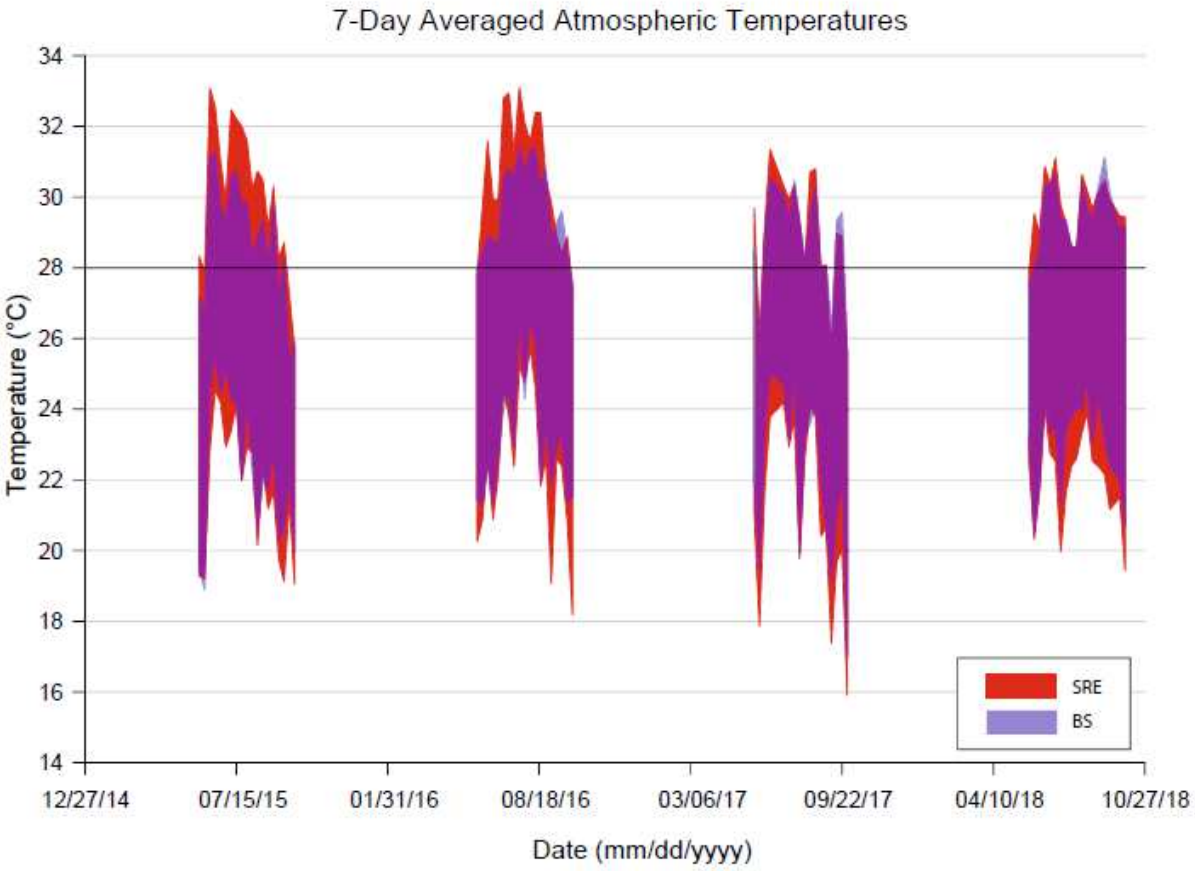

Figure 1.7 Seven-day averaged maximum and minimum temperatures (°C) for SRE (red) and BS (blue/purple due to semitransparent blue color) between May 27 and October 5 for each year within the study period. 28 °C is bolded to display the temperature above which desiccation stress occurs.

To compare the position of the growth ceiling and the OGZ among estuaries and landscape settings in different tidal regimes, we converted elevations to percent aerial exposure because exposure, not elevation per se, is the important driver of intertidal reef growth (Bishop and Peterson 2006). Aerial exposure of the reef crests varied by <13% in both estuaries and the average aerial exposure of the reef crests in BS (58.9 (±2.1)%) was greater than in the SRE (42.8 (±2.1)% ; P= 0.001; Table 1.2; Appendix 1.3 and 1.4). The average aerial exposure of the

reef crest for fringing reefs was also lower than patch reefs regardless of estuary (47.6 (±4.3)%, 54.0 (±3.5)% , respectively, P= 0.031; Table 1.2; Appendix 1.3 and 1.4). The average aerial exposure of the OGZ for the six reefs in the SRE was > the six reefs in BS (38.7 (±1.7)%, 49.9 (±2.5)% , respectively, P= 0.0009; Table 1.2; Appendix 1.3 and 1.4) and the same was found for reef-landscape setting compared among estuaries (41.0 (±3.2)%, 47.5 (±2.6)% , respectively, P=0.050; Table 1.2; Appendix 1.3 and 1.4). Fringe BS-3 was an outlier where the aerial exposure of the OGZ was 55.1%, ~13% higher than the other two fringing reefs in BS and skewed the BS mean (Figure 1.8). The difference between the aerial exposures of the reef crest and the OGZ indicates the amount of separation between these reef zones relative to their position in the tidal frame. The average difference was larger in BS (9.0 (±0.85)%) than in the SRE (4.1 (±0.77)%; P= 0.001; Figure 1.9; Appendix 1.3 and 1.4). The difference between aerial exposure at the reef crest and the OGZ was similar among landscape settings (Patch: 6.5 (±1.1)%, Fringe: 6.6 (±1.6)%; P=0.790; Table 1.2; Appendix 1.3 and 1.4).

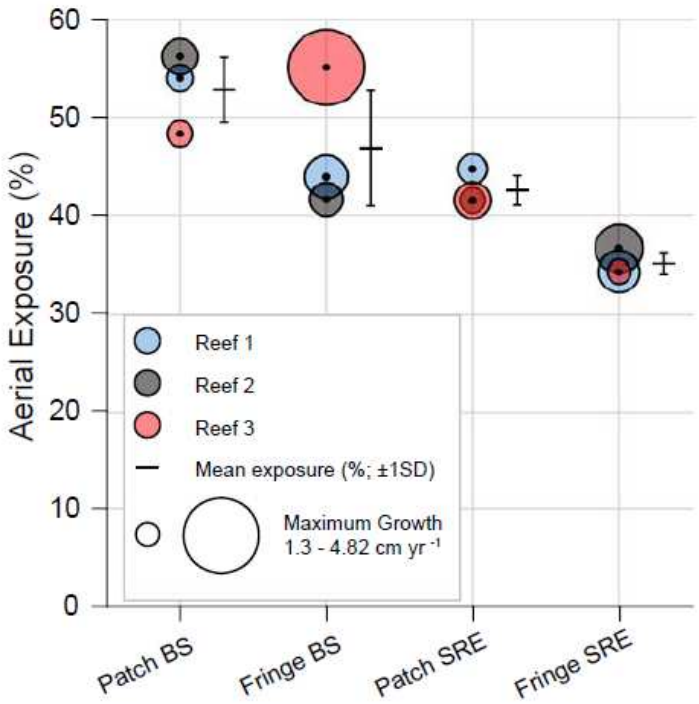

Figure 1.8 Median percent aerial exposure of the OGZ grouped by estuary and reef type. Size of the circle is scaled to median maximum growth rate (MMGR). Mean aerial exposure of the OGZ (± 1 SD) for each setting is displayed to the right and based on a sample size of three.

Reef Age

The natural reefs in this study formed at different times, ranging from 625 CE (Patch SRE-2) to 1958 (Fringe BS-1 and -3; Table 1.1). The reefs in the SRE were determined to be older than the reefs in BS and most of the patch reefs were older than the fringing reefs within each estuary, the exception being Fringe SRE-2, which was similar in age to BS patch reefs (Table 1.1; Figure 1.9). Reef age varied between the two study sites and the range was much larger in the SRE (119–1394 y) than in BS (62–137 y; Table 1.1; Figure 1.9). Despite most reefs in each landscape setting within the SRE and BS being in proximity, they formed at various times. There was a ~500-year difference in age between adjacent patch and fringing reefs in the SRE; however, in BS fringing reefs separated by a few kilometers were about the same age (Table 1.1).

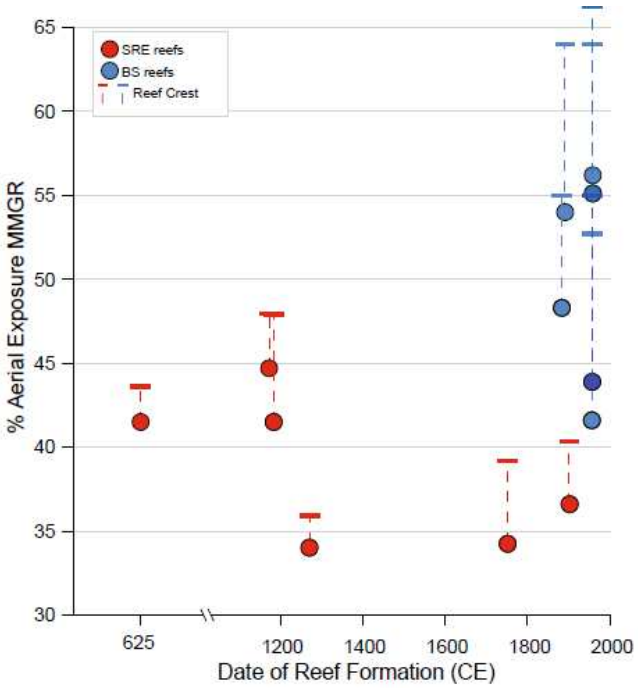

Figure 1.9 Distance between OGZ and reef crest. Median percent aerial exposure of OGZ (circles) and reef crests (capped lines) versus date of reef formation. SRE is in red and BS is in blue, with different shades of blue used to distinguish overlaying values. The length of the dashed lines is approximate difference between aerial exposures of reef crests and the OGZ. Notice break in the x-axis.

Discussion

Position in the tidal frame

Despite intertidal reef growth rates being similar among estuaries and landscape settings, the relative exposure of the OGZ and the aerial extent of the reef crest varied. Aerial exposure of oysters is important for reefs to persist in the lower parts of estuaries where salinity is higher because that niche reduces biofouling, predation, and disease (Bishop and Peterson 2006; Powers et al. 2009). Aerial exposure of the intertidal reefs examined here varied among estuaries, with the average aerial exposure of the OGZ in the SRE, where the tidal range is larger, being less than in BS. The average duration of aerial exposure of the reef crests is also lower in the SRE than BS, indicating that intertidal reefs in the SRE are simply exposed for less time than intertidal reefs in BS. Low-salinity water is another niche for oyster reefs and subtidal oyster reefs exist in the upper parts of estuaries, closer to river outlets (Bahr & Lanier 1981; White et al 1996; Byers et al. 2015). If the reefs in the SRE grew in lower salinity water than the reefs in BS, then that low-salinity niche would allow intertidal reefs to persist at lower average aerial exposures; however, salinity at the reef sites was similar among estuaries throughout the study period and cannot explain the observed differences in aerial exposure (Appendix 1.2).

Mortality of adult intertidal oysters has been tied to high air temperatures. Persistent high air temperatures are known to cause exposed *C. virginica* to re-allocate energy, typically used for growth, to metabolic maintenance (Dame 1972, Newell 1979). Furthermore, genes that are known indicators of environmental stress were expressed in *C. virginica* when they were subjected to persistent temperatures > 28°C (Chapman et al. 2011). The potential heat stress of the SRE is 26% greater than BS which would provide additional stress that should increase as the time of oyster exposure increases. Air temperature stress is likely forcing reefs in the SRE

toward positions that are lower in the tidal frame than BS. The mean aerial exposure time of the reef crests and OGZs in the SRE are 27% and 22% lower than BS, respectively. In addition, the range of aerial exposures between the reef crests and the OGZ is larger in BS than the SRE. It is important to note that the period over which growth was measured varied between estuaries, which resulted in BS fringing reefs experiencing the fewest days with Tmax > 28 °C and the least potential heat stress. The lower position in the tidal frame of the SRE reefs, attributed here to higher atmospheric temperature, may introduce other stressors like biological competition and sedimentation, both of which increase with depth (Schulte et al. 2009; Stokes et al. 2012; Fodrie et al. 2014). The reefs in the SRE are also closer to a river mouth than the reefs in BS and may be subject to a higher suspended sediment load. Neither competition nor sedimentation can be constrained with our dataset but could vary between estuaries and contribute to the observed difference in OGZ between estuaries.

In both estuaries, fringing reefs generally occupied lower elevations in the tidal frame than patch reefs. The exception is Fringe BS-3 with a reef crest elevation >10 cm higher than the other fringing reefs in BS. The elevation of Fringe BS-3 is likely an outlier because Ridge et al. (2017a) examined an adjacent fringing reef (CI-1) located 65 m east on the opposite side of the tidal channel that has a crest elevation ~5 cm lower. The vertical and horizontal growth of a fringing reef may be limited by the presence of the adjacent saltmarsh, whose vertical extent is also tightly coupled with mean sea level (Morris et al. 2002). Low flow rates along the ecotone between the saltmarsh and oyster reef likely impact growth around the crests of fringing reefs that are positioned near the saltmarsh edge. Fringing reefs have a ramp morphology and when submerged, flow is oriented along shore and impeded by the saltmarsh edge, which is different than patch reefs where flow is oriented across the mound. Subtidal mounded reefs increase flow

speed, and the growth of oysters was greater on top of reefs where flow velocities were higher and sediment deposition was reduced (Lenihan 1999). This is likely similar for intertidal patch reefs while submerged. When fringing reefs and adjacent saltmarsh are inundated, however, the saltmarsh vegetation, the crenulated saltmarsh edge, and the reef attenuates along-shore flow (Stumpf 1983; Leonard et al. 1995; Christiansen et al. 2000; Friedrichs and Perry 2001; Housego and Rosman 2016). Flow attenuation along the edge of saltmarsh platforms effect fringing reefs by decreasing the flux of seston and oxygen to the oysters, increasing sedimentation on the reef, limiting oyster growth, and increasing mortality (Lenihan et al. 1996; Grabowski et al. 2005; Reidenbach et al. 2013; Fodrie et al. 2014; Housego and Rosman 2016). Flow conditions most conducive to oyster reef growth on fringing reefs are likely to occur away from the saltmarsh edge and lower in the tidal frame than patch reefs due to differences in reef morphology (ramp vs. mound) and surrounding ecotones (structured saltmarsh vs. smooth tidal flat). The oyster reef structure also baffles flow. As the width of a reef along its short axis increases, which is commonly oriented parallel to flow, flow attenuation increases across the reef, erosion is reduced, sedimentation increases, and this can promote the colonization of vegetation on top of reef crests, such as Patch SRE-1 where a plot of saltmarsh colonized the center of the reef.

Reef growth and age

The parabolic growth pattern observed for the 12 natural reefs in this study, with the OGZ positioned along the upper flank of the reefs, is the same as previous studies that focused on restored patch reefs in BS (Rodriguez et al. 2014; Ridge et al. 2015; Ridge et al. 2017a). The position of the OGZ in the tidal frame, however, should change as a reef matures because the intertidal substrate oysters colonize is at various elevations and it takes time for the reef to

accrete to the growth ceiling. Previously studied intertidal reefs in BS displayed high growth rates, but those reefs formed on low relief (15 cm) and low elevation (<20% exposure) piles of oyster cultch. The space available for reef growth (accommodation) was at a maximum when cultch was initially installed at the base of the OGZ. The high accommodation promoted high growth rates because there was simply more intertidal space for the oysters to fill (Ridge et al. 2015). The aerial exposure of the OGZ of the only previously measured natural fringing reef (CI-1) was ~50%, much higher than the youngest restored reefs (9–23%; Ridge et al. 2017a). In addition, Rodriguez et al. (2014) investigated growth rates of patch reefs that were 1–14 years old and found evidence the position of the OGZ in the tidal frame elevates as reefs mature. The position of the OGZ on old natural reefs should be at the highest possible position in the tidal frame because the reef had enough time to accrete and fill accommodation. To investigate the time scale over which the OGZ elevates and stabilizes in the tidal frame of BS, we compared the young restored reefs included in Ridge et al. (2015, 2017a), with older natural fringing and patch reefs (Table 1.1; Figure 1.10). Of the restored reefs, 9 were ~4 years old (young reefs, Ridge et al. 2017a) and 5 were between 13 and 18 years old (decade-old reefs, Ridge et al 2015). We also include the one natural fringing intertidal reef, CI-1 from Ridge el al. (2017a) known to be ~270 years old.

The young reefs had the highest average MMGR (7.1 cm y^{-1}; n= 9) at the lowest average aerial exposures (14.3%) when compared to both the decade-old reefs (2.7 cm y^{-1}; 36.2%; n=5) and the natural reefs (2.4 cm y^{-1}; 50.00 %; n= 7; Figure 1.10). As reefs age, the MMGR decreases and the OGZ shifts towards higher aerial exposures (Figure 1.10). The crests of the young reefs are only at ~35% aerial exposure, those reefs have the most accommodation, and growth is unconstrained by mean sea level. In contrast, the crests of the older reefs extend to

higher exposures, ~60% for the decade-old restored reefs and >60% for the >50-year old natural reefs (Figure 1.10). The exposure of the OGZ for reefs that initially formed on low-elevation substrate increases over a 20–50-y period to an optimal value of ~50% for BS and the MMGR decreases over that same period due to decreasing accommodation (Figure 1.10).

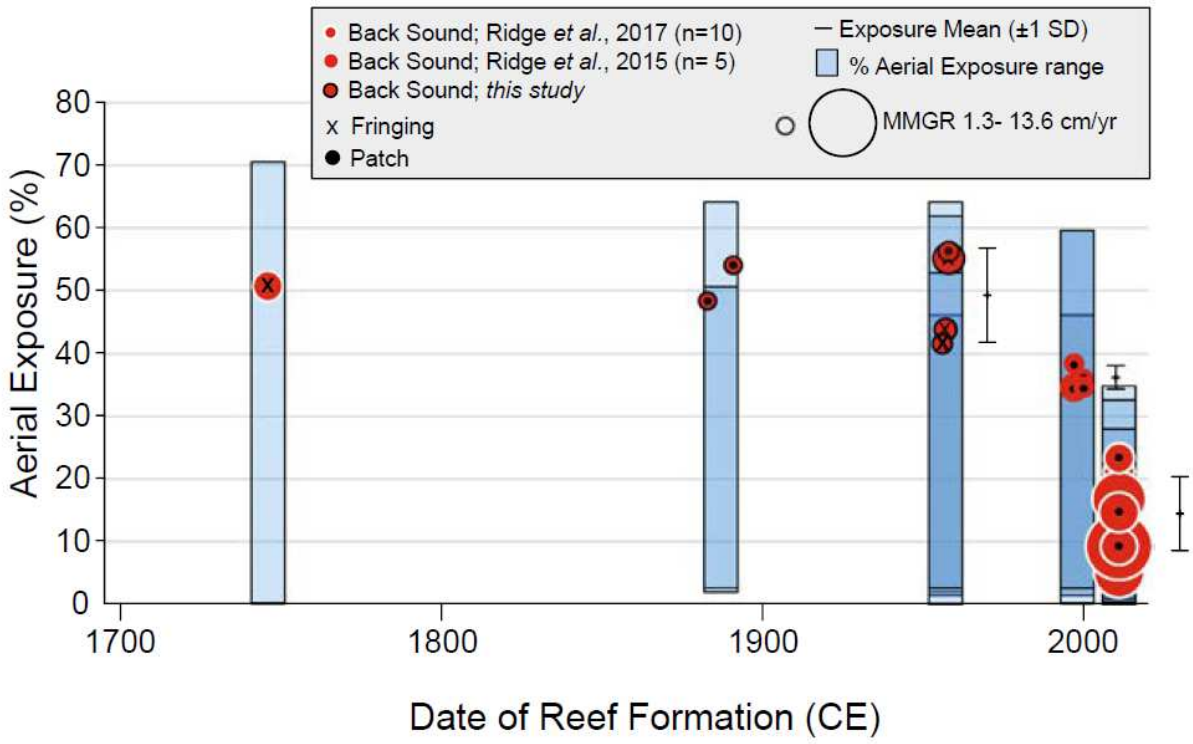

Figure 1.10 Aerial exposure of OGZ with age. Median percent aerial exposure of OGZ (circles) and range of exposures encompassed by each reef (blue bars) versus date of reef formation for restored (≥ 1997 CE) and natural reefs in BS. Size of the circle is scaled to MMGR. Mean aerial exposure of MMGR (± 1 SD) for reefs of similar age (formed within 20 years for natural reefs) shown to the right of clusters with n≥3.

Conclusions and implications for restoration

The Ridge et al. (2015) conceptual intertidal-reef growth model is applicable across landscape settings and tidal regimes. Reef growth rates follow a parabolic pattern from the reef crest, where growth rates are low and approximate the rate of SLR, increasing to the reef flank (at the OGZ), and decreasing towards the base of the reef. The natural patch and fringing reefs in the SRE exhibited peak growth at lower aerial exposures than in BS, which was likely driven by higher summertime temperatures in the SRE. The exposure of the OGZ on fringing reefs is lower than patch reefs, which may result from vegetation baffling flow and the ramp morphology preventing the acceleration of flow across the crests of fringing reefs. Although the conceptual growth model is applicable, the position of the growth ceiling and the optimal growth zone in the tidal frame varies across landscape settings and estuaries.

The position of the OGZ varies as reefs mature. A young restored reef positioned low in the tidal frame grows rapidly within 20–40% aerial exposure due to high accommodation and takes between 20–50 years to equilibrate with mean sea level. As the reef ages, the MMGR decreases and the OGZ elevates to higher aerial exposures due to accretion and associated decreasing accommodation. Once the restored reef reaches ~50 years old, the elevation of the OGZ has increased to a position that is close to mean sea level, although other factors like flow and temperature can affect the location of the OGZ in the tidal frame. While older reefs exhibit peak growth rates that are slower than young reefs, these rates still exceed the rate of relative sea-level rise (MMGR = 13–48 mm y^{-1}). However, the OGZ only spanned ~2–12 cm of the elevations occupied by the reef and other areas, such as the reef crests, grew more slowly and even experienced erosion (-1.1–19.1 mm y^{-1}).

Knowing the position in the tidal frame that maximizes intertidal reef growth and how that position varies with landscape setting, reef age, tidal regime, and air temperature will help guide restoration project design and performance expectations. The construction of intertidal oyster reefs as a nature-based defense against shoreline erosion is widespread along the mid-Atlantic and Gulf coasts, but often these efforts fail because the optimal conditions that promote reef growth are not met (Morris et al. 2019, 2020). Reef growth is essential for a restoration project to maintain its position in the tidal frame with sea-level rise and to continue to dampen wave energy. The results presented here demonstrate that restored oyster reefs thrive across a narrow range of elevations (the OGZ) but have the potential to grow above mean sea-level and extend to elevations with >70% aerial exposure maximizing their application for shoreline stabilization.

REFERENCES

Bahr, L.M., Lanier, W. P. (1981). The ecology of intertidal oyster reefs of the south Atlantic coast: a community profile, ed. U.S.F.a.W. Service, 105. Washington, D.C.: Office of Biological Services.

Beck, M. W., Brumbaugh, R. D., Airoldi, L., Carranza, A., Coen, L. D., Crawford, C., Defeo, O., Edgar, G. J., Hancock, B., Kay, M. C., Lenihan, H. S., Luckenbach, M. W., Toropova, C. L., Zhang, G., & Guo, X. (2011). Oyster Reefs at Risk and Recommendations for Conservation, Restoration, and Management. *BioScience, 61*(2), 107-116. https://doi.org/10.1525/bio.2011.61.2.5

Bilkovic, D. M., Mitchell, M., Mason, P., & Duhring, K. (2016). The Role of Living Shorelines as Estuarine Habitat Conservation Strategies. *Coastal Management, 44*(3), 161-174. https://doi.org/10.1080/08920753.2016.1160201

Bishop, M. J., & Peterson, C. H. (2006). Direct effects of physical stress can be counteracted by indirect benefits: Oyster growth on a tidal elevation gradient. *Oecologia, 147*(3), 426-433. https://doi.org/10.1007/s00442-005-0273-3

Byers, J. E., Grabowski, J. H., Piehler, M. F., Hughes, A. R., Weiskel, H. W., Malek, J. C., & Kimbro, D. L. (2015). Geographic variation in intertidal oyster reef properties and the influence of tidal prism. *Limnology and Oceanography, 60*(3), 1051-1063. https://doi.org/10.1002/lno.10073

Chapman, R. W., Mancia, A., Beal, M., Veloso, A., Rathburn, C., Blair, A., Holland, A. F., Warr, G. W., Didinato, G., Sokolova, I. M., Wirth, E. F., Duffy, E., & Sanger, D. (2011). The transcriptomic responses of the eastern oyster, Crassostrea virginica, to environmental conditions. *Molecular Ecology, 20*(7), 1431-1449. https://doi.org/10.1111/j.1365-294X.2011.05018.x

Christiansen, T., Wiberg, P. L., & Milligan, T. G. (2000). Flow and sediment transport on a tidal salt marsh surface. *Estuarine, Coastal and Shelf Science, 50*(3), 315-331. https://doi.org/10.1006/ecss.2000.0548

Dame, R.F. (1972). The ecological energies of growth, respiration, and assimilation in the intertidal American oyster Crassostrea virginica. *Marine Biology 17*: 243–250

Davies, D. J., Powell, Eric N., Stanton Jr., Robert J. (1989). Relative rates of shell dissolution and net sediment accumulation- a commentary: can shell beds form by the gradual accumulation of biogenic debris on the sea floor? *Lethaia, 22*, 207-212.

Fey, J. (2016). New nonparametric rank tests for interactions in factorial designs with repeated measures. *Journal of Modern Applied Statistical Methods* 15(1), 6: 78–99.

Fodrie, F. J., Rodriguez, A. B., Baillie, C. J., Brodeur, M. C., Coleman, S. E., Gittman, R. K.,

Keller, D. A., Kenworthy, M. D., Poray, A. K., Ridge, J. T., Theuerkauf, E. J., & Lindquist, N. L. (2014). Classic paradigms in a novel environment: Inserting food web and productivity lessons from rocky shores and saltmarshes into biogenic reef restoration. *Journal of Applied Ecology, 51*(5), 1314-1325. https://doi.org/10.1111/1365-2664.12276

Fodrie, F. J., Rodriguez, A. B., Gittman, R. K., Grabowski, J. H., Lindquist, N. L., Peterson, C. H., Piehler, M. F., & Ridge, J. T. (2017). Oyster reefs as carbon sources and sinks. *Proceedings of the Royal Society B: Biological Sciences, 284*(1859). https://doi.org/10.1098/rspb.2017.0891

Friedrichs, C.T., Perry, J.E. (2001). Tidal salt marsh morphodynamics: a synthesis. *Journal of Coastal Research, Winter 2001 Special Issue*, 27: 7-37.

Grabowski, J. H., Hughes, A. R., Kimbro, D.L., Dolan, M.A. (2005). How Habitat Setting Influences Restored Oyster Reef Communities. *Ecology, 86*(7), 1926-1935.

Grabowski, J. H., Brumbaugh, R. D., Conrad, R. F., Keeler, A. G., Opaluch, J. J., Peterson, C. H., Piehler, M. F., Powers, S. P., & Smyth, A. R. (2012). Economic Valuation of Ecosystem Services Provided by Oyster Reefs. *BioScience, 62*(10), 900-909. https://doi.org/10.1525/bio.2012.62.10.10

Grave, C. (1901). The oyster reefs of North Carolina: a geological and economic study. *Johns Hopkins University Circulars.* 151: 1–9.

Harding, J. M., Mann, Roger L. (2001). Oyster reefs as fish habitat: Opportunistic use of restored reefs. *Journal of Shellfish Research, 20*(3), 951-959.

Housego, R.M., Rosman, J.H. (2016). A model for understanding the effects of sediment dynamics on oyster reef development. *Estuaries and Coasts* 39: 495-509

Kay, M., Wobbrock, J. (2020). ARTool: Aligned Rank Transform for Nonparametric Factorial ANOVAs. doi: 10.5281/zenodo.594511, R package version 0.10.8.

Lenihan, H. S., Peterson, C.H., Allen, J.M. (1996). Does flow speed also have a direct effect on growth of active suspension-feeders: An experimental test on oysters. *Limnology and Oceanography, 41*(6), 1359-1366.

Lenihan, H. S., Peterson, C.H., Byers, J.E., Grabowskie, J.H., Thayer, G.W., Colby, D.R. (2001). Cascading of habitat degradation: oyster reefs invaded by refugee fishes escaping sress. *Ecological Applications, 11*(3), 764-782.

Lenihan, H. S., Micheli, F., Shelton, S. W., & Peterson, C. H. (1999). The influence of multiple environmental stressors on susceptibility to parasites: An experimental determination with oysters. *Limnology and Oceanography, 44*(3 II), 910-924. https://doi.org/10.4319/lo.1999.44.3_part_2.0910

Leonard, L.A., Hine, A.C., Luther, M.E. (1995).Surficial sediment transport and deposition processes in a *Juncus roemerianus* marsh, west-central Florida. *Journal of Coastal Research*, 11(2): 322-336.

Livingston, R. J., Howell IV, Robert L. Niu, Xufeng, Lewis III, F. Graham, Woodsum, G.C. (1999). Recovery of oyster reefs (*Crassostrea virginica*) in a gulf estuary following disturbance by two hurricanes. *Bulletin of Marine Science, 64*(3), 465-483.

Manis, J. E., Garvis, Stephanie K., Jachec, Steven M., Walters, Linda J. (2015). Wave attenuation experiments over living shorelines over time: a wave tank study to assess recreational boating pressures. *Journal of Coastal Conservation, 19*(1), 1-11. https://doi.org/10.1007/sl

McGill, R., Tukey, J. W., & Larsen, W. A. (1978). *Variations of Box Plots*.

Meyer, D. L., Townsend, E. C., & Thayer, G. W. (1997). Stabilization and erosion control value of oyster cultch for intertidal marsh. *Restoration Ecology, 5*(1), 93-99. https://doi.org/10.1046/j.1526-100X.1997.09710.x

Morris, J. T., Sundareshwar, P.V., Nietch, Christopher T., Kjerfve, B., Cahoon, D.R. (2002). Responses of Coastal Wetlands to Rising Sea Level. *Ecology, 83*(10), 2869-2877.

Morris, R. L., Bilkovic, D. M., Boswell, M. K., Bushek, D., Cebrian, J., Goff, J., Kibler, K. M., La Peyre, M. K., McClenachan, G., Moody, J., Sacks, P., Shinn, J. P., Sparks, E. L., Temple, N. A., Walters, L. J., Webb, B. M., & Swearer, S. E. (2019). The application of oyster reefs in shoreline protection: Are we over-engineering for an ecosystem engineer? *Journal of Applied Ecology, 56*(7), 1703-1711. https://doi.org/10.1111/1365-2664.13390

Morris, R. L., Boxshall, A., & Swearer, S. E. (2020). Climate-resilient coasts require diverse defence solutions. *Nature Climate Change*. https://doi.org/10.1038/s41558-020-0798-9

Morris, R. L., Konlechner, T. M., Ghisalberti, M., & Swearer, S. E. (2018, May). From grey to green: Efficacy of eco-engineering solutions for nature-based coastal defence. *Glob Chang Biol, 24*(5), 1827-1842. https://doi.org/10.1111/gcb.14063

Narayan, S., Beck, M. W., Reguero, B. G., Losada, I. J., van Wesenbeeck, B., Pontee, N., Sanchirico, J. N., Ingram, J. C., Lange, G. M., & Burks-Copes, K. A. (2016). The Effectiveness, Costs and Coastal Protection Benefits of Natural and Nature-Based Defences. *PLoS One, 11*(5), e0154735. https://doi.org/10.1371/journal.pone.0154735

Newell, R.C. 1979. Chapter 2: Tolerance of environmental stress. In Biology of Intertidal Animals. Elsevier, New York: 121.

Newell, R. I. E. (1988). Ecological Changes in Chesapeake Bay: Are They The Result of Overharvesting the American Oyster, *Crassostrea virginica*? Understanding the Estuary: Advances in Chesapeake Bay Research, Baltimore, Maryland.

NOAA Climate Data Online. (2020). Stations GHCND:USC00317813, GHCND:USW00093765. (2013-01-01 to 2019-01-31 23:59) accessed 2020-06-07.

NOAA Tides & Currents. (2020). Station 8656483. (1983-2001) accessed 2020-11-03.

https://tidesandcurrents.noaa.gov/reports.html?id=8656483

Piazza, B. P., Banks, P. D., & La Peyre, M. K. (2005). The potential for created oyster shell reefs as a sustainable shoreline protection strategy in Louisiana. *Restoration Ecology, 13*(3), 499-506. https://doi.org/10.1111/j.1526-100X.2005.00062.x

Pomeroy, L. R., D'Elia, Christopher F., Schaffner, Linda C. (2006, 11/07/2006). Limits to top-down control of phytoplankton by oysters in Chesapeake Bay. *Marine Ecology Progress Series, 325*, 301-309.

Powers, S. P., Peterson, C. H., Grabowski, J. H., & Lenihan, H. S. (2009). Success of constructed oyster reefs in no-harvest sanctuaries: implications for restoration. *Marine Ecology Progress Series, 389*, 159-170. https://doi.org/10.3354/meps08164

Raj, P. J. S. (2008). Oysters in a New Classification of Keystone Species. *Resonance*, 648-654.

R Core Team (2016) R: A Language and Environment for Statistical Computing. R Foundation for Statistical Computing, Vienna, Austria. https://www.R-project.org/Raj, P.J.S. 2008. Oysters in a new classification of keystone species. *Resonance*: 648–654.

Reguero, B. G., Beck, M. W., Bresch, D. N., Calil, J., & Meliane, I. (2018). Comparing the cost effectiveness of nature-based and coastal adaptation: A case study from the Gulf Coast of the United States. *PLoS One, 13*(4), e0192132. https://doi.org/10.1371/journal.pone.0192132

Reidenbach, M.A., P. Berg, A. Hume, J.C.R. Hansen, E.R. Whitman. (2013). Hydrodynamics of intertidal oyster reefs: the influence of boundary layer flow processes on sediment and oxygen exchange. *Limnology and Oceanography: Fluids and Environments* 3: 225–239.

Reimer, P.J., M.G.L. Baille, E. Bard,A. Bayliss, J.W. Beck,C.J.H. Bertrand, P.G. Blackwell, C.E. Buck, G.S. Burr, K.B. Cutler, P.E. Damon, R.L Edwards, R.G. Fairbanks, M.Friedrich, T.P. Guilderson, A.G. Hogg, K.A. Hughen, B. Kromer, G. McCormac, S. Manning, C.B. Ramsey, R.W. Reimer, S. Remmele, J. Southon, M. Stuiver, S. Talamo, F.W. Taylor, J. van der Plicht, C.E. Weyhenmeyer. (2004). IntCal04 Terrestrial radiocarbon age calibration, 26e0 ka BP. *Radiocarbon* 46: 1029–1058.

Reimer, P. J., B. Edouard, B., A. J. Bayliss, W. Beck, G.P. Blackwell,C.B. Ramsey,C.E. Buck, H.Cheng, R.L. Edwards, M. Friedrich, P.M. Grootes, T.P Guilderson, H. Haflidason, I. Hajdas, C.Hatte, T.J. Heaton, D.L. Hoffman, A.G. Hogg, K.A. Hughen, K.F. Kaiser, B. Kromer, S.W. Manning, M. Niu, R.W. Reimer, D.A. Richards, E.M. Scott, J.R. Southon, R.A. Staff, C.S.M. Turney, J. van der Plicht. (2013). IntCal13 and Marine13 Radiocarbon age calibration Curves 0–50,000 years cal BP. *Radiocarbon* 55: 1869–1887.

Ridge, J.T., A.B. Rodriguez, F.J. Fodrie, N.L. Lindquist, M.C. Brodeur, S.E. Coleman, J.H. Grabowski, and E.J. Theuerkauf. (2015). Maximizing oyster-reef growth supports green infrastructure with accelerating sea-level rise. *Nature Publishing Group*: 1–8.

Ridge, J.T., A.B. Rodriguez, and F.J. Fodrie. (2017). Evidence of exceptional oyster-reef resilience to fluctuations in sea level. *Ecology and Evolution* 7: 10409–10420.

Ridge, J. T., Rodriguez, A. B., & Fodrie, F. J. (2017). Salt marsh and fringing oyster reef transgression in a shallow temperate Estuary: implications for restoration, conservation and blue carbon. *Estuaries and Coasts* 40(4), 1013–1027. https://doi.org/10.1007/s12237-016-0196-8

Rodriguez, A. B., Fodrie, F. J., Ridge, J. T., Lindquist, N. L., Theuerkauf, E. J., Coleman, S. E., Grabowski, J. H., Brodeur, M. C., Gittman, R. K., Keller, D. A., & Kenworthy, M. D. (2014). Oyster reefs can outpace sea-level rise. *Nature Climate Change, 4*(6), 493-497. https://doi.org/10.1038/nclimate2216

Schulte, D.M., R.P. Burke,R.N. Lipcius. (2009). Unprecedented restoration of a native oyster metapopulation. *Science* 325: 1124–1128.

Scyphers, S. B., Powers, S. P., Heck, K. L., Jr., & Byron, D. (2011). Oyster reefs as natural breakwaters mitigate shoreline loss and facilitate fisheries. *PLoS One, 6*(8), e22396. https://doi.org/10.1371/journal.pone.0022396

Spalding, M. D., Ruffo, S., Lacambra, C., Meliane, I., Hale, L. Z., Shepard, C. C., & Beck, M. W. (2014). The role of ecosystems in coastal protection: Adapting to climate change and coastal hazards. *Ocean & Coastal Management, 90*, 50-57. https://doi.org/10.1016/j.ocecoaman.2013.09.007

Stokes, S., Wnderink, S., Lowe, M., Gereffi, G. (2012). *Restoring Gulf Oyster Reefs*.

Stuiver, M., and P.J. Reimer. (1993). Extended ^{14}C data base and revised CALIB 3.0 ^{14}C age calibration program. *Radiocarbon*, 35: 215–230.

Stumpf, R.P. (1983). The process of sedimentation on the surface of a salt marsh. *Estuarine, Coastal and Shelf Science*, 17: 495-508

Surge, D., Lohmann, K.C., Dettman, David L. (2001). Controls on isotopic chemistry of the American oyster, *Crassotsrea virginica*: implications for growth patterns. *Palaeogeography, Palaeoclimatology, Palaeoecology, 172*, 283-296.

Temmerman, S., Meire, P., Bouma, T. J., Herman, P. M., Ysebaert, T., & De Vriend, H. J. (2013, Dec 5). Ecosystem-based coastal defence in the face of global change. *Nature, 504*(7478), 79-83. https://doi.org/10.1038/nature12859

Walles, B., Fodrie, F. J., Nieuwhof, S., Jewell, O. J. D., Herman, P. M. J., & Ysebaert, T. (2016). Guidelines for evaluating performance of oyster habitat restoration should include tidal emersion: reply to Baggett et al. *Restoration Ecology, 24*(1), 4-7. https://doi.org/10.1111/rec.12328

White, M. E. & E.A. Wilson. (1996). Chapter 16: Predators, Pests, and Competitors. In the

eastern oyster Crassostrea virginica eds. Kennedy,V. S., Newell, R. I. E. & Eble, A. F., 559–580. Maryland Sea Grant College.

Wong, M. C., Peterson, C. H., & Piehler, M. F. (2011). Evaluating estuarine habitats using secondary production as a proxy for food web support. *Marine Ecology Progress Series, 440*, 11-25. https://doi.org/10.3354/meps09323

zu Ermgassen, P. S. E., Spalding, M. D., Grizzle, R. E., & Brumbaugh, R. D. (2012). Quantifying the Loss of a Marine Ecosystem Service: Filtration by the Eastern Oyster in US Estuaries. *Estuaries and Coasts, 36*(1), 36-43. https://doi.org/10.1007/s12237-012-9559-y

CHAPTER 2 ANTHROPOGENIC IMPACTS ON TIDAL CREEK SEDIMENTATION SINCE 1900

Introduction

Estuaries primarily receive sediment from their formative rivers. A portion of that sediment is deposited in the estuary and forms the substrate on which ecologically and economically important habitats, such as sea grass, oyster reefs, and salt marshes, colonize. The sediment supplied to estuaries also contributes to the vertical accretion of intertidal and shallow subtidal habitats and is necessary for maintaining their areal extent with accelerating sea-level rise (Barbier et al., 2011; Mudd 2011; Day et al., 2011; Fagherazzi et al., 2012). Humans have significantly modified river sediment load, discharge, and the degree to which watersheds are connected to the coast (Foley et al., 2005; James, 2013). It is important to address the degree to which upstream modifications have influenced sedimentation in estuaries because an increase in sediment supply to estuaries can have deleterious effects on habitats and fauna by increasing turbidity, sedimentation, and habitat burial (Lightbody et al., 2019, Ralston et al., 2020).

Land-cover changes, such as clearing forests, commonly promotes soil erosion, and increases sediment load in rivers with relief providing an important first-order control on the extent of landscape erosion and sediment transport (Hupp et al., 2009). Development of urban and suburban centers is associated with the channelization of catchment basins, increased flow velocities and increased connectivity between landscapes and downstream environments (Renfro, 1975; Milliman & Syvitski, 1992; Syvitski & Milliman, 2007). An inferred decrease in sediment delivery to estuaries, based on river gauges positioned ~15-100 km landward of river

outlets, has been attributed to the construction of dams, which peaked in the United States around 1950 (McCarney-Castle et al., 2010; Weston, 2014). This inference assumes land-cover changes in the lower coastal plain contribute little to estuarine sedimentation, and conflict with direct measures of increasing sediment accumulation rates in many North American estuaries (Rodriguez et al., 2020) and net global increase in deltaic land area over the past 30 years (Nienhuis et al., 2020). Coastal population has been rising for more than half a century and is a common proxy for land-use change (Beighley et al., 2003). Most of the population increase near estuaries occurs along the shoreline, removed from where the main river discharges into the head of the estuary, but is connected to the estuary via smaller watersheds confined to the coastal zone. This highlights the importance of understanding sedimentation dynamics in small coastal-zone watersheds positioned seaward of bayhead deltas and river gauges.

The objective of this study was to examine the effects of changes in land cover in small coastal zone watersheds on sediment accumulation in downstream environments. These small (<50 km^2), yet abundant lower coastal-plain watersheds are the primary conduits of sediments and nutrients between uplands and coastal waters along the margins of estuaries. While these coastal watersheds have little relief, area, and flow, they are more impacted by population growth and associated land-use change, in terms of percent watershed area relative to watershed size.

The inherent vulnerability of coastal areas to climate change, including increases in storminess and the rate of sea-level rise, is compounded with higher population densities and development pressures. Coastal county populations throughout the United States have increased by 39% since the 1970s and population density is over six times greater in coastal counties than inland ones (Crosset, et al., 2013). Populations in many North American Atlantic, Gulf, and

Pacific coastal counties that directly border an estuary have doubled since 1950 (Rodriguez et al., 2020). Additionally, coastal areas support tourism industries that host millions of visitors each year (Miller et al., 1993), suggesting that coastal development likely increases more than what the census population would suggest. Expanding coastal populations increase total risk to communities from large storms and sea-level rise; however, the associated changes in land cover also impact sediment delivery to depositional environments such as oyster reef, salt marsh, mangrove, seagrass and tidal flats that provide communities some protection from waves and flooding (Victor et al., 2004; Mattheus et al., 2010; Gunnell et al., 2013.).

Changes in sediment accumulation in the coastal zone can result in either the proliferation or demise of estuarine habitats like saltmarsh, oyster reef, and seagrass. A shift toward more frequent and/or larger pulses of sediment delivered to an estuary can force habitats to transition, such as tidal flats transitioning to intertidal saltmarsh, or sandy subtidal flats transitioning to muddy subtidal flats. If sedimentation is too high, seagrass and oyster reefs can become buried and converted to mud or sandflat environments (Fagherazzi et al., 2006). A shift in habitat type and area changes the quantity and type of ecosystem services provided by estuarine habitats (Barbier et al., 2011; Grabowski et al., 2012). A reduction in sediment supply can cause intertidal habitats like saltmarsh and mangrove to drown with sea-level rise (Bromberg & Bertness, 2005; Vermeer & Rahmstorf, 2009; Kirwan et al., 2010; Ward et al., 2016; Watson et al., 2017) and loss of the protection those habitats provide to communities from storms (McLeod & Salm, 2006; Barbier et al., 2008; Temmerman et al., 2013; Moller et al., 2014). Accelerating sea-level rise makes it important to address the connectivity between small coastal plain drainage basins that are experiencing changes in land cover with their associated estuarine and marine environments in terms of sediment transport and deposition.

Connectivity between upstream and downstream in a fluvial system generally decreases as catchment area increases because of sediment storage in floodplains, therefore, connectivity could be high in small coastal plain rivers with little to no floodplain. Higher vertical gradients are typically correlated with an increase in upstream to downstream connectivity, and low relief coastal plain rivers and are assumed to be disconnected from changes in their watershed (Phillips & Slattery, 2006); however, there are examples where that assumption does not apply. Land clearing increased sediment delivery in Plum Island Estuary, MA and the Newport River Estuary, NC resulting in marsh building, flow constriction, and a shallowing of those estuaries (Mattheus et al., 2009; Kirwan et al., 2011; Gunnel et al., 2013). In low-gradient small coastal-zone river systems, Darrow et al. (2017) reported an increase in sediment organic matter delivered to Mississippi Sound following urban development and Corbett et al. (2017) showed that an increase in suburban development in North Carolina, USA watersheds resulted in estuarine sediment accumulation rates being higher than relative sea-level rise (RSLR). We build on these previous studies that emphasize the importance of coastal landscape changes on sediment dynamics downstream by investigating small coastal watersheds that vary by orders of magnitude in drainage basin size and relief, experience different tidal ranges, and have been impacted by different types of landscape change.

While large river systems like the Mississippi contribute much of the sediment considered in the coastal ocean sediment budget, small coastal plain rivers and tidal creeks are more abundant and are likely to retain the sediment from their watersheds in their basins, fringing salt marshes, and contribute to the sediment budgets of larger estuaries or back barrier lagoons and marshes. Mapping changes in land cover of small coastal-plain watersheds, identifying periods of greatest change and comparing those periods to the depositional record

since 1900 using the radiometric tracer ^{210}Pb will provide guidance to managers and stakeholders in fisheries management on how to increase the resilience of coastal communities through wetland and soil conservation practices, which could include dredging, installation or removal of buffers along creeks, or modifications to existing or future developments (e.g., reductions in impervious surfaces).

Background

Tidal creek formation

Along passive continental margins, rivers incised valleys during glacial maxima (last glacial maxima ended 20 kya) when lower sea-level exposed the break-in-slope between the low-gradient coastal plain and the higher gradient continental shelf (Schumm, 1993; Schumm & Etheridge, 1994). Smaller drainage networks also formed on the surrounding landscapes of the lower coastal plain and carved smaller valleys into Pleistocene and older strata (Mattheus & Rodriguez, 2014). These incised valleys and small drainage networks became estuaries and tidal creeks, respectively, as the landscape flooded during sea-level rise (Dalrymple et al., 1992).

For this study, we define tidal creeks as small channel networks that drain lower-coastal plain watersheds less than 50 km^2, are tidal along their entire length, and discharge into larger estuaries, lagoons, or back-barrier sounds, and are fringed by saltmarsh complexes along their main stem. This definition excludes wetland channels (e.g., Mallin and Lewitus, 2004), which can be dynamic over century timescales and lack an upland watershed. Tidal creeks form within coastal prism and tributary incised valleys (eg. Newport River, NC and Scuppernong, NC, respectively; Mattheus & Rodriguez, 2014). Coastal prism incised valleys form across the break in slope between the low-gradient coastal plain and the steep shoreface of the previous highstand

shoreline (Suffolk Scarp; Figure 2.1). Tributary incised valleys formed along the margins of larger incised trunk valleys. The high convexity along the edge of the incised valley, between the steep valley flank and the flat coastal plain, increased stream power and promoted erosion and knickpoint migration, which ultimately evolved into tributary incised valleys. The steep relic landscape morphology when the area was subaerially exposed is why tributary incised valley dimensions are commonly larger than what would be predicted by their small drainage basin size (Mattheus & Rodriguez, 2014).

Tidal creeks are comprised of upper reaches where the channel is constricted and meandering along a fringing saltmarsh complex, and an embayed open-water region of confluence between the lower tidal-creek basin and the main estuary it drains into. In this open-water region of the tidal creek, salt marsh islands, oyster reefs, seagrass beds, and mudflats proliferate. Ensign et al. (2017) summarized marsh-mudflat morphodynamics in the embayed zone as being driven by waves, while marsh-channel morphodynamics in the meandering zone is driven by tidal currents. While the area of the embayed zone is covered by various amounts of structured subtidal and intertidal habitats, such as seagrass, oyster reef, and salt-marsh patches, the mouth of the meandering channel is always fringed by wetlands and commonly saltmarsh.

Tidal creek sedimentation

Sediment is supplied to a tidal creek from its drainage basin and from the estuary it drains into. Sediment moves primarily from upstream to downstream during rain events and sources include runoff, resuspension, and bank erosion. Tidal-creek watersheds have little relief, highly variable vegetation cover, and a wide range of anthropogenic impacts so the potential for erosion within the watershed can vary substantially across small spatial scales. Sediment moves from the

estuary into the tidal creek during flood tide or storm surge and is sourced mainly from surrounding drainage basins, offshore, resuspension, and shoreline erosion.

Sediment deposition in the embayed zone of a tidal creek is driven by sediment supply and accommodation. Accommodation is the amount of space available for sediments to accumulate in, which near the coast, is closely tied to the level of wave base and the rate of RSLR (Jervey, 1988). Sediment supply and accommodation change over a variety of timescales. Shorter timescales (annual to decadal) encompass changes in watershed land cover and storminess, which results in higher sediment flux to the tidal-creek embayment, and higher resuspension of the bed as wave base deepens, respectively. Over longer timescales (centennial) accommodation is mainly driven by RSLR and sediment flux by climate. The water depth of the lower embayed portion of tidal creeks is not necessarily in equilibrium with storm wave base, as is common for estuaries and lagoons (Nichols, 1989). The lower embayment of tidal creeks within tributary incised valleys are typically oversized in comparison to the size of the creek's watershed and could still be filling sediment accommodation to base level and contain more complete records of sedimentation (Mattheus & Rodriguez, 2014). Tidal creeks within coastal prism incised valleys could be accommodation limited because the size of the lower embayed portion does scale with the size of the tidal-creek watershed and contains numerous patches of intertidal oyster reefs and salt marshes.

In North Carolina, along the 180-km long coastline between Cape Lookout and Cape Fear there are four rivers that discharge into the heads of estuaries (North, Newport, White Oak, and New), but > 60 tidal creeks positioned seaward of bayhead deltas and 8-30 km from the ocean shoreline. The small size of tidal creek watersheds may be disproportionate to their importance as conduits for sediment transport from landscapes to estuaries and the coastal ocean

because they are abundant, located in areas of expanding populations and creek discharge is strongly impacted by storminess.

Methods

Site Selection

The North Carolina coast (NC, USA) hosts extensive estuarine systems, a broad coastal plain, and a long history of anthropogenic modifications to coastal watersheds making it an ideal study area. Sea-level fluctuations through time formed terraces and scarps along the lower coastal plain of NC (Riggs and Ames, 2003). The Suffolk Shoreline is an ~80 ka paleoshoreline (Mallinson et al., 2008) at an elevation between 6 and 14 m, parallels the NC ocean shoreline from the southwest to Morehead City, NC, where its trend abruptly changes to the North forming a right angle or paleo cape (Ewen et al., 2011). The paleo cape at Morehead City divides the study area into two distinct zones. The coastal plain seaward of the Suffolk Shoreline and north of the paleo cape is characterized by a low slope, elevation <2 m, numerous tributary incised valleys (Mallinson et al., 2018), and a tidal range of 0.95 m (NOAA Station ID 8656483). The zone west of the paleo cape is characterized by relatively steep coastal plain slopes with Carolina Bays typically positioned landward of the Suffolk Shoreline, numerous coastal prism incised valleys, and a tidal range of 1.21 m (NOAA Station ID 8658163). Carolina Bays are oval shaped depressions (<3 m deep) that vary in size (~10m – 4 km along the long axis) along the southeastern Atlantic coast and are oriented NW to SE (https://www.dnr.sc.gov/geology/carolina-bays.html). Our study includes six tidal creeks within Carteret County (CC; lower tidal range) and six tidal creeks in New Hanover County (NHC; higher tidal range). Of those 12 tidal creeks seven are within coastal prism incised valleys, six in

NHC and one in CC (Gales Creek, Site 6), and five are within tributary incised valleys, all in CC (Figure 2.1).

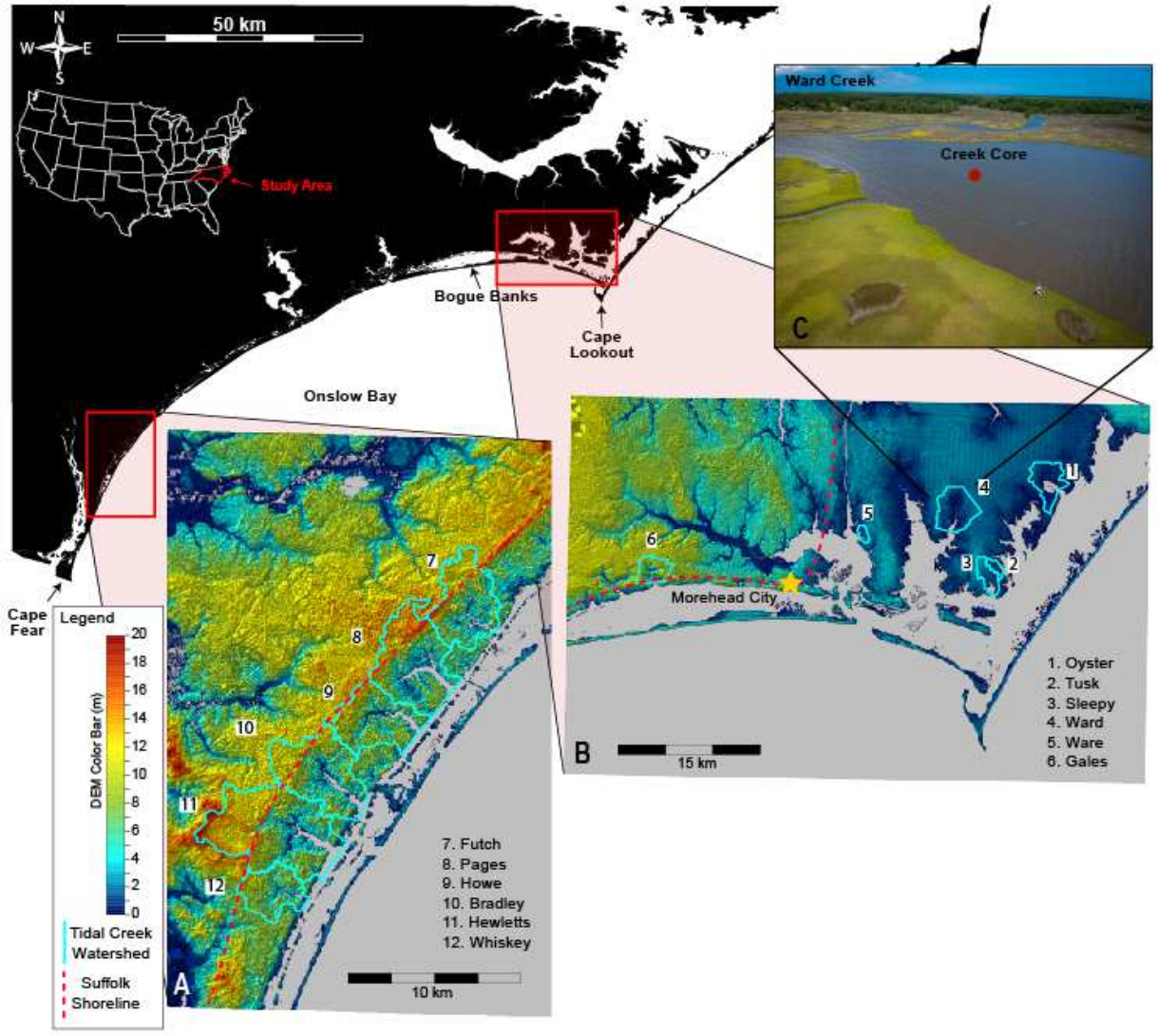

Figure 2.1 Study area map. Topography and watershed boundaries of each tidal creek. The creek numbers increase from east to west (1-12) and six creeks were sampled in both New Hanover County (A), and Carteret County (B). A core from each creek was obtained from the same general location, with respect to the creek outlet, as shown for Ward Creek (C).

Land-use change and digital elevation models

Watersheds in CC were delineated by hand in ESRI ArcGIS using digital elevation models (DEMs) from lidar data collected in 2014 (± 0.12 m vertical; NOAA OCM, 2014; Figure

2.1). NHC watersheds were obtained from the New Hanover County Open Geospatial Data portal (New Hanover County, 2015; Figure 2.1). Watershed relief was calculated as the difference between the highest and lowest 10% of elevation points of the DEM (Table 2.1, Figure 2.1).

Site ID	Creek Name	Dbs (km^2)	Watershed Relief (m)	Core Date	Core latitude (degrees)	Core longitude (degrees)	Type
1	Oyster	11.76	2.30	2016-08-05	34.8270	-76.4623	Tributary
2	Tusk	1.88	2.68	2016-08-09	34.7463	-76.5139	Tributary
3	Sleepy	5.38	3.73	2016-07-21	34.7329	-76.5272	Tributary
4	Ward	14.96	2.44	2016-07-07	34.7907	-76.5658	Tributary
5	Ware	1.54	2.49	2016-08-24	34.7750	-76.6741	Tributary
6	Gales	7.78	9.48	2016-07-28	34.7321	-76.9075	Coastal Prism
7	Futch	15.44	11.88	2016-05-10	34.3041	-77.7532	Coastal Prism
8	Pages	20.35	14.60	2016-10-04	34.2816	-77.7786	Coastal Prism
9	Howe	14.24	13.47	2016-10-05	34.2559	-77.8065	Coastal Prism
10	Bradley	18.67	12.57	2016-09-20	34.2179	-77.8395	Coastal Prism
11	Hewletts	30.23	15.08	2016-09-12	34.8270	-76.4623	Coastal Prism
12	Whiskey	8.49	8.74	2016-09-12	34.1600	-77.8626	Coastal Prism

Table 2.1 Watershed characteristics and core locations. Site ID, Creek Name, Drainage basin size (Dbs), watershed relief, core dates and locations, creek type.

Land cover of each watershed was classified at least every decade between the 1959 – 2016 study period (Table 2.2). From 1959-1993, land cover was digitized from georeferenced aerial imagery from the United States Geological Survey (USGS) Aerial Photo Single Frames records collection and National High-Altitude Photography (NHAP) program. Classifications used were forest, cleared forest, agriculture, developed, or water/intertidal. Changes between cleared forest and forest classifications were associated with silviculture operations. Land-cover from 1996-2016 was obtained from the Coastal Change Analysis Program (CCAP: NOAA, 2020) and reclassified to match the same categories as the earlier time-steps. Some of the aerial

imagery did not capture every tidal creek watershed, which resulted in land cover being classified 11 times for nine tidal creeks and 10 times for three tidal creeks (Table 2.2).

We assumed for each creek watershed that the land cover classification with the highest % contribution to the total change in land cover over the 50-year period (major land-cover change; MLCC) would be the main driver of increased sediment supply to the salt marsh. We defined the time boundary between pre- and post-MLCC as the midpoint between the dates of two land cover classification maps where a >15% gain occurred within the (Appendix 2.3).

Year	1	2	3	4	5	6	7	8	9	10	11	12
1959												
1964												
1969												
1970												
1975												
1982												
1993												
1996												
2001												
2006												
2010												
2016												

Table 2.2 Land cover data obtained. The years land-cover classes were mapped in each Tidal Creek watershed (Green). Missing land cover data (Orange). See Figure 2.1 for creek numbering.

Field sampling and radiometric dating

To ensure the sediment core captured changes in deposition, each tidal creek was sampled in 2016 where the channel widened and transitioned from wetland-dominated to embayed or within the bayhead shoreline (Simms et al., 2018; Figure 2.1). A push core (1 m) was collected from each creek bottom (water depth ~1m; Appendix 2.1) with the aid of a sledgehammer. Sediment cores were transported back to the laboratory in a vertical position, extruded into 1-cm intervals

(~10 cm^3) and frozen. Samples were then weighed, freeze-dried, and weighed again to calculate porosity. Dry bulk density values were calculated assuming quartz composition. Disaggregated subsamples were used to measure percent organic matter by loss on ignition (LOI; Heiri et al., 2001) and grain size (<2000 to 0.04 μm fraction) using a Cilas laser particle size analyzer. The remaining samples were then sorted through a 63-micrometer sieve for radioisotope analysis of the fine-grained fraction.

The fine-grained fraction (<63 microns) was used for isotope-dilution alpha spectrometry to quantify ^{210}Pb via the granddaughter isotope, ^{210}Po, which is assumed to be in secular equilibrium with ^{210}Pb (Flynn, 1968; El-Daoushy et al., 1991; Matthews et al., 2007; de Vleeschouwer et al., 2010). Raw ^{210}Pb data and dry bulk density, both of which are needed for geochronology modelling, are presented in Appendix 2.2 for each depth interval for all 12 creek cores. To obtain accumulation rates, ^{210}Pb dating methods including the Constant Flux and Constant Flux Constant Sedimentation models described in Sanchez-Cabeza and Ruiz-Fernandez (2012) were used. For this study, the Constant Flux model (CF; widely known as the Constant Rate of Supply model; Appleby and Oldfield 1978) was of the most interest because it assumes that ^{210}Pb flux to the sediment surface is constant and the initial concentrations and the mass accumulation rates (MAR) of individual layers may change, but they must be inversely proportional. Depth integrated ^{210}Pb inventories were calculated for each sediment core and used to calculate sediment accumulation rates with the CF model. This model provides ages and accumulation rates for discrete intervals within the core allowing for direct comparison with the land-use time-series data. All reported p-values are the result of t-tests assuming unequal variances between sample groupings.

Results

Drainage basin size and relief

The drainage basins of the tidal creeks vary in area and relief by an order of magnitude. Coastal prism drainage basins are generally larger and have greater relief than the tidal creeks within tributary incised valleys (Table 2.1) with Hewletts Creek (Site 11) having the largest watershed area (30.23 km^2) and relief (15.08 m), Ware Creek (Site 5) having the smallest watershed size (1.54 km^2), and Oyster Creek (Site 1) having the lowest relief (2.3 m). The drainage basin size of tidal creeks increases with relief and drainage basin size is a power function of relief except for two outliers, Oyster (Site 1) and Ward (Site 4) creeks (Figure 2.2). Both outliers are tributary incised valleys with large drainage basins relative to their low reliefs. Ward Creek is positioned along the flank of the North River incised valley, which is 8-10 m deep at the confluence (Mattheus et al., 2014). When sea level was lower and the area was exposed, the relic steep slope and high relief along the flank of the North River incised valley promoted incision, knickpoint migration, and expansion of the Ward Creek drainage basin above what would be predicted from watershed relief (Mattheus et al., 2014). The

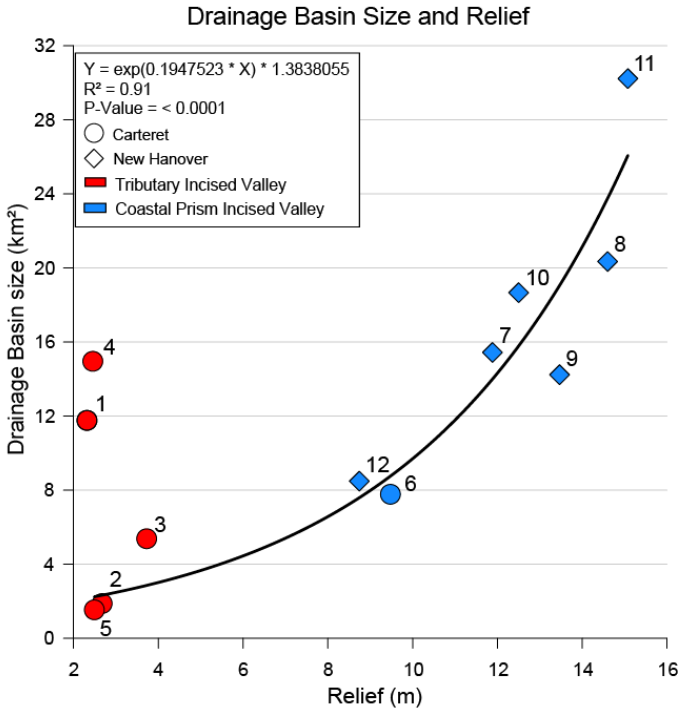

Figure 2.2 Drainage basin size vs relief. Tidal creek drainage basin size increases exponentially with relief. Tidal creeks are enumerated as shown on Figure 1. Oyster Creek (1) and Ward Creek (4) are outliers excluded from the regression.

other tidal creeks that formed within tributary incised valleys merge with their associated larger river systems on the inner continental shelf, farther seaward than where Ward Creek merges with the North River (Mallinson et al., 2018), and the size of those drainage basins, at the present headwater locations, is controlled mainly by relief. The Oyster Creek outlier has the lowest watershed relief and a disproportionately large drainage basin area that has been highly modified by humans. Extensive ditching of nearby farmland and wetlands and creation of a 1.25 km^2 waterfowl impoundment site has increased watershed area above its natural state.

Land cover 1959 to 2016

Land cover of all 12 tidal creek watersheds was dominated by forest, cleared forest, and agriculture in the 1959 imagery (Figure 2.3). During the next 57 years, development of the creek watersheds in NHC increased to an average of 50.2 ±5.5% of total watershed area, while the CC creek watersheds remained dominated by forest, cleared forest, and agriculture (Figure 3B). The creek watersheds in NHC are adjacent to the expanding Wilmington, NC urban center and developed into suburban landscapes, while the creek watersheds in CC remained relatively rural over the same period. Development of the NHC creek watersheds increased the most, ~20-26%, between the early 1970s and middle 1990s (Appendix 2.3). In the tidal creek watersheds of CC, the type of land-use change was more variable, and the percent of area that changed was lower than what occurred over the 57-year period in NHC (Appendix 2.3). Cleared forest area rapidly increased between 1982 and 2001 in the Oyster Creek watershed (Site 1) and agriculture area rapidly increased between 1975 and 1982 in the Ward Creek watershed (Site 4). The percent area of forest and cleared forest fluctuated after 1975 in Tusk (Site 2) and Sleepy creek (Site 3) watersheds, mainly the result of silviculture operations, with maximum increases in cleared

forest between 1975 and 1982 of 18% and 28% at each respective site. Land cover of the Ware Creek watershed (Site 5) changed the least throughout the period in all classes, with a maximum increase of only 11% cleared forest between 1993 and 1996. The land cover of the Gales Creek watershed (Site 6) increased 13% in developed area between 1975 and 1982 and forest and cleared forest area fluctuated after 1964, with a maximum of 9% increase in cleared forest between 1975 and 1982 (Appendix 2.3.).

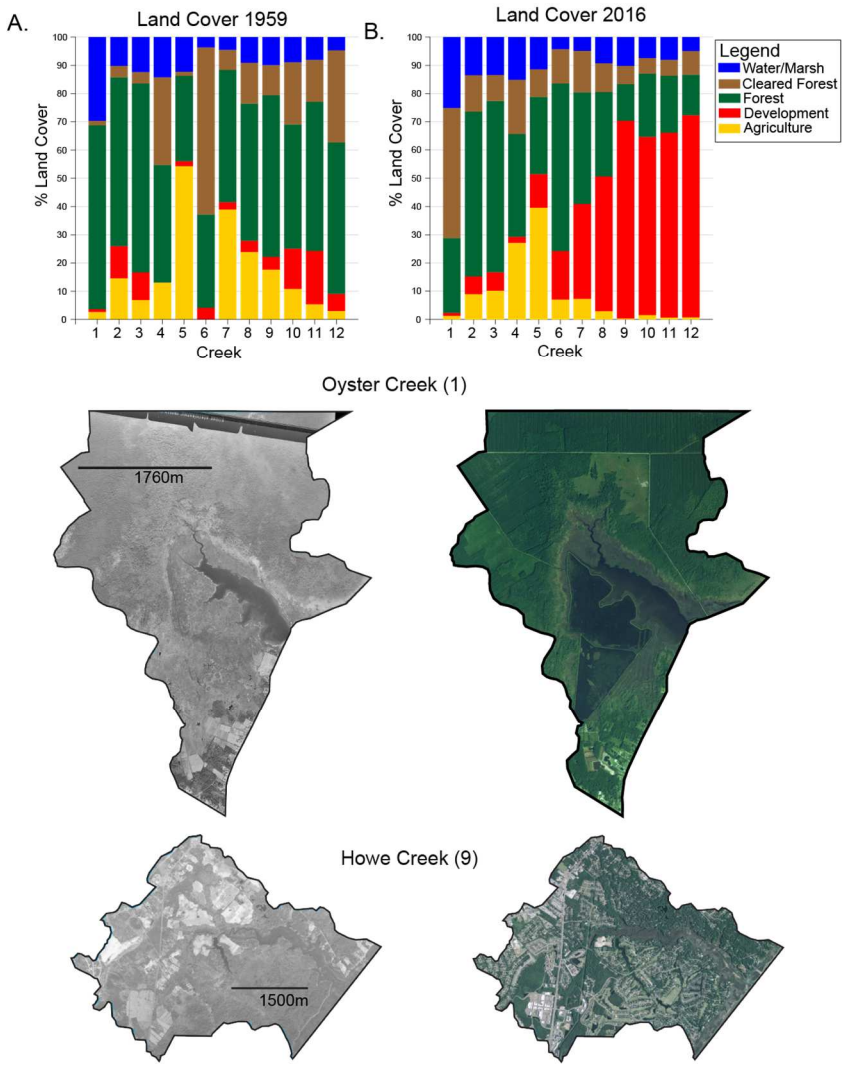

Figure 2.3 Land cover in 1959 and 2016. Tidal-creek watershed percent land cover of each class and examples of aerial imagery used for Oyster Creek (Site 1) and Howe Creek (Site 9) in 1959 (A) and 2016 (B).

Tidal creek sediment composition

Changes in sediment composition and texture with depth in a sediment core can indicate changes in sediment source or support a hypothesized change in sedimentary regime. Most of the tidal creek cores showed minor variation in sediment composition with depth, but there were some differences in texture between CC and NHC. The CC creek sites generally had less sand than the NHC creek sites. Distinct underlying depositional environments over which the watersheds formed, capacity for transporting sand, and sediment texture of adjacent source areas explains the broad differences in sediment texture between counties. The tidal creek watersheds in NHC are positioned on the sandy relatively high-relief Suffolk Scarp paleoshoreline, while the tidal creek watersheds in CC formed on old inner-continental shelf muddy substrate with low relief (Mallinson et al., 2008). In addition, the embayments of the NHC creeks are positioned closer to modern sandy tidal deltas and have a greater tidal range and capacity for transporting sand than CC creeks. The one exception is Oyster Creek (Site 1) that

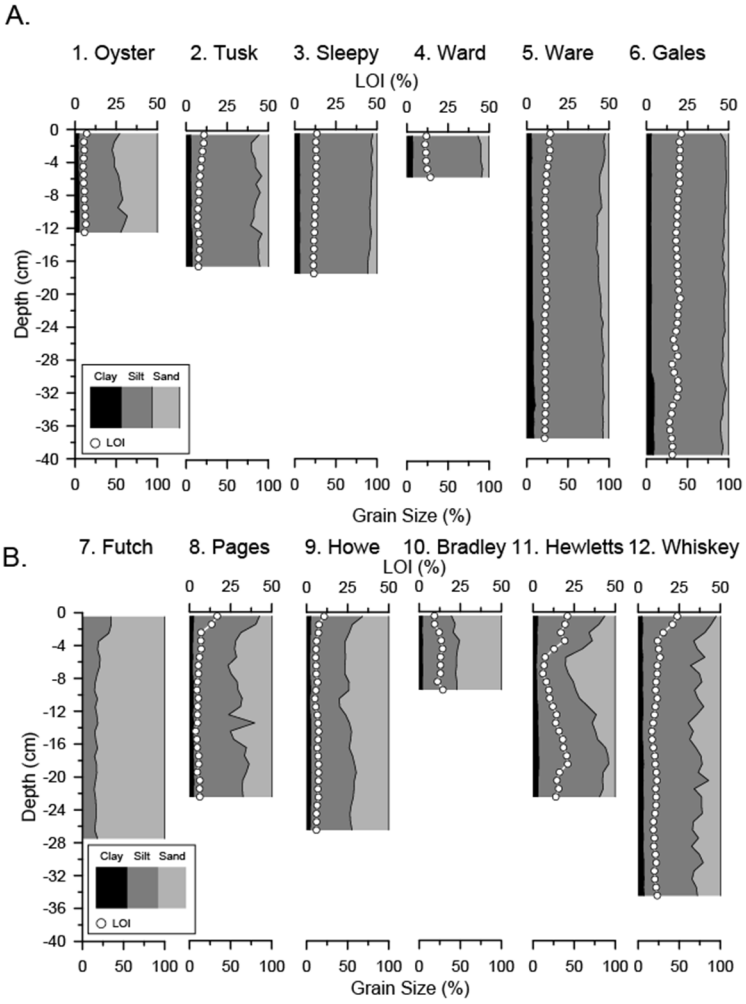

Figure 2.4 Changes in the composition of each core with depth. Cumulative percent of clay (black), silt (dark grey), and sand (light grey) and percent organic matter (while circles) are shown for each 1-cm thick core sample. Mid-point depths are plotted from the top of the bed (0 cm) to the base of the ^{210}Pb profile.

had between 37- 55% sand (Figure 2.4) throughout the sediment core. Of the CC creek sites, Oyster creek has the most direct connection to sandy Core Sound (Wells and Kim, 1989). There was also relatively little change in percent organic matter with depth for most of the cores (Figure 2.4). The top ~3 cm of the cores from the NHC sites had a higher % organic matter than what was measured below, likely due to incomplete biodegradation of surface organic carbon. Hewletts Creek (Site 11) showed some variation in organic matter and sediment composition downcore, which could be attributed to a change in sediment regime following a land-use change (Figure 2.4).

Mass accumulation rates through time

Long term average (1900-2016) MARs were higher in tidal creeks within coastal prism incised valleys than tributary incised valleys (0.21 ± 0.03 g cm^2 yr^{-1} and 0.12 ± 0.03 g cm^2 yr^{-1}, respectively, P=0.033) excluding Bradley Creek (Site 10) which was mixed throughout the profile making accumulation rates impossible to derive. Average MAR from 1900-1950 was the same in both creek valley types, but from 1950-2016, average MAR was higher in creeks within coastal prism incised valleys than tributary incised valleys (0.22 ± 0.004 and 0.14 ± 0.002 g cm^2 yr^{-1}, respectively, P= 0.032). Most creeks showed an increasing trend in MARs from 1900 to 2016 and most of the increase occurred in the second half of the century (1950-2016), the only exception being Ward Creek (Site 4) with consistently low MARs (Figure 2.5).

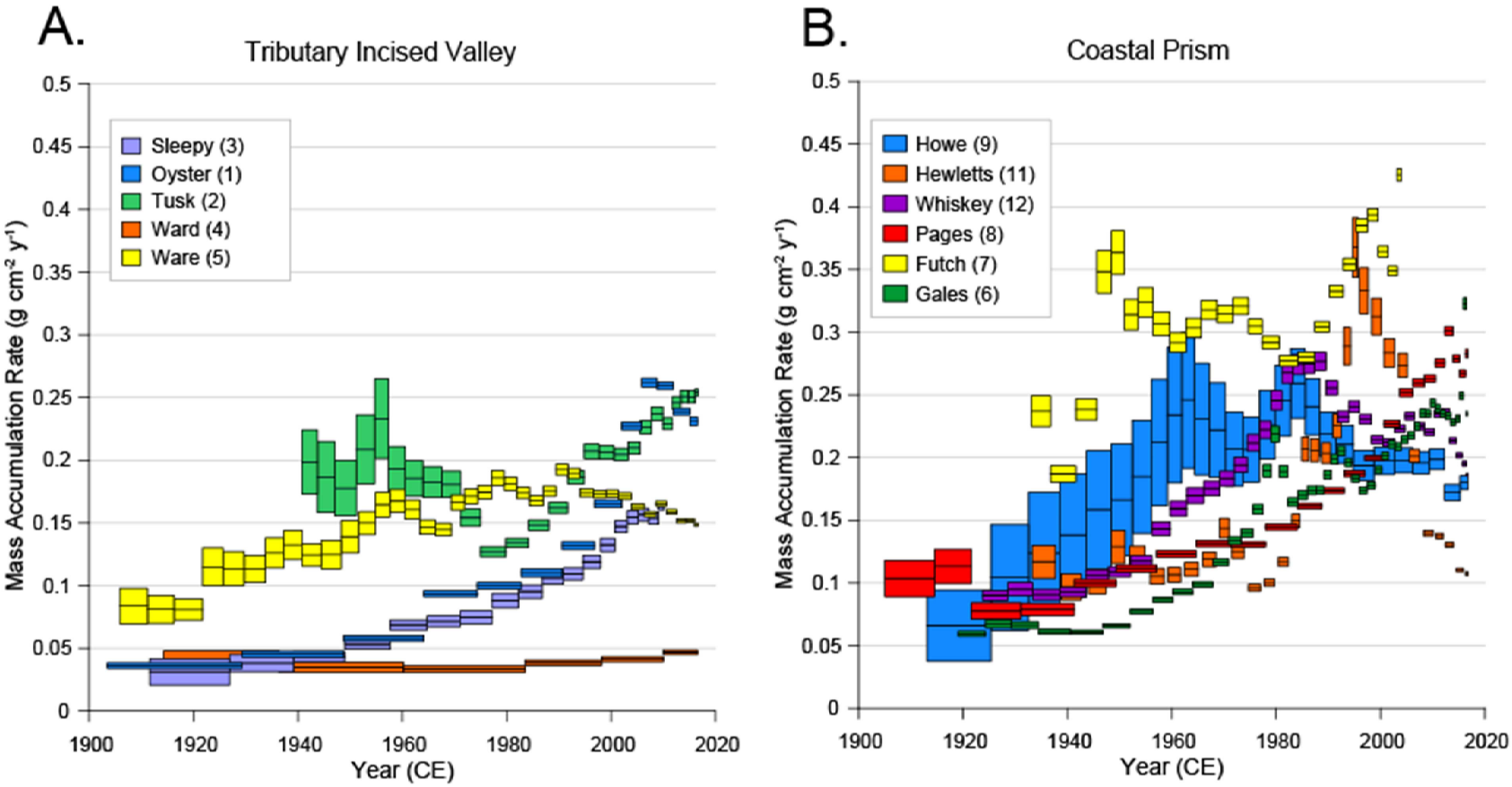

Figure 2.5 Mass accumulation rates. Tidal creeks within tributary incised valleys (A) and coastal prism incised valleys (B). Vertical errors are measurement uncertainty representative of alpha spectrometry and horizontal error shows the amount of time each 1-cm slice represents in the core.

The MARs of Oyster, Tusk, Sleepy, Gales, Futch, Pages, Hewett's, and Whiskey creeks (Sites 1-3, 6, 7, 8, 11, and 12) rapidly increased following the mid-1970s or early 1980s, reached a maximum in the 1990s or early 2000s and subsequently stabilized or decreased. In contrast, the MARs at Howe (Site 9) and Ware (Site 5) creeks increased until ~1960, the beginning of our land-cover time-series data set, but then showed small fluctuations until 2016. Ward Creek (Site 4) had consistently low MARs throughout the entire record.

Quantitatively relating MAR with LUC is impossible or not meaningful because we would have to coarsen the resolution of the accumulation rates in order to compare to the decadal record we derived for LUC. By binning accumulation rates relative to the resolution of the LUC data set, we lose trends in accumulation rates that are clearly a result of the LUC data set.

Discussion

8 of the 12 tidal creeks we studied were defined by increases in MAR post-MLCC, and those patters of sedimentation appear to be correlated with increased cleared forest for the creek sites within tributary incised valleys, and suburban development for creek sites within coastal prism incised valleys (Figure 2.6). The higher MARs recorded at sites within coastal prism incised valleys could be a partial result of accommodation differences between coastal prism and tributary incised valleys. Sediments in a tributary incised valley systems have an oversized embayed area to deposit in which would result in deposition of a thinner layer and lower recorded accumulation rates than in coastal prism incised valleys.

Constraining the relative proportions of the various sediment sources that contributed to the increase in MAR at each creek is not possible with our data set; however, given that we included numerous tidal creeks in the study, many of which are in proximity to each other, it is

possible to identify likely forcing mechanisms. Tidal creeks receive some sediment from larger rivers through their connection with estuaries and the coastal ocean and from shoreline erosion. If an increase in sediment supply to those connected water bodies caused the increase in MAR measured at most of our sites, then the timing of the increase should correspond with the sediment loading of those larger rivers and the increase recorded as a synchronous shift in depositional regime of many adjacent tidal creeks. There is no hydrological connectivity between the NHC tidal creek sites and the nearby Cape Fear River, but sediment loading in the Neuse and the Newport rivers could have influenced sedimentation in the CC tidal creeks. The timing of the increase in MAR for the tidal creeks in CC, however, occurred after 1975 CE, postdating the increase in sediment loading of the Newport River (1964; Mattheus et al., 2009) and the Neuse River (~1940; Cooper et al., 2004; Rodriguez et al., 2020; Figure 2.6).

The cores collected for this study were all from tidal creek outlets or bayhead shorelines (Simms et al., 2018) where an increase in MAR eventually forms tidal flats that become colonized with salt marsh as the creek outlet moves basin-ward. At the bayhead shoreline of tidal creeks, an increase in accumulation rate of the bed must be associated with an increase in sediment load and/or a decrease in the depth of bed erosion. Changes in storminess can promote shoreline erosion and increase sediment supply; however, it would simultaneously increase the depth of erosion at the creek outlet and increase the subtidal area. Furthermore, the proximity of the sites to each other suggests that a change in storminess would result in a change in MAR at the same time, but it differs for each creek site. An increase in storms with wind > 55.5 km h^{-1} (primarily northeasters) did occur around 2000 in the area near the CC sites (Miller et al., 2021) but increased storminess postdates the diachronous increase in MAR among creeks (Figure 2.5).

The timing of the post-MLCC increase in MAR matched large changes in land cover at eight of the creek sites (sites 1-3, 6- 8, 11, and 12; Figure 2.6). Sites 1-3 experienced variations in cleared-forest area from silviculture activities that started in the mid-1980s and early 1990s. Immediately after the initiation of silviculture, MAR accelerated. The land cover of the Gales Creek watershed (Site 6) experienced the largest change between 1964 and 1982 with a decrease in cleared forest area and an increase in developed area. This change in land cover corresponded with accelerating MARs between 1964 and 1982. The MARs of sites 7, 8, and 12 (Futch, Pages, and Whiskey creeks, respectively) accelerated rapidly during periods of increasing development in the early 1980s.

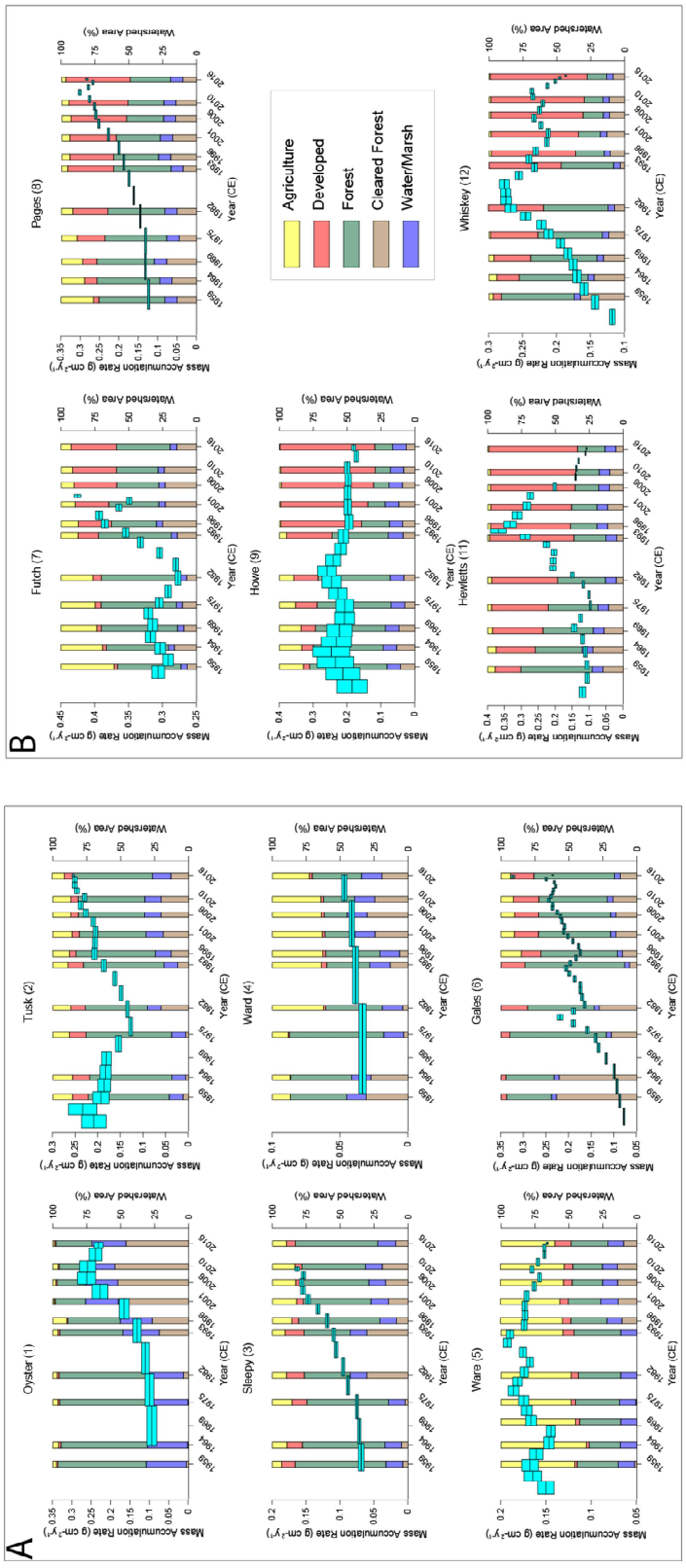

Figure 2.6 MAR vs LUC. Mass accumulation rates (cyan) and tidal creek watershed land cover since 1950.

Development of the Hewletts Creek (Site 11) watershed initiated in the 1950s, but the increase in MAR was not recorded until ~1980. The pattern of development across the Hewletts Creek watershed progressed from landward to seaward, initiating in the upper part of the watershed within a Carolina Bay depression (~3.5 km^2 within a 30.23km^2 watershed; Appendix 2.4). This depression, with a central man-made retention pond, likely acted as a natural retention area for ~11% of the total Hewletts Creek watershed, limiting drainage to the lower watershed and into the creek. The increase in development prior to 1982 occurred mostly within the confines of the Carolina Bay depression and was not recorded as an increase in MAR because the depression disconnected the modified landscape from the creek. The increase in development between 1982 and 1993 occurred outside of the Carolina Bay depression throughout the lower watershed and MAR accelerated rapidly during the same period. The core from Hewletts Creek also showed a decrease in organic matter and an increase in sand between 1982 and 1996. Only Hewletts Creek recorded changes in sediment composition as MAR accelerated and unlike the other sites, most of the increase in development occurred on the sandy Suffolk Scarp, which makes up 46% of the 30.23 km^2 watershed.

The creek sites that recorded an increase in MAR with large changes in developed land cover (Futch, Pages, Hewletts, and Whiskey) show a subsequent levelling off or decrease in MAR during the most recent part of the sedimentary record. Maintenance of constant or decreasing MAR occurred in the absence of any large changes in land cover of the creek watersheds. It is likely that surface sediment was eroded from the watershed and transported to the creeks during the construction phase of development, which included clearcutting forest, and once developed there was little sediment available that could be mobilized and exported to the tidal creeks. The creek sites impacted primarily by changes in silviculture recorded a more

persistent acceleration in MAR as forested and cleared forest areas transition back and forth with reestablishment and harvesting of pine trees.

Tidal creeks 4, 5, and 9 experienced changes in watershed land cover with no commensurate increase in MAR at the outlet. The NE trend of Ward Creek (Site 4) makes it susceptible to resuspension and flushing during SW wind events, the prevailing wind direction in the area. The Ward Creek sedimentary record consistently recorded the lowest MARs of all sites and unsupported ^{210}Pb was only measured down to 7 cm in the core, indicating the orientation of the creek is conducive to sediment bypass near the bay head shoreline, not deposition. Large changes in land cover of the Ward Creek watershed, such as the increase in cleared forest from 6-24% from 1996-2001, likely did promote an increase in sediment flux to coastal areas; however, the core was not obtained from an efficient depocenter where that would be recorded. Ware Creek (Site 5) experienced little change in land cover since 1959, but preserved some variability in sediment accumulation rates, most within error, which aligned with the timing of small changes in land-cover (Figure 2.6). The Howe Creek (Site 9) sedimentary record also preserved little changes in MAR since 1959; however, the development area of the watershed more than doubled between 1982 and 1996. Unlike the other creeks in NHC that showed an increase in MAR as developed area of the watershed increased, the Howe Creek watershed had a relatively large area dedicated to retention ponds, >2% of the watershed as compared to <0.5% in other creeks. The retention ponds function to interrupt runoff from reaching downstream areas and likely restricted sediment transport following land-cover changes.

Connectivity between creek watersheds and downstream estuaries

The stream power of tidal creeks is low because of their low slope, low discharge, and large backwater effects from lunar tides (Slattery and Philips, 2011). Despite their low sediment transport capacity, the connectivity of tidal creek watersheds to downstream bay head shorelines was high, using the time lag between when erosion of the landscape from a change in land cover initiated and when that sediment began to accumulate at the bay head shoreline as a proxy (Mattheus et al., 2009). The largest change in land cover was contemporaneous with increases in MAR near the bayhead shoreline at eight of the 11 tidal creeks, the response time being within the resolution of the remote-sensing data set (5-10 years). Land-use change is known to promote increases in sediment flux in low-relief areas (Mattheus et al., 2009; Corbett et al., 2017), but connectivity and the magnitude of the increase tends to be greater for smaller systems with higher relief (Syvitski, 1978; Milliman & Syvitski, 1992; Douglas, 1993). Creek watersheds within coastal prism incised valleys should be more connected to downstream bayhead shorelines than tributary incised valleys given their generally larger drainage basins and higher relief; however, this was not resolved with our data set. Oyster Creek (Site 1) is within a tributary incised valley, has the lowest relief watershed (2.3 m), and like the creeks within coastal prism incised valleys, the increase in MAR at the bayhead shoreline of Oyster Creek corresponded immediately with the increase in cleared forest area from silviculture activity (Figure 2.6). In addition, the ~30% greater tidal range in NHC, as compared to CC, had little influence on connectivity. The MARs of Gales Creek, the only CC creek within a coastal prism incised valley accelerated with an increase in development, like the creeks in NHC.

The MARs near the bay-head shorelines of all creeks were similar for the earlier part of the records (before MLCC), but the subsequent acceleration reached higher MAR values for

creeks within coastal prism incised valleys than creeks within tributary incised valleys. That disparity was likely due, in part, to differences in the type of land cover change, a shift from forested to suburban development, and forested to cleared forest in NHC and CC, respectively. The greater relief and drainage basin size of tidal creeks within coastal prism incised valleys also likely contributed to the higher MARs for the recent part of the record; however, we could not decouple land-use change type from watershed characteristics because all tidal creeks within coastal prism incised valleys were only subjected to increased development as the largest land use change of the period.

The reach of the tidal creeks from headwater to mouth is short, only 5-15 km in length for the creeks in this study, and the proportion of the watersheds that experienced a change in land cover was high (>50%) for most of the creeks. The short length of the creeks and large percent change in land cover explains why these small watersheds are highly connected to downstream bay head shorelines and we see no correlations between connectivity and drainage basin size or relief. Whiskey Creek (Site 12) has the smallest drainage basin area and relief in NHC; however, it recorded similar trends in MAR as adjacent Hewletts Creek (Site 11), both accelerating with an increase in development of the watersheds, despite Hewletts Creek having >three times greater drainage basin area and relief.

Coastal rain events and flooding from storm surge disproportionately affect tidal creeks as compared to large river systems due to their low elevation, small relief, and position along the shoreline. Transport of sediment by sheet flow in tidal creek watersheds occurs during storms and coastal NC has entered a wetter climatic regime where storm events are bringing more extreme precipitation patterns (Torres et al., 2003; Paerl et al., 2020). The predicted increase in storm intensity and frequency in the region (Knutson et al., 2010; Zhang & Cole, 2018), should

result in further increased connectivity between tidal creek watersheds and downstream depositional environments.

The presence of structured habitats in tidal creeks and connected estuaries are a requirement for healthy and productive ecosystems. Saltmarsh and mangrove habitats rely on sedimentation to maintain position in the tidal frame with accelerating RSLR; however, sediment loading can also have negative effects on ecosystems. Harmful heavy metals can sorb onto fine-grained particles and poor water quality from sediment loading commonly results in restrictions on commercial fishing, smothering of benthic flora and fauna, and lowered primary productivity from increased light attenuation (Gambrell et al., 1994; Sanger et al., 1999; NCAC, 2007). The two tidal creeks with high-resolution sedimentation records that did not record an increase in MAR near the bay head shoreline provide guidance on possible strategies for mitigating sediment loading. Land cover change of the Ware Creek watershed impacted <11% of the area and no corresponding increase in MAR was recorded indicating that small-scale land-use changes likely affect sediment loading less than large-scale changes. Constructing retention ponds in association with large-scale tidal creek development activities, should also help mitigate excessive sediment loading to downstream coastal habitats. The developed watershed area of Howe Creek increased from 4.5% in 1959 to 70.0% in 2016, but MAR did not rapidly increase unlike the other sites in NHC. Furthermore, initial development of the Hewletts Creek watershed occurred within a Carolina Bay depression with a central retention pond, and that phase of development was not associated with an increase in MAR, unlike the subsequent development of other watershed areas (Appendix 2.3 and 2.4). Retention ponds likely interrupted sediment transport pathways to downstream areas in both Hewletts and Howe creeks and should be applied more widely in development plans for coastal communities.

Average MAR and SAR pre and post MLCC

Average MAR accelerated after a MLCC at all creek sites except for Howe and Ward creeks (sites 4 and 9) which had similar MARs pre- and post- MLCC (within error; Figure 2.7). Creek orientation relative to the predominant NE wind direction of CC likely flushes Ward creek and inhibits long term sedimentation while a higher percentage of retention ponds in the Howe creek watershed likely limits sediment delivery to the creek. Of the five creek sites within tributary incised valleys that experienced a MLCC, average MARs more than doubled at three of those sites (Oyster, Sleepy, and Gales; Sites 1,3, and 6), but of the 5 coastal prism creek sites with a MLCC, only two sites doubled (Pages and Whiskey, sites 8 and 12, respectively). While overall, MARs were lower at sites within tributary incised valleys, the acceleration of MAR post-MLCC was faster than in coastal prism incised valleys.

Sediment accumulation rates (SAR) provide an indicator of changes in bed elevation, and in coastal depocenters SAR typically match rates of relative sea-level rise over long timescales (Nichols, 1989). Half of the creek sites experienced a doubling or more in average SAR post MLC, but all sites except Howe creek (site 9) showed an acceleration in SAR post-MLCC (Figure 2.7), despite the difference in type and percent land cover change between NHC and CC creeks. This widespread increase in average SARs can be attributed to increases in sediment load and increased accommodation through RSLR. There is a gradient in average 20th century rates of RSLR along the NC coast, increasing toward the north from 2.1 ± 0.5 mm/yr at Wilmington, near the NHC creeks to 3.5 ± 0.3 mm/yr at Tump Point, near CC creek sites (Kopp et al., 2015). Most sites experienced SARs >3.5 mm yr^{-1} and up to ~8.4 mm yr^{-1} (Gales Creek, Site 6; Figure 2.7) post-MLCC, suggesting that these tidal creeks are infilling and getting shallower. Accommodation limits SAR and some sediment is likely bypassing and entering the adjacent

estuary in CC creeks and the coastal ocean in NHC, especially during storm events, which could be contributing to higher MAR and SAR seen regionally in larger estuarine depocenters (Rodriguez et al., 2020).

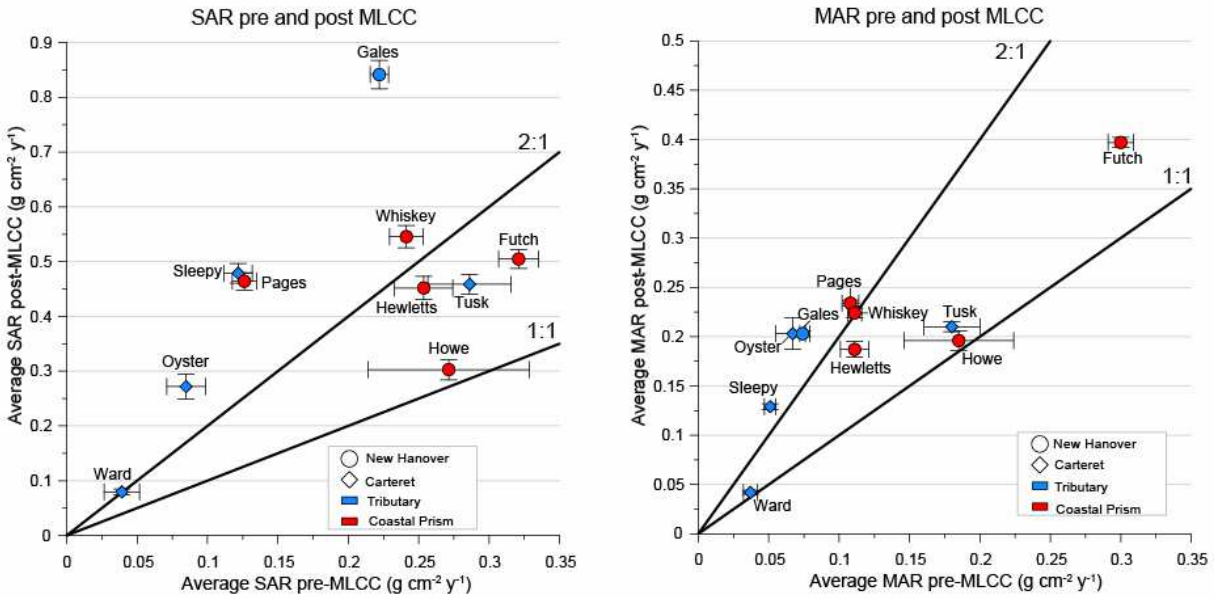

Figure 2.7 MAR and SAR pre and post MLCC. Average Pre and Post MLCC sediment accumulation rates (A) and mass accumulation rates (B) compared to a 2:1 and a 1:1 line. Error bars represent average measurement error.

Conclusion

Tidal creek watersheds are small but abundant along passive margin coasts, worldwide, and formed within tributary and coastal prism incised valleys on the lower coastal plain. Despite variations in setting, watershed area and relief, and tidal range, tidal creek watersheds are directly connected to downstream bay head shorelines. Our data set cannot be used to explicitly identify sediment sources; however, MARs measured downstream, near the bay head shoreline, accelerated at the same time large changes in land cover occurred in the watershed at eight of eleven sites. This indicates sediment transport pathways in tidal creeks are more direct and responsive to LUC than what their low relief and small watersheds would suggest. Much of the

rapid increase in population of coastal areas and associated changes in land cover over the last 50 years occurred within tidal creek watersheds, and we documented an increase in developed watershed area from <20% to >50% at four of the sites. Prior to a MLCC, the average MAR at the sites were similarly low. At the end of the 20th century, the sites within coastal prism incised valleys, where development was the largest type of land cover change, showed higher average MARs than lower relief smaller tidal creeks within tributary incised valleys, where silviculture was the largest type of land cover change. The type of LUC and/or watershed morphology influence the amount of sediment accumulating in down-stream coastal areas, and watersheds with small-scale changes in land cover or large changes in land cover with retention ponds showed little changes MAR at the tidal creek outlet. Most of the tidal creek bay head shoreline areas are accumulating sediment faster than the rate of RSLR; however, as RSLR continues to accelerate and these watersheds have little additional space to accommodate future changes in land cover, this is likely a temporary state. Tidal creeks discharge directly into the flood plain of larger river systems, estuaries, or the coastal ocean and their contribution to coastal sediment budgets is largely ignored but could partly explain the increase that occurred after 1950 at many sites across North America.

REFERENCES

Administration, N. O. a. A. (2013). National Coastal Population Report: Population Trends from 1970-2020. [Report]. *Department of Commerce*.

Appleby, P. G., & Oldfield, F. (1978). The calculation of lead-210 dates assuming a constant rate of supply of unsupported 210-Pb to the sediments. wird eine Methode zur Berechnung des Sedimentalters beschrieben , die auf 210pb. *Catena, 5*, 1-8.

Barbier, E. B., Hacker, Sally D., Kennedy, Chris, Koch, Evamaria W., Stier, Adrian C., Silliman, Brian R. (2011). The value of estuarine and coastal ecosystem services. *Ecological Monographs, 81*(2), 169-193.

Charles R. Ewen, T. R. W., R. P. Stephen Davis, Jr. . (2011). The Archaeology of North Carolina: Three Archaeological Symposia. http://www.rla.unc.edu/NCAC/Publications/NCAC30/index.html

Corbett, D. R., Walsh, J. P., & Zhao, Y. (2017). Impacts of Land-Use Change on Sedimentation in Tidal Creeks of North Carolina, USA. *Journal of Geography and Earth Sciences*. https://doi.org/10.15640/jges.v5n1a1

Dalrymple, R. W., Zaitlin, B. A., & Boyd, R. (1992). Estuarine facies models; conceptual basis and stratigraphic implications. *Journal of Sedimentary Research, 62*(6), 1130-1146. https://doi.org/10.1306/D4267A69-2B26-11D7-8648000102C1865D

Darrow, E. S., Carmichael, R. H., Calci, K. R., & Burkhardt, W. (2017). Land-use related changes to sedimentary organic matter in tidal creeks of the northern Gulf of Mexico. *Limnology and Oceanography, 62*(2), 686-705. https://doi.org/10.1002/lno.10453

Day, J. W., Christian, R. R., Boesch, D. M., Yáñez-Arancibia, A., Morris, J., Twilley, R. R., Naylor, L., Schaffner, L., & Stevenson, C. (2008). Consequences of Climate Change on the Ecogeomorphology of Coastal Wetlands. *Estuaries and Coasts, 31*(3), 477-491. https://doi.org/10.1007/s12237-008-9047-6

Day, J. W., Kemp, G. P., Reed, D. J., Cahoon, D. R., Boumans, R. M., Suhayda, J. M., & Gambrell, R. (2011). Vegetation death and rapid loss of surface elevation in two contrasting Mississippi delta salt marshes: The role of sedimentation, autocompaction and sea-level rise. *Ecological Engineering, 37*(2), 229-240. https://doi.org/10.1016/j.ecoleng.2010.11.021

de Vleeschouwer, F., Sikorski, J., & Fagel, N. (2010). Development of Lead-210 Measurement in Peat Using Polonium Extraction. A Procedural Comparison. *Geochr, 36*(-1), 1-8. https://doi.org/10.2478/v10003-010-0013-5

Edward B. Barbier, E. W. K., Brian R. Silliman, Sally D. Hacker, Eric Wolanski, Jurgenne Primavera, Elise F. Granek, Stephen Polasky, Shankar Aswani, Lori A. Cramer, David

M. Stoms, Chris J. Kennedy, David Bael, Carrie V. Kappel, Gerardo M. E. Perillo, Denise J. Reed. (2008). Coastal Ecosystem–Based Management with Nonlinear Ecological Functions and Values. *Science, 319*.

El-Daoushy, F., Olsson, K., Garcia-Tenorio, R. . (1991). Accuracies in PO-210 determination for lead-210 dating. *Hydrobiologia 214*, 43-52.

McLeod, E. (2006). Managing Mangroves for Resilience to Climate Change. *IUCN, The Nature Conservancy,* Gland, Switzerland. 64pp.

Ensign, S., Currin, C., Piehler, M., & Tobias, C. (2017). A method for using shoreline morphology to predict suspended sediment concentration in tidal creeks. *Geomorphology, 276*, 280-288. https://doi.org/10.1016/j.geomorph.2016.09.036

Fagherazzi, S., Kirwan, M. L., Mudd, S. M., Guntenspergen, G. R., Temmerman, S., Alpaos, A. D., Koppel, J. V. D., Rybczyk, J. M., Reyes, E., Craft, C., Clough, J. (2012). Numerical models of salt marsh evolution: ecological, geomorphic, and climatic factors. *Reviews of Geophysics (50)*, 1-28. https://doi.org/10.1029/2011RG000359.

Foley, J. A., Defries, R., Asner, G. P., Barford, C., Bonan, G., Carpenter, S. R., Chapin, F. S., Coe, M. T., Daily, G. C., Gibbs, H. K., Helkowski, J. H., Holloway, T., Howard, E. A., Kucharik, C. J., Monfreda, C., Patz, J. A., Prentice, I. C., Ramankutty, N., & Snyder, P. K. (2005). R EVIEW Global Consequences of Land Use. *8*(July), 570-574. https://doi.org/10.1126/science.1111772

Gambrell, R. P. (1994). Trace and Toxic Metals in Wetlands-A Review. *Journal of Environmental Quality, 23*, 883-891.

Gedan, K. B., Silliman, B. R., & Bertness, M. D. (2009). Centuries of human-driven change in salt marsh ecosystems. *Ann Rev Mar Sci, 1*, 117-141. https://doi.org/10.1146/annurev.marine.010908.163930

Grabowski, J. H., Brumbaugh, R. D., Conrad, R. F., Keeler, A. G., Opaluch, J. J., Peterson, C. H., Piehler, M. F., Powers, S. P., & Smyth, A. R. (2012). Economic Valuation of Ecosystem Services Provided by Oyster Reefs. *BioScience, 62*(10), 900-909. https://doi.org/10.1525/bio.2012.62.10.10

Gunnell, J. R., Rodriguez, A. B., & McKee, B. A. (2013). How a marsh is built from the bottom up. https://doi.org/10.1130/G34582.1

Hupp, C. R., Schenk, E. R., Richter, J. M., Peet, R. K., & Townsend, P. A. (2009). Bank erosion along the dam-regulated lower Roanoke River, North Carolina. In *Management and Restoration of Fluvial Systems with Broad Historical Changes and Human Impacts*. https://doi.org/10.1130/2009.2451(06)

James, L. A., & Lecce, S. A. (2013). 9.37 Impacts of Land-Use and Land-Cover Change on

River Systems. In *Treatise on Geomorphology* (pp. 768-793). https://doi.org/10.1016/b978-0-12-374739-6.00264-5

James P. M. Syvitski, J. D. M. (2007). Geology, Geography, and Humans Battle for Dominance over the Delivery of FluvialSediment to the Coastal Ocean. *The Journal of Geology, 115*(1), 1-19. https://doi.org/https://doi.org/10.1086/509246

Jervey, M. T., Wilgus, C. K., Hastings, B. S., Posamentier, H., Wagoner, J. V., Ross, C. A., & Kendall, C. G. S. C. (1988). Quantitative Geological Modeling of Siliciclastic Rock Sequences and Their Seismic Expression. In *Sea-Level Changes: An Integrated Approach* (Vol. 42, pp. 0). SEPM Society for Sedimentary Geology. https://doi.org/10.2110/pec.88.01.0047

Milliman, J.D., Milliman, J.P.M.S. (1992). Geomorphic/Tectonic Control of Sediment Discharge to the Ocean: The Importance of Small Mountainous Rivers. *The Journal of Geology, 100*(5), 525-544. https://www.jstor.org/stable/30068527

Phillips, J.D. (2006). Sediment storage, sea level, and sediment delivery to the ocean by coastal plain rivers. *Progress in Physical Geography, 30*(4), 613-540. https://doi.org/10.1191/0309133306pp494ra

Jones, M. C., Bernhardt, C. E., Krauss, K. W., & Noe, G. B. (2017). The Impact of Late Holocene Land Use Change, Climate Variability, and Sea Level Rise on Carbon Storage in Tidal Freshwater Wetlands on the Southeastern United States Coastal Plain. *Journal of Geophysical Research: Biogeosciences, 122*(12), 3126-3141. https://doi.org/10.1002/2017jg004015

Bromber, K.D. (2005). Reconstructing Historical Maps New England Salt Marsh Losses Using. *Estuaries, 28*(6), 823-832.

Kirwan, M. L., Guntenspergen, G. R., D'Alpaos, A., Morris, J. T., Mudd, S. M., & Temmerman, S. (2010). Limits on the adaptability of coastal marshes to rising sea level. *Geophysical Research Letters, 37*(23), 1-5. https://doi.org/10.1029/2010GL045489

Kirwan, M. L., Murray, A. B., Donnelly, J. P., & Corbett, D. R. (2011). Rapid wetland expansion during European settlement and its implication for marsh survival under modern sediment delivery rates. *Geology, 39*(5), 507-510. https://doi.org/10.1130/g31789.1

Lightbody, A. F., Kui, L., Stella, J. C., Skorko, K. W., Bywater-Reyes, S., & Wilcox, A. C. (2019). Riparian Vegetation and Sediment Supply Regulate the Morphodynamic Response of an Experimental Stream to Floods. *Frontiers in Environmental Science, 7*. https://doi.org/10.3389/fenvs.2019.00040

Mallin, M. A., & Lewitus, A. J. (2004). The importance of tidal creek ecosystems. *Journal of Experimental Marine Biology and Ecology, 298*(2), 145-149. https://doi.org/10.1016/S0022-0981(03)00356-3

Mallinson, D., Culver, S., Leorri, E., Mitra, S., Mulligan, R., & Riggs, S. (2018). Barrier Island and Estuary Co-evolution in Response to Holocene Climate and Sea-Level Change: Pamlico Sound and the Outer Banks Barrier Islands, North Carolina, USA. In *Barrier Dynamics and Response to Changing Climate* (pp. 91-120). https://doi.org/10.1007/978-3-319-68086-6_3

Martin Vermeera, S. R. (2009). Global sea level linked to global temperature. *PNAS, 106*(51), 21527–21532.

Mattheus, C. R., & Rodriguez, A. B. (2014). Controls On Lower-Coastal-Plain Valley Morphology and Fill Architecture. *Journal of Sedimentary Research, 84*(4), 314-325. https://doi.org/10.2110/jsr.2014.30

Mattheus, C. R., Rodriguez, A. B., & McKee, B. A. (2009). Direct connectivity between upstream and downstream promotes rapid response of lower coastal-plain rivers to land-use change. *Geophysical Research Letters, 36*(20). https://doi.org/10.1029/2009gl039995

Mattheus, C. R., Rodriguez, A. B., McKee, B. A., & Currin, C. A. (2010). Impact of land-use change and hard structures on the evolution of fringing marsh shorelines. *Estuarine, Coastal and Shelf Science, 88*(3), 365-376. https://doi.org/10.1016/j.ecss.2010.04.016

Matthews, K. M., Kim, C.-k., & Martin, P. (2007). Determination of Po in environmental materials : A review of analytical methodology. *65*, 267-279. https://doi.org/10.1016/j.apradiso.2006.09.005

McCarney-Castle, K., Voulgaris, G., & Kettner, A. J. (2010). Analysis of Fluvial Suspended Sediment Load Contribution through Anthropocene History to the South Atlantic Bight Coastal Zone, U.S.A. *The Journal of Geology, 118*(4), 399-416. https://doi.org/10.1086/652658

Miller, C. B., Rodriguez, A. B., & Bost, M. C. (2021). Sea-level rise, localized subsidence, and increased storminess promote saltmarsh transgression across low-gradient upland areas. *Quaternary Science Reviews, 265*. https://doi.org/10.1016/j.quascirev.2021.107000

Miller, M. L. (1993). The rise of coastal and marine tourism. *Ocean & Coastal Management, 20*(3), 181-199. https://doi.org/10.1016/0964-5691(93)90066-8

Möller, I., Kudella, M., Rupprecht, F., Spencer, T., Paul, M., van Wesenbeeck, B. K., Wolters, G., Jensen, K., Bouma, T. J., Miranda-Lange, M., & Schimmels, S. (2014). Wave attenuation over coastal salt marshes under storm surge conditions. *Nature Geoscience, 7*(10), 727-731. https://doi.org/10.1038/ngeo2251

New Hanover County, 2015, Open Geospatial Data Portal: Watersheds, http://geo.nhcgov.com/gis/rest/services/Layers/Watersheds/MapServer/0, accessed June 2016.

NOAA (National Oceanic and Atmospheric Administration) National Ocean Service, 2013,

National Coastal Population Report, 20p. Available at: http://oceanservice.noaa.gov/facts/coastal-population-report.pdf.

NOAA OCM (National Oceanic and Atmospheric Administration, Office for Coastal Management), 2016, Coastal Change Analysis Program (C-CAP) Regional Land Cover, www.coast.noaa.gov/ccapftp: accessed December 2017.

NOAA OCM (National Oceanic and Atmospheric Administration, Office for Coastal Management), 2014, North Carolina Floodplain Mapping Program, https://coast.noaa.gov/dataviewer/#/lidar/search/where:ID=4954: accessed December 2017.

Nichols, M. A. (1989). Sediment Accumulation Rates and Relative Sea-Level Rise in Lagoons. *Marine Geology, 88*, 209-219.

Nienhuis, J. H., Ashton, A. D., Edmonds, D. A., Hoitink, A. J. F., Kettner, A. J., Rowland, J. C., & Tornqvist, T. E. (2020, Jan). Global-scale human impact on delta morphology has led to net land area gain. *Nature, 577*(7791), 514-518. https://doi.org/10.1038/s41586-019-1905-9

Ralston, D. K., Yellen, B., Woodruff, J. D., & Fernald, S. (2020). Turbidity Hysteresis in an Estuary and Tidal River Following an Extreme Discharge Event. *Geophysical Research Letters, 47*(15). https://doi.org/10.1029/2020gl088005

Renfro, A. A., Cochran, J. K., Hirschberg, D. J., Bokuniewicz, H. J., & Goodbred, S. L. (2016). The sediment budget of an urban coastal lagoon (Jamaica Bay, NY) determined using ^{234}Th and ^{210}Pb. *Estuarine, Coastal and Shelf Science, 180*, 136-149. https://doi.org/10.1016/j.ecss.2016.06.008

Renfro, G.W. (1975). Use of erosion equations and sediment-delivery ratios for predicting sediment yield. *U.S. Department of Agriculture, S-40*, 33-45.

Rodriguez, A. B., McKee, B. A., Miller, C. B., Bost, M. C., & Atencio, A. N. (2020, Jun 26). Coastal sedimentation across North America doubled in the 20(th) century despite river dams. *Nat Commun, 11*(1), 3249. https://doi.org/10.1038/s41467-020-16994-z

Victor, S. Wolanski, E., Richmond, R.H. (2004). Fine sediment trapping in two mangrove-fringed estuaries exposed to contrasting land-use intensity, Palau, Micronesia. *Wetlands Ecology and Management, 12*, 277–283.

Sanchez-Cabeza, J. A., & Ruiz-Fernández, A. C. (2012). 210Pb sediment radiochronology: An integrated formulation and classification of dating models. *Geochimica et Cosmochimica Acta, 82*, 183-200. https://doi.org/10.1016/j.gca.2010.12.024

Sanger, D. M., Holland, A.F., Scott, G.I. . (1999). Tidal Creek and Salt Marsh Sediments in

South Carolina Coastal Estuaries: I. Distribution ofTrace Metals. *Archives of Environmental Contamination and Toxicology, 37*, 445-457.

Schumm, S. A. (1993). Managing Mangroves for Resilience to Climate Change. *The Journal of Geology, 101*(2), 279-294. https://www.jstor.org/stable/30081152

Schumm, S. A., & Etheridge, F. G. (1994). Origin, Evolution and Morphology of Fluvial Valleys. *Incised Valley Systems: Origin and Sedimentary Sequenses, 51*, 11-27.

Fagherazzi, S. D'Alpaos, L., Defina, A. (2006). Critical Bifurcation of Shallow Microtidal Landforms in Tidal Flats and Salt Marshes. *PNAS, 102*(33), 8337-8341.

Syvitski, J. P. M. (1978). Sediment fluxes and rates of sedimentation. In *Sedimentology* (pp. 980-992). Springer Berlin Heidelberg. https://doi.org/10.1007/3-540-31079-7_180

Temmerman, S., Meire, P., Bouma, T. J., Herman, P. M., Ysebaert, T., & De Vriend, H. J. (2013, Dec 5). Ecosystem-based coastal defence in the face of global change. *Nature, 504*(7478), 79-83. https://doi.org/10.1038/nature12859

Torres, R., Mwamba, M.J., Goni, M.A. (2003) Properties of intertidal marsh sediment mobilized by rainfall. *Limnology and Oceanography, 48* (3), 1245-1253.

Ward, R. D., Friess, D. A., Day, R. H., & Mackenzie, R. A. (2016). Impacts of climate change on mangrove ecosystems: a region by region overview. *Ecosystem Health and Sustainability, 2*(4). https://doi.org/10.1002/ehs2.1211

Watson, E. B., Wigand, C., Davey, E. W., Andrews, H. M., Bishop, J., & Raposa, K. B. (2017, May 1). Wetland loss patterns and inundation-productivity relationships prognosticate widespread salt for southern New England. *Estuaries Coast, 40*(3), 662-681. https://doi.org/10.1007/s12237-016-0069-1

Wells, J. T., Kim, S. (1989). Sedimentation in the Albemarle-Pamlico lagoonal system: synthesis and hypothesis. *Marine Geology, 88*, 263-284.

Weston, N. B. (2014). Declining Sediments and Rising Seas: an Unfortunate Convergence for Tidal Wetlands. *Estuaries and Coasts, 37*(1), 1-23. https://doi.org/10.1007/s12237-013-9654-8

Yeager, K. M., Santschi, P. H., Schindler, K. J., Andres, M. J., & Weaver, E. A. (2006). The relative importance of terrestrial versus marine sediment sources to the Nueces-Corpus Christi Estuary, Texas: An isotopic approach. *Estuaries and Coasts, 29*(3), 443-454. https://doi.org/10.1007/BF02784992

CHAPTER 3 RESPONSE OF FRINGING SALT MARSH ACCRETION TO LAND-USE CHANGE OF TIDAL CREEK WATERSHEDS

Introduction

The salt marsh depositional environment must accrete vertically over decadal to centennial time scales at rates equal to, or greater than, sea-level rise to persist. This accretion makes them resilient ecosystems and valuable recorders of environmental changes, such as sea level (de Plassche et al. 1998, Engelhart et al. 2011, Kemp et al., 2017) and storms (Donnelly et al., 2001, Boldt et al., 2010, de Groot et al., 2011). Salt marsh area has declined over the last century, globally, along with the valuable ecosystem services they provide, motivating restoration, conservation, and management efforts (Lotze et al., 2006; Duarte et al., 2005; Airoldi and Beck, 2008; Gedan et al., 2009). Salt marsh ecosystem services and the success of restoration projects hinge on vertical accretion and maintaining aerial extent (Peterson and Turner 1994; Sousa et al., 2010; Mcleod et al., 2011; Theuerkauf et al., 2015, Barbier et al., 2008; Moller et al., 2014; Neumeier and Ciavoloa, 2004; Howes et al., 2010).

Salt marsh is an important blue carbon habitat and carbon burial is closely tied with accretion (McTigue et al., 2019). Vertical accretion of salt marsh sediments allows for the continual draw down of CO_2 from the atmosphere and below-ground storage of carbon for decades to millennia. Salt marshes can accrete through various ecogeomorphic feedbacks. With increased inundation through relative sea-level rise (RSLR), the marsh is supplied with more allogenic inorganic sediments (if supply to the estuary is constant) which in turn enhances belowground biomass and production (Pethick 1981; Kirwan & Guntenspergen, 2012). These processes support vertical accretion, carbon accumulation, and often a net gain in marsh platform

elevation (Morris et al., 2002; Drexler., 2011). The culmination of vertical accretion and the increasing volume of stored carbon is measured as carbon accumulation rates (CAR; g C m^{-2} y^{-1}) which are tied closely with mass accumulation rates (MAR g m^{-2} y^{-1}) and known to be impacted by land-use change (LUC).

The installation of dams and reservoirs caused a ubiquitous decline in suspended sediment loads reaching the coastal plain (Walling and Fang, 2003; Meade & Moody, 2010; Syvitski & Kettner, 2011; Jalowska et al., 2015). Sediment loads have been reduced up to ~50% in the Mississippi River system alone which has resulted in 25% loss of deltaic wetlands (Blum and Roberts, 2009). In contrast, LUC has been shown to increase sediment load and enhance marsh expansion locally. Salt marsh area expanded in Plum Island, MA following deforestation associated with European settlement in the 18^{th} and 19^{th} centuries (Kirwan et al., 2011). Many coastal plain river systems are not dammed and, in the Newport River, NC, there was rapid lateral marsh expansion following intensified upstream silviculture operations in the 1960s (Mattheus et al., 2009). In addition, anthropogenic backwater areas within the Hudson River basin were colonized with marsh within 18 years of widespread urban development (Yellen et al., 2020). These gains in salt marsh area increased the services provided and enhanced the drawdown of CO_2.

Rodriguez et al. (2020) reported a doubling in sedimentation rates in 25 North American coastal depocenters since 1950, driven predominantly by population growth in coastal counties and associated LUC, but adjacent marshes at some sites were found to be degrading and accreting at rates below RSLR, despite the acceleration of sedimentation rates on the bay bottom (Hartig et a., 2002; Lagomasino et al., 2013; Kearney and Turner 2016; Raposa et al., 2017; Peteet et al., 2018; Gunderson et al., 2021). The contrast between accelerating sedimentation

rates in coastal depocenters and the degradation of adjacent fringing salt marshes suggests salt marshes are buffered from LUC and the associated increase in sediment loads. Considering the same water that supplies subtidal areas with sediment inundates adjacent salt marshes, alternatively, salt marshes could have responded to LUC by increasing accretion rates, like subtidal areas, but are still degrading because accretion is <RSLR. To address this, we investigated fringing salt marsh accretion rates in 12 tidal creeks in North Carolina that have undergone localized LUC and show a commensurate increase in accretion rates of the subtidal creek bed.

Methods

Site Selection

The North Carolina coast (NC, USA) hosts many tidal creeks with a long history of anthropogenic modifications to coastal watersheds. Our study includes six tidal creek fringing salt marshes within Carteret County (CC; lower tidal range, 0.321–0.943 m) and six within New Hanover County (NHC; higher tidal range, 1.191–1.248 m; Figure 3.1, Table 3.1). RSLR is higher in CC than in NHC (3.79 mm y^{-1} and 2.65 mm y^{-1}, respectively; NOAA Station IDs 8656483, 8658120; Figure 3.1). Tidal creeks, are small channel networks (<50 km^2) that drain lower-coastal plain watersheds, are tidal along their entire length, and discharge into larger estuaries, lagoons, or back-barrier sounds. The main stems of these creeks are characterized by fringing salt marsh complexes and all sampled marsh sites were characteristic low marsh, dominated by *Spartina alterniflora.*

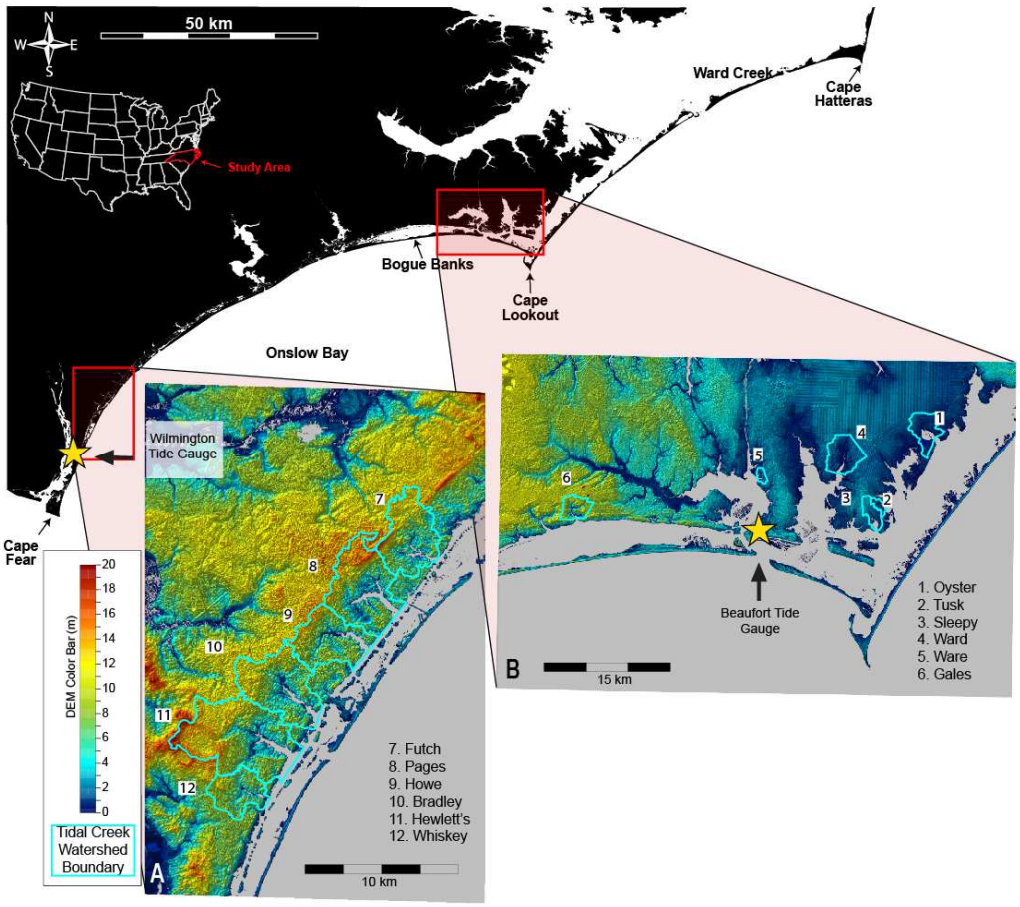

Figure 3.1 Study area map. New Hanover Creek DEM (A) and Carteret County creek DEMs (B) including creek watershed boundaries and ID numbers. (Wilmington NOAA Station ID: 8658120; Beaufort NOAA Station ID: 8656483).

Tidal creeks form as the landscape floods during sea-level rise and can be categorized into two morphological distinctions based on the type of incised valley they occupy: coastal prism and tributary incised valleys (Mattheus & Rodriguz, 2014). Coastal prism incised valleys formed as sea level fell after the last interglacial period and exposed the break in slope between the low-gradient coastal plain and the steeper shoreface of the previous highstand shoreline termed Suffolk Scarp in eastern NC. Tributary incised valleys formed as larger rivers incised trunk valleys and created a break in slope between the flat area seaward of the Suffolk Scarp (the exposed Pleistocene continental shelf) and the steep valley flank along the edge of the incised valleys. Marsh sites 1-5 in CC are within tributary incised valleys with low-relief watersheds

(2.30 –3.73 m) and marsh sites 6-12 (Gales, Site 6, in CC and sites 7-12 in NHC; Figure 3.1) are within coastal prism incised valleys with high relief watersheds (8.74–15.08 m; Table 2.2).

Land cover of the 12 tidal creek watersheds that discharge near the fringing marsh sites was classified from 1959 – 2016. From 1959 – 1993, land cover was digitized from georeferenced aerial imagery from the United States Geological Survey (USGS) Aerial Photo Single Frames records collection and National High-Altitude Photography (NHAP) program. Land-cover from 1996-2016 was obtained from the Coastal Change Analysis Program (CCAP: NOAA, 2020) and reclassified to match the same categories as the earlier time-steps. Land cover of each watershed was classified as forest, cleared forest, agriculture, developed, or water/intertidal every decade between the 1959 – 2016 study period (Table 2.1) and changes between cleared forest and forest classifications were largely associated with silviculture operations. We assumed for each creek watershed that the land cover classification with the highest % contribution to the total change in land cover over the 50-year period (major land-cover change; MLCC) would be the main driver of increased sediment supply to the salt marsh. Watershed changes with the highest % contribution to the total change in CC were dominated by shifts in % cleared forest, forest, and agriculture while watersheds in NHC were dominated by increases in % suburban development (Figure 3.2). Bost et al. (in review) showed mass accumulation rates measured from subtidal creek bed sites located within 100 m of the salt marsh sites examined here, generally increased with major changes to those same land cover types. We defined the time boundary between pre- and post-MLCC as the midpoint between the dates of two land cover classification maps where a >15% gain occurred within the (Table 2.1).

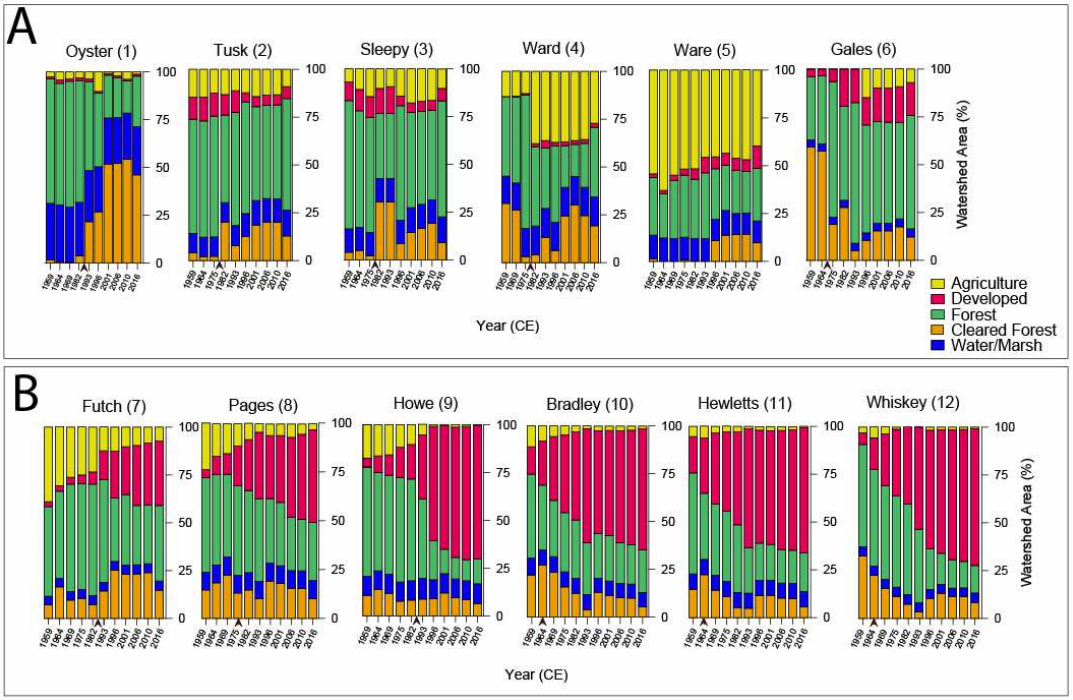

Figure 3.2 Land cover through time. Proportion of land cover every decade from 1959-2016. (A) CC creek watersheds, (B) NHC creek watersheds. Arrows indicate date divisor of >15% decadal change.

Inundation

Marsh elevation relative to the tidal frame plays a role in inundation duration, which impacts the amount of sediment that can be deposited on the platform. Storm surge elevation and frequency is an additional factor that defines the duration a salt marsh is inundated; however, over decadal to centennial time scales this is difficult to quantify. We calculated the fractional inundation time ($1 \geq \vartheta \geq 0$) for the marsh sites and used that as a proxy for inundation time using the elevation of the marsh (z) relative to mean high (MHW) and mean low water (MLW) measured in m relative to NAVD88 after Morris et al. (2021).

$$\vartheta \approx \frac{MHW - Z}{MHW - MLW} \quad (1)$$

The MHW and MLW were determined at each site using the NOAA Online Vertical Datum Transformation tool (US Department of Commerce, 2022; Table 3.1).

Creek Name	Creek Type	Elevation (m; NAVD88)	Mean Sea Level (m; NAVD88)	Tidal range (m)*	Inundation ϑ
1. Oyster	Tributary	0.19	-0.08	0.32	-0.34
2. Tusk	Tributary	0.17	-0.09	0.36	-0.21
3. Sleepy	Tributary	0.12	-0.09	0.42	0.00
4. Ward	Tributary	0.44	-0.01	0.54	-0.51
5. Ware	Tributary	0.16	-0.11	0.94	0.21
6. Gales	Coastal Prism	0.05	-0.07	0.52	0.24
7. Futch	Coastal Prism	0.23	-0.11	1.22	0.23
8. Pages	Coastal Prism	-0.23	-0.11	1.20	0.60
9. Howe	Coastal Prism	0.23	-0.12	1.19	0.21
10. Bradley	Coastal Prism	0.11	-0.12	1.24	0.32
11. Hewletts	Coastal Prism	0.17	-0.12	1.24	0.27
12. Whiskey	Coastal Prism	0.21	-0.12	1.25	0.24

* Astronomical tidal range obtained from V-Datum

Table 3.1 Salt marsh elevation information at the core locations.

Field sampling and radiometric dating

At each fringing salt marsh site, we collected a push core (~1 m long) approximately 10 m from the estuarine shoreline with the aid of a sledgehammer. Elevation was taken using a RTK Trimble GPS at each coring location. Stem densities within randomly selected plots were measured in proximity to the core location by counting all live stems within a 0.25 m^2 quadrat at 9 locations. Cores were transported back to the laboratory in a vertical position, extruded into 1-cm intervals (~10 cm^3) and frozen. Samples were then weighed, freeze-dried, and weighed again for porosity. Dry bulk density was calculated assuming quartz composition. Disaggregated subsamples were used to measure percent organic matter by loss on ignition (LOI; Heiri et al., 2001). LOI was converted to percent organic carbon based on the relationship from Craft (1991) which was derived from NC salt marshes. The remaining sample portions were then sorted through a 63-micrometer sieve for radioisotope analysis of the fine-grained fraction.

The fine-grained fraction (<63 microns) was used for isotope-dilution alpha spectrometry to quantify ^{210}Pb via the granddaughter isotope, ^{210}Po, which is assumed to be in secular equilibrium with ^{210}Pb (Flynn, 1968; El-Daoushy et al., 1991; Matthews et al., 2007; de Vleeschouwer et al., 2010). Raw ^{210}Pb data and dry bulk density, both of which are needed for geochronology modelling are presented in Appendix 3.2. Depth integrated ^{210}Pb inventories were calculated for each sediment core and used to derive mass and sediment accumulation rates (MAR and SAR, respectively) with the Constant Flux (CF) model (Sanchez-Cabeza & Ruiz-Fernandez, 2012; Arias-Ortiz et al., 2018). This model provides ages and accumulation rates for discrete intervals within the core. Carbon accumulation rates (CAR) for each interval were calculated by multiplying the CF-derived MARs by the C-fraction derived from the Craft (1991) equation. We assessed differences between means using a two-sample t-test assuming unequal variances. All reported values include the mean ± standard error followed by the p-value unless they are derived from a regression analysis in which case an R^2 and p-value were reported.

Results

Astronomical Inundation

The elevation of the marsh platforms across the study sites is a contributing factor to inundation time. The elevations of the salt marshes were similar with an average of 0.16 ± 0.06 (1 SD), excluding two outlier sites; Ward Creek (Site 4) with an elevation of 44 cm NAVD88

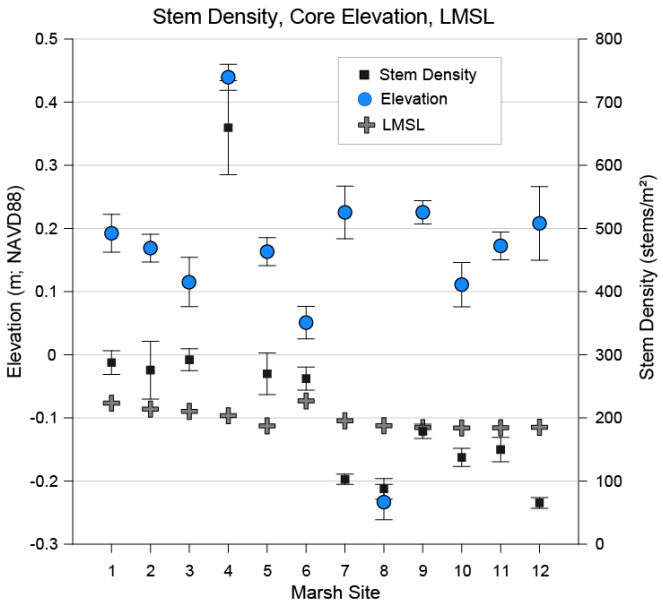

Figure 3.3 Stem density, marsh elevation, and local mean sea level (LMSL). Stem density (black squares) and marsh elevation (blue circle) at coring site. Stem density values are average ± standard error of the 9 sampling points at each marsh site. LMSL (gray crosses) at each marsh sites from V-Datum.

and Pages Creek (Site 8) with an elevation of -23 cm NAVD88 (Figure 3.3). Pages Creek (Site 9) was the only site where the elevation of the marsh was below local mean sea level (LMSL).

Allogenic sedimentation occurs when the marsh is under water and inundation time at the sites from astronomical tides ranged between -51 to 60% (Table 3.1). Oyster, Tusk, and Ward creeks were the only sites with negative inundation values, which are due to the marsh elevation being above MHW (see equation 1). Negative inundation values do not indicate the marsh is always subaerially exposed and all sites are characterized by low marsh flora that require submergence to persist. The inundation fraction for marsh sites located east of Beaufort Inlet (Sites 1-4) were lower than the other marsh sites (-26.2 ± 10.7 and 28.9 ± 0.06 %, respectively; P=0.009). In addition to small astronomical tides, inundation at Oyster, Tusk, Sleepy, and Ward creeks is also influenced by wind tides in Pamlico Sound generated during the prevailing NE and SW wind directions (Giese et al., 1985; Luettich et al., 2002; Reed et al., 2008). The other eight marsh sites experience a range of astronomical inundation from 21% at Ware to >60% at Pages marsh (sites 5 and 8, respectively).

Accumulation Rates (MAR and CAR)

Most marsh sediment records in this study showed an increasing trend in MARs since 1900 with much of that increase occurring in the latter half of the study period (Sites 1–4, 6, 8, and 10; Figure 3.4). Average long term (1900–2016) MAR was higher at marsh sites within tributary incised valleys than sites within coastal prism incised valleys (0.12 ± 0.02 g cm^{-2} y^{-1} and 0.07 ± 0.01, respectively; P= 0.0238). The difference is mainly driven by the MARs within tributary incised valleys being more variable and reaching higher maximum values at marsh sites (minimum 0.03 g cm^{-2} y^{-1} between 1922-1935 at Ward– 0.26 g cm^{-2} y^{-1} in 2007 at Sleepy) than marshes within coastal prism incised valleys (minimum of 0.02 g cm^{-2} y^{-1} from 1902-1928 at Gales– 0.17 in 2016 at Bradley Creek; Figure 3.4).

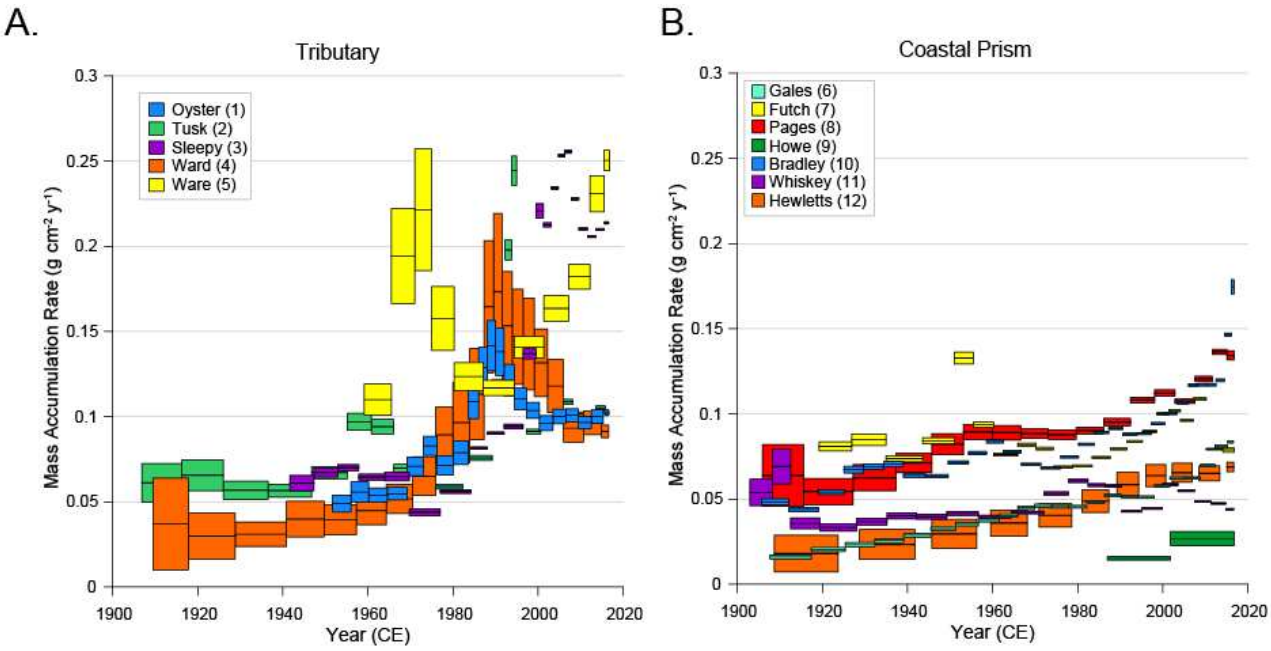

Figure 3.4 MAR since 1900 for (A) marsh sites within tributary incised valleys (B) marsh sites within coastal prism incised valleys.

Stem densities play an important role in promoting sedimentation (Leonard & Luther, 1995). The average stem densities of marsh sites in CC, where MLCC was agriculture, forest, and cleared forest, the marshes mainly occupy tributary incised valleys (excluding Gales), and

the average tidal range is <1 m were higher than marsh sites in NHC where the MLCC was development, the marshes occupy coastal prism incised valleys, and the average tidal range is > 1m (341.1 ± 63.8 stems/m^2 and 120.2 ± 17.3 stems/m^2, respectively; P=0.008; Table 3.1, Figure 3.3).

The MARs at 4 of the 5 sites within tributary incised valleys increased to a maximum during the 1990s and then decreased towards 2016 or stabilized at some value less than the maximum before 2016 (Oyster, Tusk, Sleepy, Ward; Sites 1-4). The marsh site at Ware creek (Site 5) showed a peak in MAR early in the record (~1970), followed by a decrease to pre-peak values (~1990), with an increase to a maximum MAR in 2016. The marshes within coastal prism incised valleys did not record periods of increasing and decreasing MARs (Sites 6-12). The MARs at Gales, Pages, Bradley, and Hewletts marshes (sites 6, 8,10, and 11) steadily increased in MAR from 1900–2016, while Futch and Whiskey marshes (Sites 7 and 12) showed minor variability in MAR defined by < 3 data points, with rates being largely constant throughout the record. The ^{210}Pb profile from Howe Creek marsh (Site 9) reached supported levels at 3 cm depth, likely indicating an erosional setting, and is excluded from further analyses (Appendix 3.2).

Average LOI among all sites varied from 4.14 ± 0.47 % at Ware (Site 5) – 43.78 ± 1.16% at Gales (Site 6) and was not different between marsh sites within coastal prism and tributary incised valleys (20.2 ± 5.0 % and 18.7 ± 4.7%, respectively; P= 0.832, Figure 3.5) nor county and the associated MLCC they represent (22.9 ± 5.7 % in CC and 16.3 ± 3.7 % in NHC; P=0.26; Figure 3.5).

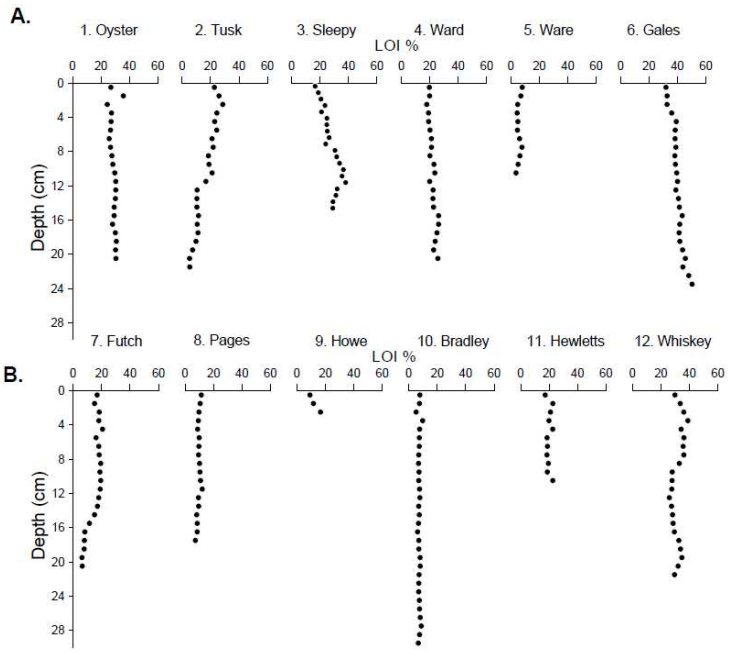

Figure 3.5 Marsh LOI %. LOI % for (A) CC sites and (B) NHC sites.

Although LOI was not significantly different between the salt marsh settings or counties, there were differences in carbon accumulation rates (CAR). Long term average CAR (1900-2016) was higher at marsh sites within tributary incised valleys than sites within coastal prism incised valleys (103.1 ± 21.5 g C m^{-2} y^{-1} and 53.8 ± 9.2 g C m^{-2} y^{-1}, P= 0.044) and in CC than in NHC (100.2 ± 17.8 g C m^{-2} y^{-1} and 47.3 ± 8.1 g C m^{-2} y^{-1}, respectively; P= 0.030). The difference being Gales Creek marsh, the only site in CC within a coastal prism incised valley.

Long term MAR (1900–2016) showed a strong positive correlation with astronomical inundation fraction (ϑ) for marsh sites within tributary incised valleys (R^2= 0.91, P=0.012); however, there was no relationship between MAR and ϑ for sites within coastal prism incised valleys (R^2= 0.36, P=0.206; Figure 3.7). Post-MLCC, average CAR was negatively correlated with astronomical inundation (R^2= 0.42; P=0.042; Figure 3.6).

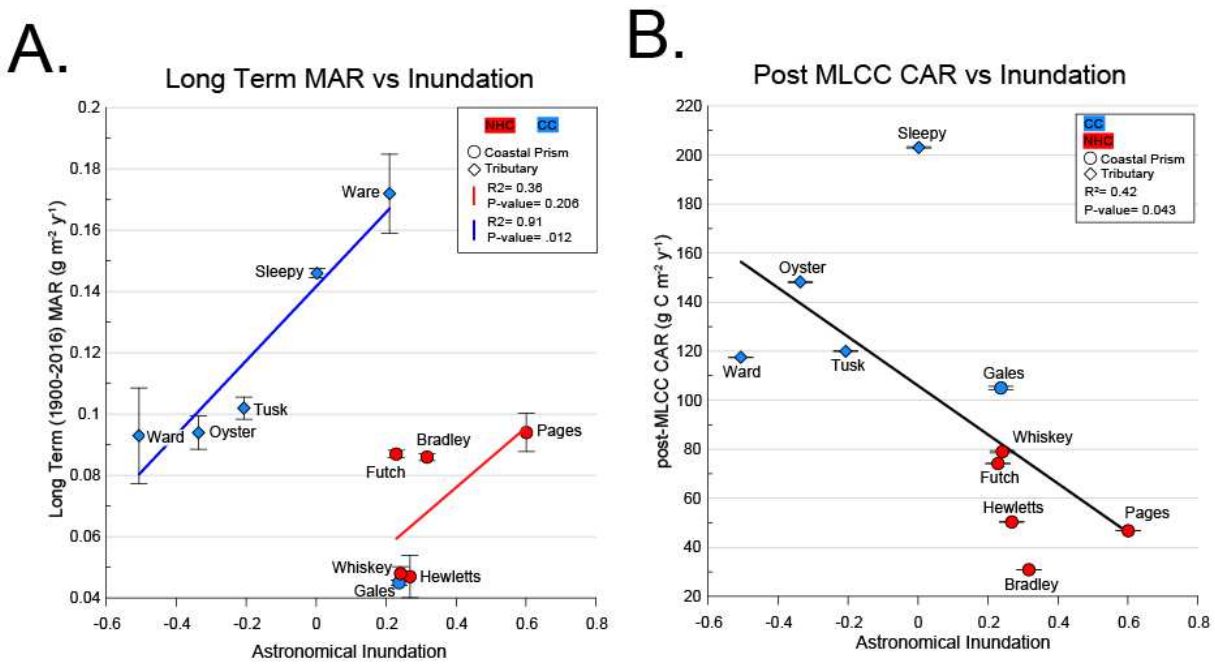

Figure 3.6 Inundation and accumulation. (A) Astronomical inundation fraction (ϑ) and average MAR (g cm^{-2} y^{-1}) from 1900-2016. (B) Average CAR (g C m^{-2} y^{-1}) post-MLCC and astronomical inundation fraction (ϑ) for all marsh sites.

Accumulation rates after land-use change

Before the MLCC occurred in any of the creek watersheds, average MARs were similar between marsh sites within tributary incised valleys and those within coastal prism incised valleys (0.064 ± 0.006 g cm^{-2} y^{-1} and 0.054 ± 0.011 g m^{-2} y^{-1}, respectively; P=0.418; Figure 3.6). After the MLCC, average MARs were higher at marsh sites within tributary incised valleys than those in coastal prism incised valleys (0.135 ± 0.015 and 0.074 ± 0.011 g cm^{-2} y^{-1}, respectively; P= 0.022A). Within each creek watershed, after the MLCC occurred, MAR was significantly higher at all sites except for Futch and Whiskey (Sites 7 and 12, respectively; Figure 3.6), both of which are within NHC coastal prism incised valleys. The difference between the top quartile for pre-MLCC and the bottom quartile for post-MLCC was larger for sites within tributary incised

valleys suggesting that the magnitude of the increase in MAR post-MLCC was higher at marsh sites within tributary incised valleys than sites within coastal prism incised valleys.

Before the MLCC, CARs were similar between marsh sites within tributary incised valleys and those within coastal prism incised valleys (67.77 ± 16.95 and 40.59 ± 8.38 g C m^{-2} y^{-1}, respectively; P=0.224; Figure 3.6). After watershed MLCC, average CARs were higher at marsh sites within tributary incised valleys than those within coastal prism incised valleys (147.22 ± 19.89 and 64.33 ± 10.94 g C m^{-2} y^{-1}, respectively; P=0.015; Figure 3.6). Average CARs were higher post- MLCC at all sites within tributary incised valleys, but only at 3 of the 6 sites within coastal prism incised valleys (Figure 3.6). Like the MARs, the range between CARs pre- MLCC and post- MLCC upper and lower quartiles, respectively, were larger for marsh sites within tributary incised valleys.

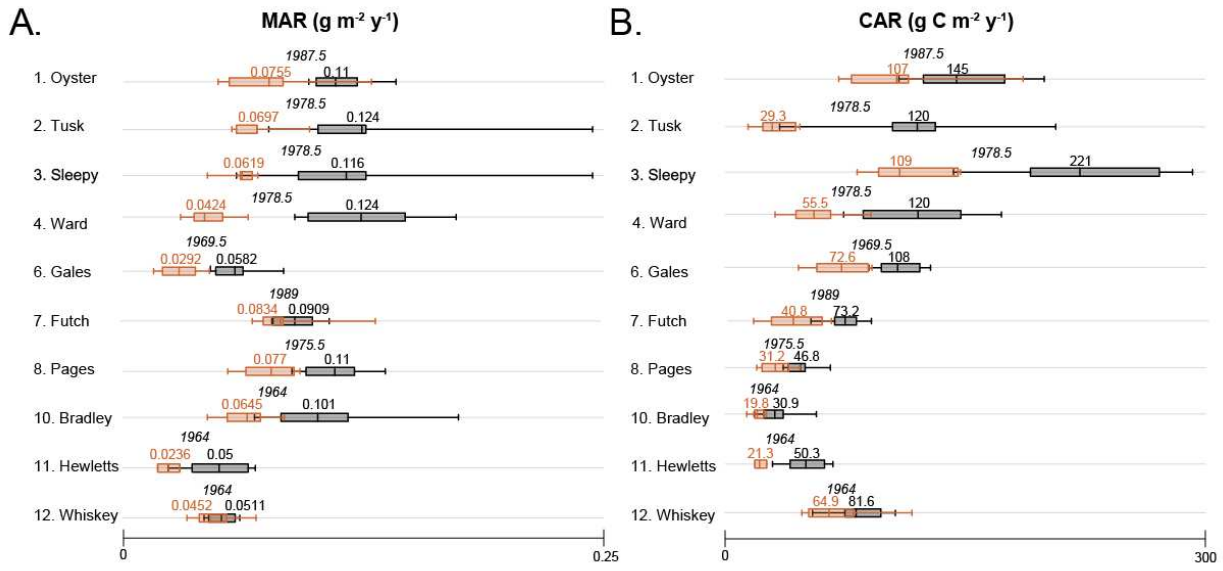

Figure 3.7 Accumulation pre- and post- MLCC. (A) MAR and (B) CAR for each marsh site pre- (orange) and post-MLCC (black). Each bar represents the first and third quartiles, mean accumulation rate, and whiskers are max and min values. Date dividing pre- and post-MLCC for each creek watershed in italics above.

Sediment Accumulation Rates (SAR) provides an indicator of elevation change across a marsh platform. Long-term (1900-2016) SARs were similar between marsh sites within tributary incised valleys and those within coastal prism incised valleys (2.9 ± 0.3 mm y^{-1} and 2.1 ± 0.3 mm y^{-1}, P=0.063) and between marsh sites in CC and NHC (2.8 ± 0.3 mm y^{-1} and 2.0 ± 0.3 mm y^{-1}, respectively; P= 0.096). Average SARs since 1950 were higher at marsh sites within tributary incised valleys than coastal prism incised valleys (3.4 ± 0.3 mm y^{-1} and 2.4±0.3 mm y^{-1}, respectively; P=0.024), but similar between sites within CC and NHC (3.0 ±0.3 mm y^{-1} and 2.3 ± 0.4 mm y^{-1}, respectively; P=0.155). This is likely a manifestation of RSLR being higher in CC, including Gales creek which the only site in CC that is a coastal prism incised valley, than NHC over the period (3.79 mm y^{-1} and 2.65 mm y^{-1}, respectively; NOAA Station IDs 8656483, 8658120; Figure 3.1). When RSLR was subtracted from average SAR since 1950 for each site, all sites were negative accept two, Sleepy and Bradley (Sites 3 and 10, respectively) indicating that for 9 of the marsh sites in this study, RSLR > SAR (Figure 3.8).

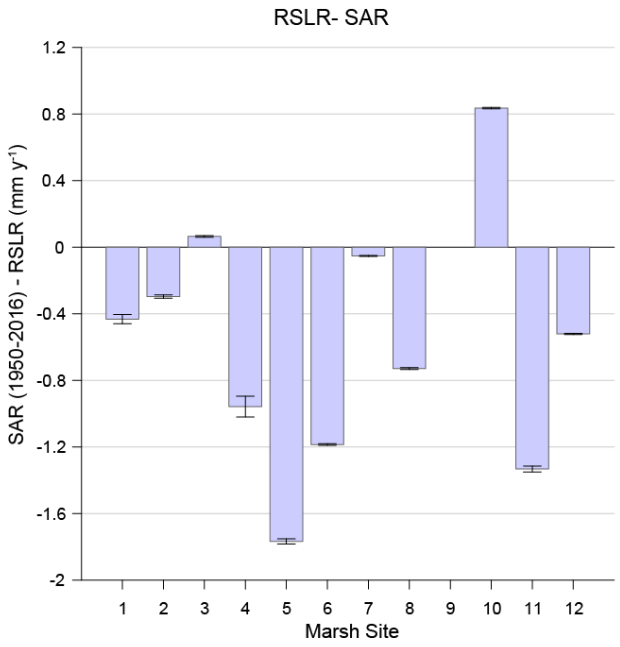

Figure 3.8 SAR minus RSLR. Average SAR minus RSLR at each marsh site. RSLR based on linear regression of monthly mean sea level at the Beaufort (1953-2020) and Wilmington (1935-2020) tide gauges for sites 1-6 and 7-12, respectively.

Discussion

Mass accumulation rates, land cover and creek morphology

Previous research has documented accelerated subtidal accretion rates and local marsh expansion in response to LUC (Mattheus et al., 2009; Kirwan et al., 2011; Rodriguez et al., 2020; Yellen et al., 2020) and the 12 tidal creek basins in this study and their adjacent fringing salt marshes complement these findings as they recorded accelerated MARs after the MLCC in the watersheds. Storm events are known to impact sediment transport at the coast but increased sediment supply from storms would result in a synchronous increase in MAR across marsh sites due to their proximity to each other. The significant increase in MAR at 8 of 12 marsh sites occurred at different times among sites and corresponds with the MLCC, of cleared forest in CC and developed in NHC. An increase in storms with wind > 55.5 km h^{-1} (primarily northeasters) did occur around 2000 in the area near the CC sites (Miller et al., 2021) but increased storminess postdates the increase in MAR among the sites in this study. In addition to an increase in watershed development, the NHC marsh sites all have higher tidal ranges and ϑ than the sites in CC making it difficult to disentangle the relative impacts of MLCC and tidal range. The marsh site at Ware Creek (Site 5) with a similar ϑ to other CC marsh sites, however, had no MLCC in the watershed and MAR peaks and troughs did not correspond with any known regional or local modifications. Furthermore, the Ware Creek bed recorded a consistent MAR throughout the record. Changes in the land cover of watersheds is an important determinant of MAR at both subtidal creek-bed and adjacent salt-marsh settings.

The average MARs prior to the MLCC were similar among subtidal creek beds and among adjacent marshes. After the MLCC and the associated increase in sediment supply, creek-basin morphology, which is related to the type of incised valley the creek formed on, controlled

the magnitude of the increase in MAR of creek beds and adjacent saltmarshes. Tidal creeks within tributary incised valleys have a relatively oversized embayed portion compared to the size of the watershed while tidal creeks within coastal prism incised valleys have a smaller embayed portion, which scales with watershed area, and numerous patches of intertidal structured habitats (Mattheus & Rodriguez, 2014). With RSLR creating sediment accommodation, an oversized open-water embayment has a greater accommodation, and an increase in sediment supply should be recorded as lower vertical accretion rates (Rodriguez et al., 2005). This is supported by the accretion rates measured in the creek bed as MARs after the MLCC were lower in tributary incised valleys than in coastal prism incised valleys. In contrast, MARs at marsh sites within tributary incised valleys were higher than those in coastal prism incised valleys. Unlike subtidal areas, allogenic sediment is only available to salt marsh when it is inundated and inundation conditions, such as duration and mechanism vary between the sites within coastal prism and tributary incised valleys.

Mass accumulation rates and inundation

For many marshes to persist with accelerating RSLR, autogenic organic sediment must be supplemented with allogenic sediment, which is only supplied when the platform is submerged (Kirwan et al., 2012; Morris et al., 2021). In addition to the concentration of sediment in the water flooding a salt marsh, the contribution of allogenic sediment to vertical accretion hinges on inundation time, which is often bound to astronomical tides and dependent on the relative elevation of the marsh. Long-term MAR was directly correlated with ϑ only for the marsh sites within tributary incised valleys; however, ϑ is only a proxy for inundation and the range of ϑ at sites within tributary incised valleys is 50% greater than coastal prism incised

valleys, which could be driving those differences. In addition, the MARs for the marshes within coastal prism incised valleys after the MLCC were much lower than the other marshes.

The sites in NHC had a larger astronomical tidal range than the sites in CC and the associated higher tidal energy could have promoted resuspension and export (Traynum & Styles, 2007) which would explain lower MARs at those marsh sites. Additionally, the narrower channels and more restricted basins present in coastal prism incised valleys likely impacted the flood-ebb dominance at those marsh sites, as deeper, narrower channels promote high tidal velocities, increasing sediment resuspension (Fleri et al., 2019). Gales Creek marsh is the only site within a coastal prism incised valley with a lower tidal range, but also recorded lower MARs through time that were similar to the other coastal prism systems, likely a result of the restricted basin.

The easternmost marsh sites in CC had the lowest astronomical tidal range and $\vartheta \leq 0.0$ (Oyster, Tusk, Sleepy, and Ward). Wind-driven tides and storm events are important contributors to inundation time at those sites and are not captured in ϑ. The true inundation time of those four marsh sites must be > 0.0 because a system flooded infrequently by basin water would likely transition to high marsh or a terrestrial landscape, altering the plant species present, but all marsh sites in this study were dominated by *Spartina alterniflora,* a key low salt marsh macrophyte species throughout the eastern US. Water level fluctuations in tributary incised valleys are controlled by the adjacent estuaries they are connected to, unlike coastal prism incised valleys that are more connected to the open ocean via adjacent inlets. Water levels in adjacent Pamlico Sound, a large northeast trending lagoon, are principally wind-driven and influence water levels at sites 1-4 by connection with Core Sound (Pietrafesa and Janowitz, 1988; Luettich et al., 2002). In addition, the creek embayment within tributary incised valleys included larger open-water

area than the creek embayment within coastal prism incised valleys that had narrower channels, marsh islands, and inundation mainly driven by astronomical tides. The larger fetch of the creek embayment within tributary incised valleys coupled with wind-driven marsh inundation could have supplied coastal sediment sourced from eroding shorelines and resuspension of the creek bed to those marshes more frequently and for longer durations than the coastal prism systems. This coastal sediment that supplemented upstream watershed sources to marshes in tributary incised valleys supports the higher MARs measured at those sites.

Sediment Accumulation Rates and Sea Level

The resilience of salt marsh to accelerating RSLR is commonly assessed by SAR, with SAR<RSLR indicating high vulnerability to drowning and conversion to subtidal mudflats or sandflats. The average post 1950 SARs of 9 marsh sites are < RSLR suggesting high vulnerability. Most of these marshes, however, (all but Pages marsh, Site 8) are currently above the elevation of LMSL (average 10 cm above LMSL) and after the MLCC the MARs at most of the marsh sites increased indicating an abundant supply of sediment. The low SARs could reflect that accommodation is limited by high elevation at many of the marshes and as SLR continues to accelerate, SARs will be able to keep pace (Kirwan et al., 2010).

Carbon accumulation rates

Stem density is directly related to sedimentation on a marsh platform as the canopy slows water flow (Gleasonet al., 1979; Stumpf, 1983). Additionally, salt marsh plants contribute a large quantity of organic matter and carbon to the marsh sediments and promotes vertical accretion (Morris et al., 2016). In North Carolina, McTigue et al (2019) reported CARs of 141 g C m^{-2} y^{-1}

for the top 32 cm of a core taken from 5.6 m into the marsh from the estuarine edge and Choi and Wang (2004) reported values of 130 ± 9 g C m^{-2} y^{-1}. The CARs measured at sites within tributary incised valleys post-MLCC were within this range but were >2x the rates measured at marsh sites within coastal prism incised valleys post-MLCC. Variability in salt marsh carbon is driven by latitude, inundation, the dominant macrophyte, and stem density. Latitude between the two counties is arguably too similar to confound trends in a N-S direction and the dominant macrophyte was the same between all sites.

Stem densities were only measured in 2016 so it is impossible to compare those to accumulation rates over 100 years prior, but if stem densities changed through time, a change in organic matter downcore would be expected. Since none of the marsh sites exhibited a shift, we area assuming stem density is similar through time. The higher stem densities at marsh sites within tributary incised valleys may be a result of the smaller tidal prism which likely contributed to longer residence times of nutrients in the water column, a higher proportion of marsh organic matter to mineral matter, and ultimately higher MARs and CARs (Elsey-Quirk & Unger, 2018). Furthermore, Ouyang and Lee (2014) reported higher CAR in microtidal settings due to the belowground carbon processes, root biomass, and decomposition. While all sites in this study are within microtidal ranges (<2 m), there is a negative correlation between post-MLCC CARs and inundation fraction which supports previous findings (Ouyang & Lee, 2014; Elsey-Quirk & Unger, 2018). Lower stem densities at marsh sites within coastal prism incised valleys, combined with the higher tidal energy associated with the larger tidal prism in NHC, implies less sediment retention and supply of organic matter than the marsh sites within tributary incised valleys, which may also contribute to both lower MARs and CARs at (Elsey-Quirk & Unger, 2018; Fleri et al., 2019).

Higher average CARs post-MLCC were likely driven by higher MARs at sites within tributary incised valleys. Gales Creek marsh (Site 6) recorded the highest CARs post-MLCC among coastal prism systems despite MARs and an inundation fraction like other coastal prism systems. In contrast to other coastal prism incised valleys, Gales Creek marsh had and the highest stem densities, like the other sites in CC, emphasizing the important role that stem density plays in CARs within fringing marsh sites.

Conclusion

The evolution of an established salt marsh is dependent on sediment accumulation which is controlled by accommodation, sediment supply, inundation duration, and stem density. In tidal creeks, the SARs and MARs of fringing salt marshes accelerated post-MLCC; however, despite an abundance of sediment available, most of the marsh sites in this study are accreting slower than RSLR. This could indicate vulnerability to accelerating RSLR but is more likely reflecting limited accommodation space. The magnitude of accelerations in MARs and CARs post-MLCC in tidal creek fringing salt marshes differed depending on the morphology of the creek basins. The highest accretion rates were measured at marsh sites within tributary incised valleys, which contrasts with the adjacent creek beds where accretion rates were higher in coastal prism incised valleys (Chapter 2). The larger open water area of tributary incised valleys supported wind-driven inundation during events when water was turbid while the higher astronomical tidal range and narrower channels within coastal prism systems resulted in higher inundation durations and likely promoted faster water flow velocities on ebb and flood tides. Additionally, higher stem densities of *Spartina alterniflora* at sites within tributary incised valleys likely provided more autogenic sediment (organic matter) and an efficient trap for allogenic sediment retention.

This study highlights a potential disconnect between faster bay bottom accretion rates and slower fringing marsh accretion rates that may be resulting in overall marsh loss. While this could be the manifestation of some marsh sites having reached their accretion ceiling, this is not the case for all sites, and some, specifically in NHC where accumulation rates are the lowest, could be drowning. The disconnect between the creek beds that are rapidly accumulating sediment and infilling and the adjacent marshes that are slowly accumulating sediment challenges the assumption that the creek bottom and marsh respond at similar magnitudes to climate or anthropogenic impacts. High sediment loads in the tidal creek after the MLCC built salt marsh elevation capital in most of the tributary systems, which limited inundation, caused SAR and MAR to decrease, and suppressed the function of saltmarsh as a buffer of sediment loading to downstream areas. Salt marshes in most of the coastal prism tidal creeks showed consistently accelerating SARs and MARs after the MLCC indicating a lack of elevation capital and vulnerability to accelerating RSLR. Our findings show that marshes have a dampened response to MLCC than adjacent tidal creek bottoms due to intermittent inundation and that comparing SAR to RSLR to assess vulnerability may be misleading by ignoring that marshes can be accommodation limited.

REFERENCES

Airoldi, L., Balata, D., & Beck, M. W. (2008). The Gray Zone: Relationships between habitat loss and marine diversity and their applications in conservation. *Journal of Experimental Marine Biology and Ecology*. https://doi.org/10.1016/j.jembe.2008.07.034

Arias-Ortiz, A., Masqué, P., Garcia-Orellana, J., Serrano, O., Mazarrasa, I., Marbà, N., Lovelock, C. E., Lavery, P. S., & Duarte, C. M. (2018). Reviews and syntheses: Pb-derived sediment and carbon accumulation rates in vegetated coastal ecosystems – setting the record straight. *Biogeosciences, 15*(22), 6791-6818. https://doi.org/10.5194/bg-15-6791-2018

Barbier, E. B., Koch, E. W., Silliman, B. R., Hacker, S. D., Wolanski, E., Primavera, J., Granek, E. F., Polasky, S., Aswani, S., Cramer, L. A., Stoms, D. M., Kennedy, C. J., Bael, D., Kappel, C. V., Perillo, G. M. E., & Reed, D. J. (2008). Coastal Ecosystem–Based Management with Nonlinear Ecological Functions and Values. *Science, 319*, 4.

Blum, M. D., & Roberts, H. H. (2009). Drowning of the Mississippi Delta due to insufficient sediment supply and global sea-level rise. *Nature Geoscience, 2*(7), 488-491. https://doi.org/10.1038/ngeo553

Boldt, K. V., Lane, P., Woodruff, J. D., & Donnelly, J. P. (2010). Calibrating a sedimentary record of overwash from Southeastern New England using modeled historic hurricane surges. *Marine Geology, 275*(1-4), 127-139. https://doi.org/10.1016/j.margeo.2010.05.002

Bost et al (*in review*). (2022) Anthropogenic impacts on tidal creek sedimentation since 1900

Choi, Y., & Wang, Y. (2004). Dynamics of carbon sequestration in a coastal wetland using radiocarbon measurements. *Global Biogeochemical Cycles, 18*(4), n/a-n/a. https://doi.org/10.1029/2004gb002261

Craft, C. B., Seneca, E. D., & Broome, S. W. (1991). Loss on ignition and kjeldahl digestion for estimating organic carbon and total nitrogen in estuarine marsh soils: Calibration with dry combustion. *Estuaries, 14*(2), 175-179. https://doi.org/10.2307/1351691

de Groot, A. V., Veeneklaas, R. M., & Bakker, J. P. (2011). Sand in the salt marsh: Contribution of high-energy conditions to salt-marsh accretion. *Marine Geology, 282*(3-4), 240-254. https://doi.org/10.1016/j.margeo.2011.03.002

de Vleeschouwer, F., Sikorski, J., & Fagel, N. (2010). Development of Lead-210 Measurement in Peat Using Polonium Extraction. A Procedural Comparison. *Geochr, 36*(-1), 1-8. https://doi.org/10.2478/v10003-010-0013-5

Donnelly, J. P., Bryant, S. S., Butler, J., Dowling, J., Fan, L., Hausmann, N., Newby, P., Shuman, B., Stern, J., Westover, K., & Thompson Webb, I. (2001). 700 yr sedimentary

record of intense hurricane landfalls in southern New England. *GSA Bulletin, 113*(6), 13. https://doi.org/10.1130/0016-7606(2001)113<0714:YSROIH>2.0.CO;2

Drexler, J. Z. (2011). Peat Formation Processes Through the Millennia in Tidal Marshes of the Sacramento–San Joaquin Delta, California, USA. *Estuaries and Coasts, 34*(5), 900-911. https://doi.org/10.1007/s12237-011-9393-7

Duarte, C. M., Middelburg, J. J., & Caraco, N. (2005). Major role of marine vegetation on the oceanic carbon cycle. *Biogeosciences, 2*, 9.

El-Daoushy, F., Olsson, K., Garcia-Tenorio, R. . (1991). Accuracies in PO-210 determination for lead-210 dating. *Hydrobiologia 214*, 43-52.

Elsey-Quirk, T., & Unger, V. (2018). Geomorphic influences on the contribution of vegetation to soil C accumulation and accretion in <i>Spartina alterniflora</i> marshes. *Biogeosciences, 15*(1), 379-397. https://doi.org/10.5194/bg-15-379-2018

Engelhart, S. E., Horton, B. P., & Kemp, A. C. (2011). Holocene sea-level changes along the united states' Atlantic coast. *Oceanography, 24*(2), 10.

Fleri, J. R., Lera, S., Gerevini, A., Staver, L., & Nardin, W. (2019). Empirical observations and numerical modelling of tides, channel morphology, and vegetative effects on accretion in a restored tidal marsh. *Earth Surface Processes and Landforms, 44*(11), 2223-2235. https://doi.org/10.1002/esp.4646

Flynn, W. W. (1968). The determination of low levels of Polonium-210 in environmental materials. *Anal. Chim. Acta, 43*, 7.

Gedan, K. B., Silliman, B. R., & Bertness, M. D. (2009). Centuries of human-driven change in salt marsh ecosystems. *Ann Rev Mar Sci, 1*, 117-141. https://doi.org/10.1146/annurev.marine.010908.163930

GIESE, G. L., WILDER, H. B., & G. G. PARKER, J. (1985). *Hydrology of Major Estuaries And Sounds of North Carolina* (United States Geological Survey
Water-Supply Paper 2221, Issue.

Gleason, M. L., Elmer, D. A., Pien, N. C., & Fisher, J. S. (1979). Effects of Stem Density Upon Sediment Retention by Salt Marsh Cord grass, Spartina alterniflora Loisel. *Estuaries, 2*(4), 3.

Gundersen, G., Corbett, D. R., Long, A., Martinez, M., & Ardón, M. (2021). Long-Term Sediment, Carbon, and Nitrogen Accumulation Rates in Coastal Wetlands Impacted by Sea Level Rise. *Estuaries and Coasts, 44*(8), 2142-2158. https://doi.org/10.1007/s12237-021-00928-z

Hartig, E. K., Gornitz, V., Kolker, A., Muschacke, F., & Fallon, D. (2002). Anthropogenic and climate-change impacts on salt marshes of Jamaica Bay, New York City. *Wetlands, 22*(1), 19.

Hartig, E. K., Gornitz, V., Kolker, A., Mushacke, F., & Fallon, D. (2001). Anthropogenic and climate-change impacts on salt marshes of Jamaica Bay, New York City. *Wetlands, 22*(1), 19.

Heiri, O., Lotter, A. F., & Lemcke, G. (2001). Loss on ignition as a method for estimating organic and carbonate content in sediments: reproducibility and comparability of results. *Journal of Paleolimnology 25*, 10.

Howes, N. C., FitzGerald, D. M., Hughes, Z. J., Georgiou, I. Y., Kulp, M. A., Miner, M. D., Smith, J. M., & Barras, J. A. (2010, Aug 10). Hurricane-induced failure of low salinity wetlands. *Proc Natl Acad Sci U S A, 107*(32), 14014-14019. https://doi.org/10.1073/pnas.0914582107

Jalowska, A. M., Rodriguez, A. B., & McKee, B. A. (2015). Responses of the Roanoke Bayhead Delta to variations in sea level rise and sediment supply during the Holocene and Anthropocene. *Anthropocene, 9*, 41-55. https://doi.org/10.1016/j.ancene.2015.05.002

Jr., R. A. L., Carra, S. D., Reynolds-Fleming, J. V., Fulchera, C. W., & McNinch, J. E. (2002). Semi-diurnal seiching in a shallow, micro-tidal lagoonal estuary. *Continental Shelf Research, 22*, 1669–1681.

Kearney, M. S., & Turner, E. R. (2016). Microtidal Marshes: Can These Widespread and Fragile Marshes Survive Increasing Climate–Sea Level Variability and Human Action? *Journal of Coastal Research, 32*(3). https://doi.org/10.2112/jcoastres-d-15-00069.1

Kemp, A. C., Wright, A. J., Barnett, R. L., Hawkes, A. D., Charman, D. J., Sameshima, C., King, A. N., Mooney, H. C., Edwards, R. J., Horton, B. P., & van de Plassche, O. (2017). Utility of salt-marsh foraminifera, testate amoebae and bulk-sediment δ13C values as sea-level indicators in Newfoundland, Canada. *Marine Micropaleontology, 130*, 43-59. https://doi.org/10.1016/j.marmicro.2016.12.003

Kirwan, M. L., & Guntenspergen, G. R. (2012). Feedbacks between inundation, root production, and shoot growth in a rapidly submerging brackish marsh. *Journal of Ecology, 100*(3), 764-770. https://doi.org/10.1111/j.1365-2745.2012.01957.x

Kirwan, M. L., Guntenspergen, G. R., D'Alpaos, A., Morris, J. T., Mudd, S. M., & Temmerman, S. (2010). Limits on the adaptability of coastal marshes to rising sea level. *Geophysical Research Letters, 37*(23), 1-5. https://doi.org/10.1029/2010GL045489

Kirwan, M. L., Murray, A. B., Donnelly, J. P., & Corbett, D. R. (2011). Rapid wetland expansion during European settlement and its implication for marsh survival under modern sediment delivery rates. *Geology, 39*(5), 507-510. https://doi.org/10.1130/g31789.1

Lagomasino, D., Corbett, D. R., & Walsh, J. P. (2013). Influence of Wind-Driven Inundation and Coastal Geomorphology on Sedimentation in Two Microtidal Marshes, Pamlico River Estuary, NC. *Estuaries and Coasts, 36*(6), 1165-1180. https://doi.org/10.1007/s12237-013-9625-0

Lotze, H. K., Lenihan, H. S., Bourque, B. J., Bradbury, R. H., Cooke, R. G., Kay, M. C., Kidwell, S. M., Kirby, M. X., Peterson, C. H., & Jackson, J. B. C. (2006). Depletion, Degradation, and Recovery Potential of Estuaries and Coastal Seas. *Science, 312*, 4.

Mattheus, C. R., & Rodriguez, A. B. (2014). Controls On Lower-Coastal-Plain Valley Morphology and Fill Architecture. *Journal of Sedimentary Research, 84*(4), 314-325. https://doi.org/10.2110/jsr.2014.30

Mattheus, C. R., Rodriguez, A. B., & McKee, B. A. (2009). Direct connectivity between upstream and downstream promotes rapid response of lower coastal-plain rivers to land-use change. *Geophysical Research Letters, 36*(20). https://doi.org/10.1029/2009gl039995

Matthews, K. M., Kim, C.-k., & Martin, P. (2007). Determination of Po in environmental materials : A review of analytical methodology. *65*, 267-279. https://doi.org/10.1016/j.apradiso.2006.09.005

McLeod, E., Chmura, G. L., Bouillon, S., Salm, R., Björk, M., Duarte, C. M., Lovelock, C. E., Schlesinger, W. H., & Silliman, B. R. (2011). A blueprint for blue carbon: Toward an improved understanding of the role of vegetated coastal habitats in sequestering CO2. *Frontiers in Ecology and the Environment, 9*(10), 552-560. https://doi.org/10.1890/110004

McTigue, N., Davis, J., Rodriguez, A. B., McKee, B., Atencio, A., & Currin, C. (2019). Sea Level Rise Explains Changing Carbon Accumulation Rates in a Salt Marsh Over the Past Two Millennia. *Journal of Geophysical Research: Biogeosciences, 124*(10), 2945-2957. https://doi.org/10.1029/2019jg005207

Meade, R. H., & Moody, J. A. (2010). Causes for the decline of suspended-sediment discharge in the Mississippi River system, 1940-2007. *Hydrological Processes*, n/a-n/a. https://doi.org/10.1002/hyp.7477

Miller, C. B., Rodriguez, A. B., & Bost, M. C. (2021). Sea-level rise, localized subsidence, and increased storminess promote saltmarsh transgression across low-gradient upland areas. *Quaternary Science Reviews, 265*. https://doi.org/10.1016/j.quascirev.2021.107000

Möller, I., Kudella, M., Rupprecht, F., Spencer, T., Paul, M., van Wesenbeeck, B. K., Wolters, G., Jensen, K., Bouma, T. J., Miranda-Lange, M., & Schimmels, S. (2014). Wave attenuation over coastal salt marshes under storm surge conditions. *Nature Geoscience, 7*(10), 727-731. https://doi.org/10.1038/ngeo2251

Morris, J. T., Sundareshwar, P.V., Nietch, C.T., Kjerfve, B., Cahoon, D.R. (2002). Response of Coastal Wetlands to Rising Sea Level. *Ecology, 83*(10), 2869-2877. http://www.jstor.org/stable/3072022

Morris, J. T. (2021). Marsh Equilibrium Theory: Implications for Responses to Rising Sea Level. In D. M. Fitzgerald & Z. J. Hughes (Eds.), *Salt Marshes* (pp. 157-177). Cambridge University Press.

Morris, J. T., Barber, D. C., Callaway, J. C., Chambers, R., Hagen, S. C., Hopkinson, C. S., Johnson, B. J., Megonigal, P., Neubauer, S. C., Troxler, T., & Wigand, C. (2016, Apr). Contributions of organic and inorganic matter to sediment volume and accretion in tidal wetlands at steady state. *Earths Future, 4*(4), 110-121. https://doi.org/10.1002/2015EF000334

Neumeier, U., & Ciavola, P. (2004). Flow Resistance and Associated Sedimentary Processes in a Spartina maritima Salt-Marsh. *Journal of Coastal Research, 202*, 435-447. https://doi.org/10.2112/1551-5036(2004)020[0435:Fraasp]2.0.Co;2

New Hanover County, 2015, Open Geospatial Data Portal: Watersheds, http://geo.nhcgov.com/gis/rest/services/Layers/Watersheds/MapServer/0, accessed June 2016.

NOAA (National Oceanic and Atmospheric Administration) National Ocean Service, 2020, National Coastal Population Report, 20p. Available at: http://oceanservice.noaa.gov/facts/coastal-population-report.pdf.

NOAA OCM (National Oceanic and Atmospheric Administration, Office for Coastal Management), 2016, Coastal Change Analysis Program (C-CAP) Regional Land Cover, www.coast.noaa.gov/ccapftp: accessed December 2017.

NOAA OCM (National Oceanic and Atmospheric Administration, Office for Coastal Management), 2014, North Carolina Floodplain Mapping Program, https://coast.noaa.gov/dataviewer/#/lidar/search/where:ID=4954: accessed December 2017.

Ouyang, X., & Lee, S. Y. (2014). Updated estimates of carbon accumulation rates in coastal marsh sediments. 5057-5071. https://doi.org/10.5194/bg-11-5057-2014

Peteet, D. M., Nichols, J., Kenna, T., Chang, C., Browne, J., Reza, M., Kovari, S., Liberman, L., & Stern-Protz, S. (2018, Oct 9). Sediment starvation destroys New York City marshes' resistance to sea level rise. *Proc Natl Acad Sci U S A, 115*(41), 10281-10286. https://doi.org/10.1073/pnas.1715392115

Peterson, G. W., & Turner, R. E. (1994). The Value of Salt Marsh Edge vs Interior as a Habitat for Fish and Decapod Crustaceans in a Louisiana Tidal Marsh. *Estuaries, 17*(1B), 28.

Pethick, J. S. (1981). Long-term accretion rates on tidal salt marshes *Journal of Sedimentary Petrology, 51*(2), 7.

Pietrafesa, L. J., Janowitz, G. S., Brown, K. S., Gabriel, C., & Salzillo, L. A. (1988). *The invasion of red tides on North Carolina coastal waters*.

Plassche, O. v. d., Borg, K. v. d., & Jong, A. F. M. d. (1998). Sea level–climate correlation during the past 1400 yr. *Geology, 26*(4), 4.

Raposa, K. B., Cole Ekberg, M. L., Burdick, D. M., Ernst, N. T., & Adamowicz, S. C. (2016). Elevation change and the vulnerability of Rhode Island (USA) salt marshes to sea-level rise. *Regional Environmental Change, 17*(2), 389-397. https://doi.org/10.1007/s10113-016-1020-5

Reed, R. E., Dickey, D. A., Burkholder, J. M., Kinder, C. A., & Brownie, C. (2008). Water level variations in the Neuse and Pamlico Estuaries, North Carolina due to local and remote forcing. *Estuarine, Coastal and Shelf Science, 76*(2), 431-446. https://doi.org/10.1016/j.ecss.2007.05.049

Rodriguez, A.B., Anderson, J.B., Simms, A. (2005) Terrace inundation as an autocyclic mechanism for parasequence formation: Galveston estuary, Texas, U.S.A. *Journal of Sedimentary Research, 75,* 608-620

Rodriguez, A. B., McKee, B. A., Miller, C. B., Bost, M. C., & Atencio, A. N. (2020, Jun 26). Coastal sedimentation across North America doubled in the 20(th) century despite river dams. *Nat Commun, 11*(1), 3249. https://doi.org/10.1038/s41467-020-16994-z

Sanchez-Cabeza, J. A., & Ruiz-Fernández, A. C. (2012). 210Pb sediment radiochronology: An integrated formulation and classification of dating models. *Geochimica et Cosmochimica Acta, 82*, 183-200. https://doi.org/10.1016/j.gca.2010.12.024

Sousa, A. I., Lillebo, A. I., Pardal, M. A., & Cacador, I. (2010). The influence of Spartina maritima on carbon retention capacity in salt marshes from warm-temperate estuaries. *Mar Pollut Bull, 61*(4-6), 215-223. https://doi.org/10.1016/j.marpolbul.2010.02.018

Stumpf, R. P. (1983). The process of sedimentation on the surface of a salt marsh. *Estuarine, Coastal and Shelf Science, 17*, 14.

Syvitski, J. P. M., & Kettner, A. (2011). Sediment flux and the Anthropocene. *Philosophical Transactions of the Royal Society A: Mathematical, Physical and Engineering Sciences, 369*(1938), 957-975. https://doi.org/10.1098/rsta.2010.0329

Theuerkauf, E. J., Stephens, J. D., Ridge, J. T., Fodrie, F. J., & Rodriguez, A. B. (2015). Carbon

export from fringing saltmarsh shoreline erosion overwhelms carbon storage across a critical width threshold. *Estuarine, Coastal and Shelf Science, 164*, 367-378. https://doi.org/10.1016/j.ecss.2015.08.001

Traynum, S., & Styles, R. (2007). Flow, Stress and Sediment Resuspension in a Shallow Tidal Channel. *Estuaries and Coasts, 30*(1), 8.

US Department of Commerce, N. O. and A. A. (2022, March 15). NOAA/Nos Web Vertical Datums transformation.
NOAA/NOS's VDatum 4.4: Vertical Datums Transformation. Retrieved March 17, 2022, from https://vdatum.noaa.gov/vdatumweb/

Walling, D. E., & Fang, D. (2003). Recent trends in the suspended sediment loads of the world's rivers. *Global and Planetary Change, 39*(1-2), 111-126. https://doi.org/10.1016/s0921-8181(03)00020-1

Yellen, B., Woodruff, J., Ladlow, C., Ralston, D. K., Fernald, S., & Lau, W. (2020). Rapid tidal marsh development in anthropogenic backwaters. *Earth Surface Processes and Landforms, 46*(3), 554-572. https://doi.org/10.1002/esp.5045

APPENDIX 1.1 SALINITY

Salinity data from Station 6 and Station 18 including site (SRE and BS), date, salinity, and tidal stage (FLD= flood, and ebb; North Carolina Department of Marine Fisheries 2014, 2015, 2017).

Site	Date	Salinity	Tide
SRE	2011-01-24	36	LAST FLD
SRE	2011-03-01	29	LAST EBB
SRE	2011-04-27	31	LAST EBB
SRE	2011-05-16	35	1/4 EBB
SRE	2011-07-18	39	HIGH
SRE	2011-09-07	31	LAST EBB
SRE	2012-02-14	34	1/2 FLD
SRE	2012-04-12	35	1/2 FLD
SRE	2012-05-29	31	1ST FLD
SRE	2012-07-10	34	1/4 FLD
SRE	2012-09-11	25	LAST EBB
SRE	2012-10-03	32	LAST FLD
SRE	2013-01-15	33	LAST FLD
SRE	2013-04-10	33	1/2 EBB
SRE	2013-06-18	30	LOW
SRE	2013-07-10	31	LAST FLD
SRE	2013-08-13	31	1/2 FLD
SRE	2013-09-25	35	3/4 FLD
SRE	2014-02-10	32	LAST EBB
SRE	2014-06-02	34	1/2 FLD
SRE	2014-07-02	35	3/4 FLD
SRE	2014-09-02	30	1/4 FLD
SRE	2014-10-02	27	1/4 FLD
SRE	2014-10-27	35	3/4 FLD
SRE	2015-03-09	32	HIGH
SRE	2015-03-25	30	1/2 FLD
SRE	2015-04-21	31	LAST FLD
SRE	2015-05-21	32	LAST FLD
SRE	2015-08-06	34	1/4 FLD

SRE	2015-09-23	34	1/4 FLD
BS	2010-05-17	35	1/2 FLD
BS	2010-07-12	36	1ST EBB
BS	2010-08-13	36	1/2 FLD
BS	2010-12-22	32	LAST FLD
BS	2011-02-22	32	1/2 FLD
BS	2011-03-13	34	1ST FLD
BS	2011-04-11	32	LAST EBB
BS	2011-05-03	35	1/2 FLD
BS	2011-07-27	36	2/3 EBB
BS	2011-09-15	35	3/4 FLD
BS	2011-10-17	30	No data
BS	2011-11-16	28	1/4 FLD
BS	2012-01-25	35	LAST FLD
BS	2012-02-13	36	1/4 FLD
BS	2012-03-14	35	1ST FLD
BS	2012-05-07	36	LAST FLD
BS	2012-07-23	38	3/4 FLD
BS	2012-09-25	35	LAST EBB
BS	2013-03-13	32	LAST FLD
BS	2013-05-02	28	1ST FLD
BS	2013-06-13	35	1/2 FLD
BS	2013-08-07	35	LAST FLD
BS	2013-10-22	31	LAST FLD
BS	2013-12-06	32	1/4 FLD
BS	2014-02-10	30	3/4 FLD
BS	2014-02-24	32	LAST EBB
BS	2014-04-09	32	3/4 EBB
BS	2014-05-05	33	1ST FLD
BS	2014-07-21	35	LAST EBB
BS	2014-10-07	32	1/4 EBB
BS	2015-01-26	32	1ST FLD
BS	2015-03-24	28	3/4 FLD
BS	2015-04-08	32	1/4 FLD
BS	2015-06-01	35	1/4 EBB

BS	2015-08-18	36	1/2 FLD
BS	2015-09-02	34	1/2 FLD
BS	2016-01-11	30	LAST FLD
BS	2016-03-17	34	1/4 EBB
BS	2016-04-12	35	1ST FLD
BS	2016-05-25	32	3/4 FLD
BS	2016-10-04	28	1/2 FLD
BS	2016-11-09	30	1/4 FLD
BS	2017-01-19	32	1/4 FLD
BS	2017-03-27	36	LAST FLD
BS	2017-04-18	35	1/2 EBB

APPENDIX 1.2 REEF AND LOGGER INFORMATION

Reef and logger locations, scan dates, study duration, and heat stress or # degree days Tmax > 28°C

Reef and Logger ID	Easting	Northing	Initial Date	End Date	Time Period (yr)	HS/ # days Tmax > 28 °C
Patch SRE-1	744654	3757389	2015-10-26	2018-04-27	2.5	568.6
Patch SRE-2	744592	3757410	2016-03-11	2018-06-21	2.3	606.5
Patch SRE-3	744555	3757429	2016-03-11	2018-06-21	2.3	606.5
Fringe SRE-1	744106	3757237	2016-03-10	2018-06-20	2.3	603.9
Fringe SRE-2	744132	3757236	2016-03-10	2018-06-20	2.3	603.9
Fringe SRE-3	744160	3757236	2016-03-10	2018-06-20	2.3	603.9
Patch BS-1	354329	3838040	2015-04-17	2018-06-15	3.2	595.4
Patch BS-2	354345	3837984	2015-07-01	2018-06-15	3.0	535.9
Patch BS-3	354259	3837989	2015-07-01	2018-06-15	3.0	535.9
Fringe BS-1	354533	3838221	2016-03-08	2018-07-11	2.3	475.7
Fringe BS-2	354727	3838352	2016-08-18	2018-08-07	2.0	337
Fringe BS-3	349763	3841257	2016-07-05	2018-05-16	1.9	375.8
BS Logger	744323	3757211	2015-07-30	2018-03-03	2.6	N/A
SRE Logger	354505	3837929	2015-10-26	2018-02-11	2.3	N/A

APPENDIX 1.3 ANOVA P-VALUES

Results of rank transformation ANOVA from ARTool Package in R (p-values).

Parameter	Estuary	Reef Type	Estuary x Reef Type
MMGR Elevation (m)	0.00062*	0.0033*	0.202
Growth rate at reef crest (cm yr^{-1})	0.788	0.688	0.416
MMGR (cm yr^{-1})	0.582	0.109	0.399
Relief (m)	0.030*	0.785	0.413
Reef base elevation (m)	0.0009*	0.029*	0.415
Reef crest elevation (m)	0.001*	0.005*	0.112
Aerial Exposure of reef crest (%)	0.001*	0.031*	0.490
Aerial exposure at MMGR (%)	0.0009*	0.050*	1.000
Crest Exposure – MMGR Exposure (%)	0.001	0.790	0.206

∗Significant P-value

APPENDIX 1.4 ANOVA EFFECTS SIZES

Results of rank transformation ANOVA from ARTool Package in R (effect sizes; partial eta squared).

Parameter	Estuary	Reef Type	Estuary x Reef Type
MMGR Elevation (m)	0.786***	0.682***	0.195
Growth rate at reef crest (cm yr^{-1})	0.009	0.021	0.084
MMGR (cm yr^{-1})	0.040	0.289	0.090
Relief (m)	0.464*	0.009	0.085
Reef base elevation (m)	0.767***	0.469*	0.084
Reef crest elevation (m)	0.760**	0.606**	0.284
Aerial Exposure of reef crest (%)	0.760**	0.460*	0.061
Aerial exposure at MMGR (%)	0.770***	0.400*	0.000
Crest Exposure – MMGR Exposure (%)	0.760**	0.009	0.191

⁎Magnitude of effect 0= negligible, 1= small effect, 2= medium effect, 3= large effect

REFERENCES

North Carolina Division of Marine Fisheries. 2014. Report of sanitary survey, area E-7, Back Sound area [2010: May 2010–2014: October], Retrieved from https://digital.ncdcr.gov/digital/collection/p16062coll9/id/166544/rec/96

North Carolina Division of Marine Fisheries. 2015. Report of sanitary survey, area A-2, Shallotte River area [2011: January–2015: September], Retrieved from https://digital.ncdcr.gov/digital/collection/p16062coll9/id/328687/rec/64

North Carolina Division of Marine Fisheries. 2017. Report of sanitary survey, area E-7, Back Sound area [2012: May–2017: April], Retrieved from https://digital.ncdcr.gov/digital/collection/p16062coll9/id/333806/rec/33

APPENDIX 2.1 CREEK CORING LOCATIONS

Site Number	Creek Name	Core Date	Core latitude (decimal degrees)	Core longitude (decimal degrees)	Approximate Core Water Depth (m)
1	Oyster	2016-08-05	34.8270	-76.4623	1.1
2	Tusk	2016-08-09	34.7463	-76.5139	1.2
3	Sleepy	2016-07-21	34.7329	-76.5272	0.8
4	Ward	2016-07-07	34.7907	-76.5658	1.1
5	Ware	2016-08-24	34.7750	-76.6741	0.8
6	Gales	2016-07-28	34.7321	-76.9075	1.2
7	Futch	2016-05-10	34.3041	-77.7532	0.75
8	Pages	2016-10-04	34.2816	-77.7786	1.1
9	Howe	2016-10-05	34.2559	-77.8065	1.1
10	Bradley	2016-09-20	34.2179	-77.8395	1
11	Hewlett's	2016-09-12	34.8270	-76.4623	1.5
12	Whiskey	2016-09-12	34.1600	-77.8626	1.1

APPENDIX 2.2 RAW CREEK PB-210 DATA

Site Number	Midpoint Depth (cm)	DBD (g cm^{-3})	Measurement error	Total ^{210}Pb (dpm/g)	Measurement error
1	0.5	0.68	0.01	2.56	0.04
1	1.5	0.84	0.02	2.23	0.06
1	2.5	0.77	0.02	2.09	0.05
1	3.5	0.79	0.02	2.01	0.07
1	4.5	0.88	0.02	2.19	0.06
1	5.5	0.83	0.02	2.44	0.04
1	6.5	0.80	0.02	2.29	0.05
1	7.5	0.86	0.02	2.39	0.05
1	8.5	0.89	0.02	1.82	0.07
1	9.5	0.90	0.02	2.05	0.06
1	10.5	0.82	0.02	1.95	0.06
1	11.5	0.98	0.02	1.54	0.11
1	12.5	0.82	0.02	1.41	0.12
1	13.5	0.83	0.02	1.26	0.15
1	14.5	0.75	0.01	0.96	0.23
1	15.5	0.79	0.02	1.10	0.18
1	16.5	0.74	0.01	1.13	0.15
1	17.5	0.90	0.02	0.89	0.27
1	18.5	0.70	0.01	0.68	0.47
1	19.5	0.79	0.02	0.46	0.99
2	0.5	0.32	0.01	5.10	0.03
2	1.5	0.35	0.01	5.38	0.03
2	2.5	0.36	0.01	4.71	0.03
2	3.5	0.41	0.01	5.20	0.03
2	4.5	0.45	0.01	4.82	0.03
2	5.5	0.52	0.01	4.48	0.03
2	6.5	0.47	0.01	4.67	0.03
2	7.5	0.50	0.01	4.52	0.03
2	8.5	0.60	0.01	4.31	0.03
2	9.5	0.59	0.01	3.86	0.03
2	10.5	0.59	0.01	3.78	0.03
2	11.5	0.57	0.01	3.94	0.03
2	12.5	0.59	0.01	4.00	0.03
2	13.5	0.56	0.01	3.74	0.03
2	14.5	0.60	0.01	3.90	0.03

2	15.5	0.63	0.01	3.20	0.04
2	16.5	0.57	0.01	2.43	0.05
2	17.5	0.73	0.01	2.38	0.05
2	18.5	0.58	0.01	2.06	0.06
2	19.5	0.63	0.01	2.14	0.06
2	20.5	0.63	0.01	1.74	0.08
2	21.5	0.64	0.01	1.69	0.10
2	22.5	0.79	0.02	1.78	0.08
2	23.5	0.65	0.01	1.73	0.08
2	24.5	0.61	0.01	1.55	0.10
3	0.5	0.22	0.00	5.39	0.02
3	1.5	0.35	0.01	5.40	0.02
3	2.5	0.30	0.01	5.20	0.02
3	3.5	0.29	0.01	5.43	0.02
3	4.5	0.31	0.01	5.38	0.02
3	5.5	0.34	0.01	5.22	0.02
3	6.5	0.31	0.01	5.66	0.02
3	7.5	0.27	0.01	5.17	0.02
3	8.5	0.34	0.01	5.11	0.02
3	9.5	0.32	0.01	4.75	0.02
3	10.5	0.37	0.01	5.01	0.02
3	11.5	0.36	0.01	4.88	0.02
3	12.5	0.43	0.01	5.17	0.02
3	13.5	0.37	0.01	4.58	0.02
3	14.5	0.48	0.01	4.69	0.02
3	15.5	0.41	0.01	4.27	0.03
3	16.5	0.44	0.01	4.34	0.02
3	17.5	0.46	0.01	4.21	0.02
3	18.5	0.47	0.01	3.45	0.03
3	19.5	0.47	0.01	3.51	0.03
3	20.5	0.44	0.01	3.51	0.03
3	21.5	0.41	0.01	3.11	0.03
3	22.5	0.49	0.01	2.85	0.04
3	23.5	0.48	0.01	2.36	0.06
3	24.5	0.51	0.01	1.97	0.08
3	25.5	0.55	0.01	1.48	0.12
3	26.5	0.59	0.01	1.43	0.13
3	27.5	0.43	0.01	1.48	0.11
3	28.5	0.54	0.01	1.52	0.11
3	29.5	0.40	0.01	1.46	0.12
3	30.5	0.48	0.01	1.52	0.12

3	31.5	0.49	0.01	1.26	0.20
3	32.5	0.50	0.01	1.45	0.17
3	33.5	0.46	0.01	1.33	0.15
3	34.5	0.45	0.01	1.28	0.19
4	0.5	0.48	0.01	4.34	0.06
4	1.5	0.33	0.01	3.67	0.06
4	2.5	0.44	0.01	3.38	0.06
4	3.5	0.53	0.01	2.48	0.07
4	4.5	0.38	0.01	1.81	0.09
4	5.5	0.30	0.01	1.67	0.10
4	6.5	0.30	0.01	1.56	0.11
4	7.5	0.24	0.00	1.22	0.15
4	8.5	0.25	0.00	1.25	0.14
4	9.5	0.20	0.00	1.15	0.17
4	10.5	0.19	0.00	1.25	0.16
4	11.5	0.17	0.00	1.54	0.11
4	12.5	0.13	0.00	1.30	0.16
4	13.5	0.14	0.00	1.26	0.16
4	14.5	0.11	0.00	1.55	0.12
4	15.5	0.12	0.00	1.46	0.13
4	16.5	0.13	0.00	1.45	0.13
4	17.5	0.13	0.00	1.34	0.13
4	18.5	0.13	0.00	1.23	0.14
4	19.5	0.10	0.00	0.99	0.26
5	0.5	0.21	0.00	10.45	0.01
5	1.5	0.28	0.01	9.75	0.01
5	2.5	0.29	0.01	9.48	0.01
5	3.5	0.31	0.01	8.01	0.01
5	4.5	0.34	0.01	8.02	0.01
5	5.5	0.36	0.01	7.80	0.01
5	6.5	0.45	0.01	6.59	0.01
5	7.5	0.41	0.01	6.29	0.01
5	8.5	0.42	0.01	5.67	0.02
5	9.5	0.44	0.01	5.60	0.02
5	10.5	0.43	0.01	4.89	0.02
5	11.5	0.44	0.01	4.36	0.02
5	12.5	0.44	0.01	4.29	0.02
5	13.5	0.43	0.01	4.50	0.02
5	14.5	0.45	0.01	4.05	0.02
5	15.5	0.42	0.01	3.77	0.02
5	16.5	0.45	0.01	3.42	0.03

5	17.5	0.44	0.01	3.27	0.03
5	18.5	0.47	0.01	3.36	0.03
5	19.5	0.40	0.01	2.96	0.03
5	20.5	0.45	0.01	3.19	0.03
5	21.5	0.43	0.01	3.17	0.03
5	22.5	0.44	0.01	2.74	0.03
5	23.5	0.50	0.01	2.53	0.04
5	24.5	0.45	0.01	2.32	0.05
5	25.5	0.48	0.01	2.36	0.05
5	26.5	0.47	0.01	2.31	0.05
5	27.5	0.47	0.01	1.00	0.18
5	28.5	0.48	0.01	2.29	0.05
5	29.5	0.44	0.01	1.99	0.06
5	30.5	0.48	0.01	1.95	0.07
5	31.5	0.40	0.01	1.86	0.07
5	32.5	0.49	0.01	1.97	0.06
5	33.5	0.46	0.01	1.60	0.09
5	34.5	0.43	0.01	1.80	0.07
5	35.5	0.43	0.01	1.92	0.07
5	36.5	0.43	0.01	1.49	0.10
5	37.5	0.43	0.01	1.72	0.09
5	38.5	0.49	0.01	1.67	0.10
5	39.5	0.41	0.01	1.43	0.13
5	40.5	0.43	0.01	1.40	0.13
5	41.5	0.44	0.01	1.22	0.15
5	42.5	0.39	0.01	1.07	0.23
5	43.5	0.41	0.01	1.27	0.15
5	44.5	0.42	0.01	1.13	0.18
5	45.5	0.42	0.01	1.16	0.17
5	46.5	0.39	0.01	1.39	0.12
5	47.5	0.40	0.01	1.16	0.15
5	48.5	0.41	0.01	1.14	0.17
5	49.5	0.45	0.01	1.06	0.32
5	50.5	0.48	0.01	0.98	0.31
6	0.5	0.15	0.00	5.51	0.02
6	1.5	0.17	0.00	7.98	0.02
6	2.5	0.21	0.00	8.61	0.02
6	3.5	0.18	0.00	8.70	0.02
6	4.5	0.24	0.00	8.42	0.02
6	5.5	0.22	0.00	7.91	0.02
6	6.5	0.22	0.00	7.90	0.02

6	7.5	0.22	0.00	7.28	0.02
6	8.5	0.23	0.00	7.30	0.02
6	9.5	0.23	0.00	7.34	0.02
6	10.5	0.27	0.01	6.92	0.02
6	11.5	0.23	0.00	7.45	0.02
6	12.5	0.29	0.01	6.91	0.02
6	13.5	0.26	0.01	7.15	0.02
6	14.5	0.26	0.01	6.75	0.02
6	15.5	0.26	0.01	6.61	0.02
6	16.5	0.25	0.00	6.81	0.02
6	17.5	0.24	0.00	6.78	0.02
6	18.5	0.27	0.01	7.14	0.02
6	19.5	0.27	0.01	6.45	0.02
6	20.5	0.25	0.00	6.05	0.02
6	21.5	0.27	0.01	5.36	0.02
6	22.5	0.27	0.01	5.28	0.02
6	23.5	0.24	0.00	5.28	0.02
6	24.5	0.28	0.01	5.50	0.02
6	25.5	0.25	0.00	5.45	0.02
6	26.5	0.34	0.01	5.10	0.02
6	27.5	0.28	0.01	5.13	0.02
6	28.5	0.32	0.01	4.95	0.02
6	29.5	0.34	0.01	3.66	0.03
6	30.5	0.30	0.01	3.79	0.03
6	31.5	0.30	0.01	4.23	0.03
6	32.5	0.32	0.01	4.58	0.02
6	33.5	0.32	0.01	4.64	0.02
6	34.5	0.33	0.01	4.36	0.02
6	35.5	0.36	0.01	5.07	0.03
6	36.5	0.38	0.01	4.78	0.02
6	37.5	0.34	0.01	4.60	0.02
6	38.5	0.32	0.01	4.43	0.02
6	39.5	0.34	0.01	4.57	0.02
6	40.5	0.35	0.01	4.48	0.03
6	41.5	0.40	0.01	3.93	0.03
6	42.5	0.36	0.01	3.25	0.03
6	43.5	0.34	0.01	2.76	0.04
6	44.5	0.33	0.01	2.64	0.04
7	0.5	0.19	0.00	7.56	0.02
7	1.5	0.23	0.00	8.18	0.02
7	2.5	0.33	0.01	7.00	0.02

7	3.5	0.61	0.01	6.24	0.02
7	4.5	0.67	0.01	7.72	0.02
7	5.5	0.55	0.01	10.63	0.03
7	6.5	0.65	0.01	10.36	0.03
7	7.5	0.75	0.01	8.78	0.03
7	8.5	0.81	0.02	8.16	0.03
7	9.5	0.88	0.02	8.17	0.03
7	10.5	0.84	0.02	8.29	0.03
7	11.5	0.95	0.02	7.95	0.03
7	12.5	0.78	0.02	8.26	0.03
7	13.5	1.00	0.02	7.91	0.03
7	14.5	0.99	0.02	6.87	0.03
7	15.5	0.94	0.02	6.02	0.03
7	16.5	0.67	0.01	5.45	0.03
7	17.5	1.17	0.02	4.96	0.03
7	18.5	0.83	0.02	4.69	0.03
7	19.5	1.04	0.02	4.29	0.03
7	20.5	0.78	0.02	4.32	0.03
7	21.5	1.00	0.02	4.00	0.03
7	22.5	0.99	0.02	3.40	0.03
7	23.5	0.94	0.02	3.26	0.06
7	24.5	0.67	0.01	3.12	0.04
7	25.5	1.17	0.02	2.42	0.07
7	26.5	0.83	0.02	2.98	0.03
7	27.5	1.04	0.02	3.55	0.04
7	28.5	0.78	0.02	3.34	0.04
7	29.5	1.09	0.02	2.04	0.09
8	0.5	0.31	0.01	9.77	0.02
8	1.5	0.29	0.01	10.80	0.02
8	2.5	0.43	0.01	8.36	0.02
8	3.5	0.47	0.01	8.87	0.02
8	4.5	0.53	0.01	8.93	0.02
8	5.5	0.56	0.01	8.63	0.02
8	6.5	0.62	0.01	8.11	0.02
8	7.5	0.63	0.01	7.98	0.02
8	8.5	0.72	0.01	8.46	0.02
8	9.5	0.72	0.01	8.29	0.02
8	10.5	0.76	0.01	7.69	0.02
8	11.5	0.71	0.01	7.58	0.02
8	12.5	0.81	0.02	6.89	0.02
8	13.5	0.89	0.02	6.96	0.02

8	14.5	0.86	0.02	5.61	0.02
8	15.5	0.84	0.02	5.03	0.02
8	16.5	0.97	0.02	4.48	0.02
8	17.5	0.76	0.01	3.93	0.03
8	18.5	0.78	0.02	3.83	0.03
8	19.5	0.74	0.01	3.73	0.03
8	20.5	0.75	0.01	2.29	0.05
8	21.5	0.78	0.02	1.93	0.08
8	22.5	0.90	0.02	2.07	0.07
8	23.5	0.77	0.02	1.74	0.10
8	24.5	0.71	0.01	1.64	0.10
8	25.5	0.87	0.02	1.59	0.11
8	26.5	0.68	0.01	1.39	0.15
8	27.5	0.78	0.02	1.24	0.17
8	28.5	0.81	0.02	1.12	0.20
8	29.5	0.87	0.02	0.96	0.30
9	0.5	0.49	0.01	6.12	0.07
9	1.5	0.54	0.01	4.66	0.07
9	2.5	0.62	0.01	4.20	0.07
9	3.5	0.64	0.01	4.08	0.07
9	4.5	0.75	0.01	3.45	0.07
9	5.5	0.79	0.02	3.44	0.07
9	6.5	0.74	0.01	2.87	0.08
9	7.5	0.70	0.01	2.57	0.08
9	8.5	0.66	0.01	2.34	0.08
9	9.5	0.69	0.01	1.97	0.09
9	10.5	0.72	0.01	1.92	0.10
9	11.5	0.73	0.01	1.88	0.11
9	12.5	0.64	0.01	1.89	0.10
9	13.5	0.67	0.01	1.88	0.10
9	14.5	0.71	0.01	1.65	0.12
9	15.5	0.67	0.01	1.54	0.13
9	16.5	0.59	0.01	1.43	0.14
9	17.5	0.64	0.01	1.34	0.14
9	18.5	0.65	0.01	1.39	0.14
9	19.5	0.69	0.01	1.34	0.15
9	20.5	0.64	0.01	1.43	0.14
9	21.5	0.71	0.01	1.32	0.17
9	22.5	0.76	0.01	1.33	0.15
9	23.5	0.67	0.01	1.29	0.25
9	24.5	0.77	0.02	1.27	0.17

9	25.5	0.74	0.01	1.24	0.18
9	26.5	0.71	0.01	1.54	0.12
9	27.5	0.85	0.02	1.19	0.18
9	28.5	0.84	0.02	1.10	0.19
9	29.5	0.92	0.02	0.80	0.31
9	30.5	0.90	0.02	0.74	0.42
9	31.5	0.95	0.02	0.63	0.64
9	32.5	0.91	0.02	0.60	0.62
9	33.5	0.81	0.02	0.69	0.53
9	34.5	0.73	0.01	0.64	0.62
9	35.5	0.60	0.01	0.49	0.93
9	36.5	0.54	0.01	0.54	0.77
9	37.5	0.74	0.01	0.49	0.96
9	38.5	0.86	0.02	0.34	1.75
9	39.5	0.93	0.02	0.25	3.14
10	0.5	0.55	0.01	6.64	0.03
10	1.5	0.50	0.01	7.78	0.03
10	2.5	0.50	0.01	7.06	0.03
10	3.5	0.52	0.01	6.76	0.03
10	4.5	0.48	0.01	6.43	0.03
10	5.5	0.43	0.01	6.26	0.03
10	6.5	0.46	0.01	6.28	0.03
10	7.5	0.49	0.01	6.45	0.03
10	8.5	0.62	0.01	6.39	0.03
10	9.5	0.40	0.01	6.60	0.03
10	10.5	0.48	0.01	5.17	0.03
10	11.5	0.53	0.01	5.03	0.03
10	12.5	0.49	0.01	5.25	0.03
10	13.5	0.42	0.01	5.58	0.03
10	14.5	0.36	0.01	4.68	0.03
10	15.5	0.42	0.01	4.84	0.03
10	16.5	0.31	0.01	4.92	0.03
10	17.5	0.34	0.01	4.68	0.03
10	18.5	0.30	0.01	5.21	0.03
10	19.5	0.28	0.01	5.08	0.04
10	20.5	0.41	0.01	4.95	0.03
10	21.5	0.41	0.01	4.75	0.03
10	22.5	0.61	0.01	4.49	0.03
10	23.5	0.65	0.01	5.10	0.03
10	24.5	0.57	0.01	5.51	0.03
10	25.5	0.70	0.01	5.24	0.04

10	26.5	1.01	0.02	4.98	0.03
10	27.5	1.04	0.02	4.68	0.03
11	0.5	0.17	0.00	9.31	0.01
11	1.5	0.26	0.01	8.03	0.01
11	2.5	0.24	0.00	6.08	0.01
11	3.5	0.28	0.01	6.86	0.01
11	4.5	0.46	0.01	5.16	0.02
11	5.5	0.55	0.01	3.19	0.03
11	6.5	0.76	0.01	3.21	0.03
11	7.5	0.71	0.01	2.67	0.04
11	8.5	0.79	0.02	2.61	0.04
11	9.5	0.53	0.01	2.23	0.05
11	10.5	0.53	0.01	2.24	0.05
11	11.5	0.49	0.01	2.75	0.03
11	12.5	0.44	0.01	2.84	0.03
11	13.5	0.45	0.01	2.89	0.03
11	14.5	0.36	0.01	2.53	0.04
11	15.5	0.33	0.01	2.71	0.04
11	16.5	0.31	0.01	3.54	0.02
11	17.5	0.30	0.01	3.49	0.02
11	18.5	0.26	0.01	3.90	0.02
11	19.5	0.37	0.01	3.23	0.03
11	20.5	0.35	0.01	2.32	0.04
11	21.5	0.37	0.01	2.56	0.04
11	22.5	0.40	0.01	2.61	0.04
11	23.5	0.36	0.01	2.43	0.04
11	24.5	0.32	0.01	2.43	0.04
11	25.5	0.45	0.01	2.19	0.05
11	26.5	0.46	0.01	1.85	0.07
11	27.5	0.48	0.01	1.85	0.07
11	28.5	0.45	0.01	2.07	0.06
11	29.5	0.56	0.01	1.61	0.09
12	0.5	0.10	0.00	11.39	0.02
12	1.5	0.22	0.00	10.43	0.02
12	2.5	0.26	0.01	10.10	0.02
12	3.5	0.29	0.01	8.73	0.02
12	4.5	0.33	0.01	7.88	0.02
12	5.5	0.38	0.01	8.21	0.02
12	6.5	0.43	0.01	8.03	0.02
12	7.5	0.45	0.01	7.07	0.02
12	8.5	0.43	0.01	6.86	0.02

12	9.5	0.46	0.01	6.91	0.02
12	10.5	0.46	0.01	6.65	0.02
12	11.5	0.52	0.01	6.05	0.02
12	12.5	0.49	0.01	5.18	0.02
12	13.5	0.51	0.01	5.14	0.02
12	14.5	0.51	0.01	4.89	0.02
12	15.5	0.63	0.01	3.93	0.03
12	16.5	0.60	0.01	3.95	0.03
12	17.5	0.56	0.01	3.57	0.03
12	18.5	0.56	0.01	3.63	0.03
12	19.5	0.51	0.01	3.36	0.03
12	20.5	0.50	0.01	3.78	0.03
12	21.5	0.51	0.01	3.50	0.03
12	22.5	0.49	0.01	3.67	0.03
12	23.5	0.50	0.01	3.55	0.03
12	24.5	0.50	0.01	3.55	0.03
12	25.5	0.56	0.01	3.32	0.03
12	26.5	0.53	0.01	3.23	0.03
12	27.5	0.49	0.01	3.16	0.03
12	28.5	0.50	0.01	3.26	0.04
12	29.5	0.46	0.01	3.52	0.03
12	30.5	0.47	0.01	2.97	0.04
12	31.5	0.45	0.01	3.10	0.04
12	32.5	0.48	0.01	2.92	0.04
12	33.5	0.44	0.01	2.57	0.04
12	34.5	0.47	0.01	2.30	0.05

Table S2. Raw ^{210}Pb data. Site number, sample midpoint depth, measured ^{210}Pb activity and measurement error, and dry bulk density (DBD).

APPENDIX 2.3 LAND COVER THROUGH TIME

Land cover classes shown as percent area of tidal creek watershed for each site in Carteret County (A) and New Hanover County (B). Land cover was classified at least once per decade.

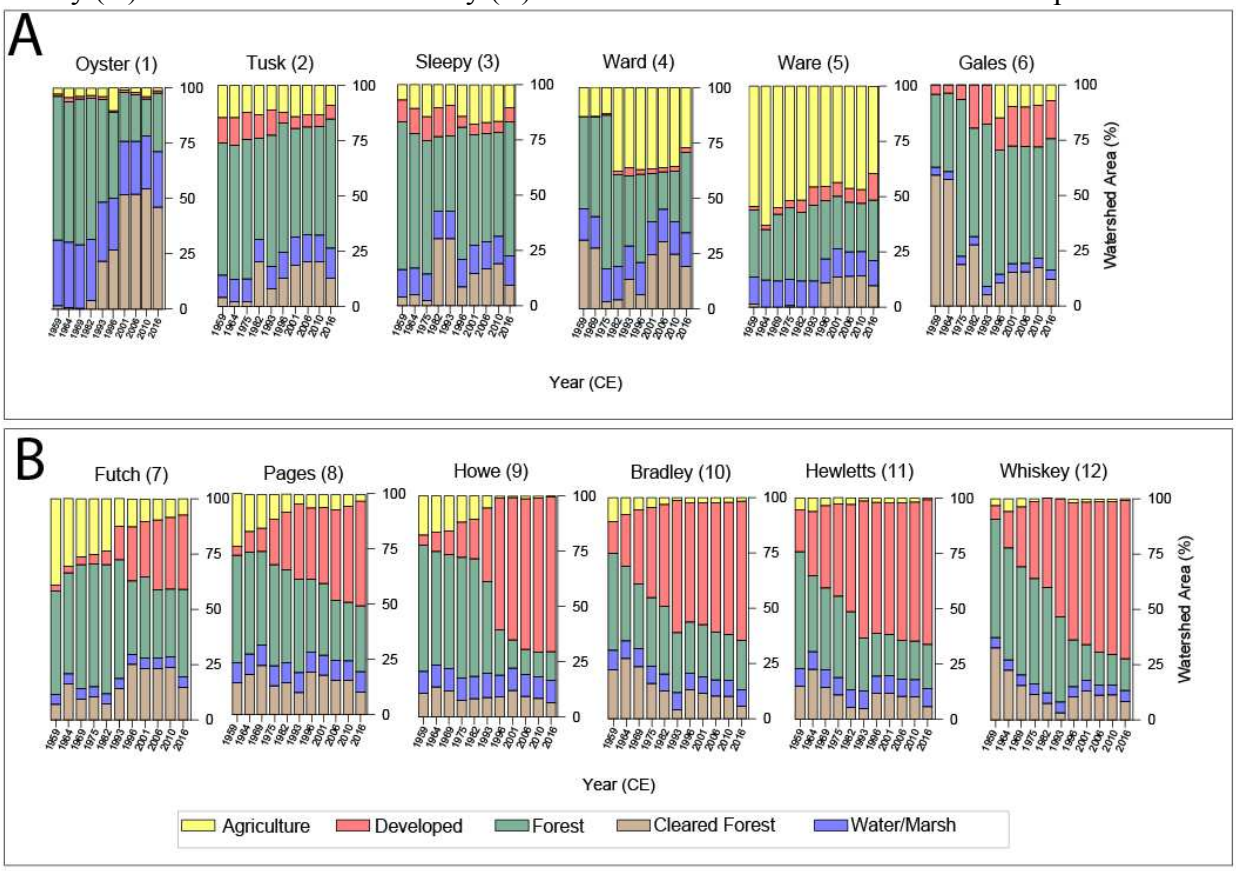

APPENDIX 2.4 DEM OF HEWLETTS CREEK WATERSHED

(Site 11) Highlighting the Carolina Bay with a central retention pond in the northwestern part of the water.

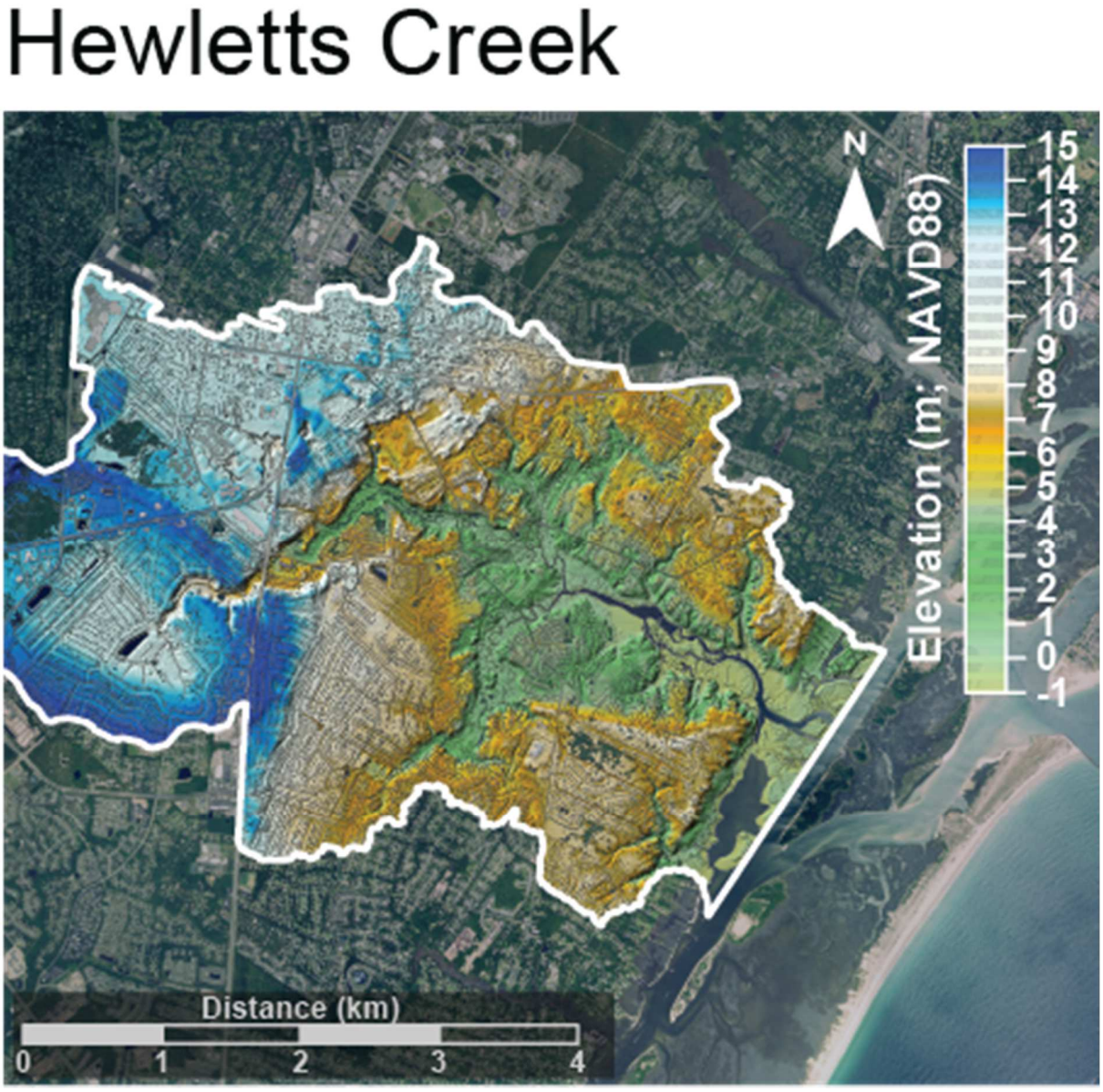

APPENDIX 3.1 MARSH CORING LOCATIONS

Site Number	Creek Name	Core Date	Core latitude (decimal degrees)	Core longitude (decimal degrees)
1	Oyster	8/5/2016	34.827507	-76.459886
2	Tusk	8/9/2016	34.746557	-76.512871
3	Sleepy	7/21/2016	34.732907	-76.527258
4	Ward	7/20/2016	34.791042	-76.566637
5	Ware	9/16/2016	34.77611	-76.67374
6	Gales	7/28/2016	34.732679	-76.907815
7	Futch	10/5/2016	34.304563	-77.752908
8	Pages	10/4/2016	34.281334	-77.777964
9	Howe	9/20/2016	34.25586	-77.80646
10	Bradley	9/20/2016	34.21834	-77.83934
11	Hewletts	9/12/2016	34.19279	-77.858891
12	Whiskey	9/12/2016	34.15864	-77.862412

APPENDIX 3.2 RAW MARSH PB-210 DATA

Site Number	Midpoint Depth (cm)	Dry Bulk Density (g cm^{-3})	Total ^{210}Pb (dpm/g)	Measurement error
1	0.5	0.26	11.69	0.027
1	1.5	0.29	11.23	0.027
1	2.5	0.29	10.44	0.027
1	3.5	0.31	8.74	0.028
1	4.5	0.30	9.23	0.027
1	5.5	0.32	7.77	0.028
1	6.5	0.32	6.80	0.028
1	7.5	0.31	5.81	0.028
1	8.5	0.29	5.27	0.029
1	9.5	0.27	4.18	0.033
1	10.5	0.27	4.32	0.031
1	11.5	0.26	4.46	0.031
1	12.5	0.27	5.24	0.029
1	13.5	0.27	6.47	0.028
1	14.5	0.27	4.91	0.029
1	15.5	0.28	4.24	0.031
1	16.5	0.26	5.32	0.029
1	17.5	0.24	5.20	0.029
1	18.5	0.23	4.11	0.031
1	19.5	0.23	4.16	0.031
2	0.5	9.39	0.09	0.087
2	1.5	10.72	0.09	0.087
2	2.5	9.27	0.09	0.087
2	3.5	8.67	0.09	0.087
2	4.5	6.92	0.09	0.087
2	5.5	5.62	0.09	0.087
2	6.5	7.70	0.09	0.087
2	7.5	7.04	0.09	0.087
2	8.5	3.35	0.09	0.090
2	9.5	2.92	0.09	0.093
2	10.5	4.14	0.09	0.088
2	11.5	5.63	0.09	0.087
2	12.5	7.05	0.09	0.087

2	13.5	5.08	0.09	0.087
2	14.5	3.64	0.09	0.089
2	15.5	2.52	0.09	0.094
2	16.5	3.07	0.09	0.091
2	17.5	3.03	0.09	0.093
2	18.5	2.61	0.10	0.097
2	19.5	2.04	0.11	0.108
2	20.5	1.71	0.11	0.113
2	21.5	1.74	0.13	0.126
2	22.5	1.62	0.14	0.136
2	23.5	1.34	0.17	0.171
2	24.5	1.50	0.14	0.140
3	0.5	0.43	5.09	0.029
3	1.5	0.41	5.19	0.029
3	2.5	0.40	4.71	0.030
3	3.5	0.45	4.53	0.030
3	4.5	0.38	3.63	0.033
3	5.5	0.38	3.54	0.033
3	6.5	0.39	3.42	0.034
3	7.5	0.40	3.71	0.033
3	8.5	0.39	3.65	0.031
3	9.5	0.37	3.17	0.035
3	10.5	0.41	6.52	0.027
3	11.5	0.44	5.32	0.028
3	12.5	0.30	5.59	0.028
3	13.5	0.32	5.23	0.028
3	14.5	0.40	8.25	0.027
3	15.5	0.26	4.29	0.028
3	16.5	0.47	3.78	0.029
3	17.5	0.33	2.93	0.031
3	18.5	0.37	2.72	0.031
3	19.5	0.38	2.43	0.034
4	0.5	0.37	6.07	0.031
4	1.5	0.42	7.15	0.031
4	2.5	0.47	4.97	0.032
4	3.5	0.42	4.22	0.034
4	4.5	0.40	3.46	0.038
4	5.5	0.38	3.28	0.039
4	6.5	0.37	2.86	0.044

4	7.5	0.36	2.69	0.046
4	8.5	0.34	2.19	0.060
4	9.5	0.36	2.64	0.045
4	10.5	0.39	3.23	0.040
4	11.5	0.38	2.75	0.046
4	12.5	0.35	3.11	0.042
4	13.5	0.33	3.74	0.036
4	14.5	0.32	3.04	0.042
4	15.5	0.30	3.30	0.040
4	16.5	0.31	2.69	0.047
4	17.5	0.36	2.40	0.052
4	18.5	0.37	2.42	0.047
4	19.5	0.35	1.59	0.092
5	0.5	0.62	5.05	0.034
5	1.5	0.86	5.90	0.034
5	2.5	0.94	5.98	0.034
5	3.5	0.97	5.09	0.034
5	4.5	0.94	5.47	0.034
5	5.5	0.78	4.47	0.035
5	6.5	0.94	3.57	0.039
5	7.5	0.78	1.94	0.078
5	8.5	0.94	1.89	0.071
5	9.5	0.78	2.55	0.053
6	0.5	0.24	16.67	0.174
6	1.5	0.24	17.31	0.174
6	2.5	0.24	18.37	0.174
6	3.5	0.22	17.14	0.174
6	4.5	0.22	14.76	0.174
6	5.5	0.20	16.23	0.174
6	6.5	0.20	14.81	0.174
6	7.5	0.20	12.65	0.174
6	8.5	0.20	11.59	0.174
6	9.5	0.20	11.58	0.174
6	10.5	0.19	9.98	0.174
6	11.5	0.19	9.19	0.174
6	12.5	0.18	7.58	0.174
6	13.5	0.18	7.93	0.174
6	14.5	0.18	7.20	0.174
6	15.5	0.19	7.02	0.174

6	16.5	0.19	5.95	0.174
6	17.5	0.19	6.04	0.174
6	18.5	0.18	5.24	0.175
6	19.5	0.17	5.19	0.174
6	20.5	0.16	4.18	0.176
6	21.5	0.16	4.60	0.174
6	22.5	0.16	3.85	0.175
6	23.5	0.16	2.74	0.177
6	24.5	0.15	2.38	0.178
6	25.5	0.15	1.93	0.186
6	26.5	0.16	1.77	0.206
6	27.5	0.17	1.57	0.207
6	28.5	0.16	1.31	0.245
6	29.5	0.16	1.09	0.296
6	30.5	0.17	0.87	0.372
6	31.5	0.17	0.93	0.441
6	32.5	0.16	0.75	0.594
7	0.5	0.33	18.55	0.028
7	1.5	0.31	9.02	0.028
7	2.5	0.33	10.42	0.028
7	3.5	0.27	9.34	0.028
7	4.5	0.28	8.10	0.028
7	5.5	0.29	8.09	0.028
7	6.5	0.31	8.14	0.028
7	7.5	0.30	7.73	0.028
7	8.5	0.32	7.45	0.028
7	9.5	0.31	6.79	0.029
7	10.5	0.32	6.66	0.029
7	11.5	0.31	5.18	0.030
7	12.5	0.34	4.45	0.031
7	13.5	0.37	4.58	0.031
7	14.5	0.47	4.14	0.033
7	15.5	0.53	3.06	0.041
7	16.5	0.59	2.98	0.041
7	17.5	0.61	3.03	0.039
7	18.5	0.70	2.51	0.044
7	19.5	0.70	2.30	0.050
8	0.5	0.47	6.29	0.028
8	1.5	0.47	5.89	0.028

8	2.5	0.50	6.46	0.028
8	3.5	0.52	5.58	0.028
8	4.5	0.56	4.79	0.029
8	5.5	0.64	4.74	0.029
8	6.5	0.58	4.29	0.030
8	7.5	0.58	3.88	0.030
8	8.5	0.57	3.36	0.031
8	9.5	0.58	3.00	0.033
8	10.5	0.62	2.62	0.038
8	11.5	0.60	2.39	0.049
8	12.5	0.61	2.32	0.057
8	13.5	0.59	2.16	0.063
8	14.5	0.63	2.06	0.066
8	15.5	0.66	1.82	0.082
8	16.5	0.72	1.48	0.115
8	17.5	0.76	1.46	0.108
8	18.5	0.88	1.39	0.131
8	19.5	0.93	1.38	0.113
8	20.5	0.94	1.32	0.127
9	0.5	0.63	7.16	0.524
9	1.5	0.59	5.31	0.524
9	2.5	0.65	1.12	0.566
9	3.5	0.64	0.68	0.755
10	0.5	0.23	7.99	0.028
10	1.5	0.24	11.32	0.027
10	2.5	0.24	10.50	0.027
10	3.5	0.24	10.60	0.027
10	4.5	0.26	9.29	0.027
10	5.5	0.27	9.50	0.027
10	6.5	0.29	9.57	0.027
10	7.5	0.29	9.03	0.027
10	8.5	0.30	9.08	0.027
10	9.5	0.30	8.42	0.027
10	10.5	0.30	7.65	0.028
10	11.5	0.30	6.62	0.028
10	12.5	0.31	6.81	0.028
10	13.5	0.30	6.24	0.028
10	14.5	0.32	6.61	0.028
10	15.5	0.33	5.67	0.028

10	16.5	0.33	5.04	0.029
10	17.5	0.33	3.90	0.031
10	18.5	0.32	3.92	0.031
10	19.5	0.33	3.67	0.033
10	20.5	0.34	3.61	0.031
10	21.5	0.34	3.47	0.032
10	22.5	0.33	2.86	0.037
10	23.5	0.33	2.63	0.039
10	24.5	0.32	2.51	0.042
10	25.5	0.31	2.33	0.044
10	26.5	0.31	2.69	0.039
10	27.5	0.31	2.29	0.043
10	28.5	0.32	2.05	0.048
10	29.5	0.32	1.96	0.052
11	0.5	0.43	2.53	0.164
11	1.5	0.42	2.04	0.170
11	2.5	0.40	1.68	0.184
11	3.5	0.40	1.48	0.195
11	4.5	0.42	1.33	0.203
11	5.5	0.42	1.32	0.209
11	6.5	0.43	1.47	0.196
11	7.5	0.42	1.31	0.217
11	8.5	0.42	1.35	0.212
11	9.5	0.41	1.32	0.210
11	10.5	0.37	1.20	0.240
11	11.5	0.34	0.84	0.403
11	12.5	0.36	0.62	0.650
12	0.5	0.18	11.00	0.029
12	1.5	0.16	10.41	0.029
12	2.5	0.21	9.02	0.029
12	3.5	0.22	7.11	0.029
12	4.5	0.21	7.20	0.030
12	5.5	0.21	8.70	0.029
12	6.5	0.21	5.69	0.030
12	7.5	0.23	5.49	0.030
12	8.5	0.26	4.89	0.030
12	9.5	0.30	4.61	0.031
12	10.5	0.31	4.78	0.031
12	11.5	0.32	4.73	0.031

12	12.5	0.32	3.90	0.033
12	13.5	0.29	3.85	0.033
12	14.5	0.29	3.37	0.036
12	15.5	0.27	3.39	0.037
12	16.5	0.27	3.11	0.040
12	17.5	0.28	3.21	0.038
12	18.5	0.27	2.63	0.042
12	19.5	0.30	2.66	0.043
12	20.5	0.27	2.67	0.043
12	21.5	0.29	2.56	0.050
12	22.5	0.28	2.81	0.047
12	23.5	0.30	2.69	0.046
12	24.5	0.30	2.57	0.046
12	25.5	0.29	2.70	0.046
12	26.5	0.30	2.25	0.057
12	27.5	0.29	2.53	0.050
12	28.5	0.30	2.48	0.049
12	29.5	0.29	2.37	0.049

APPENDIX 3.3 MARSH MASS ACCUMULATION RATES WITH MLCC

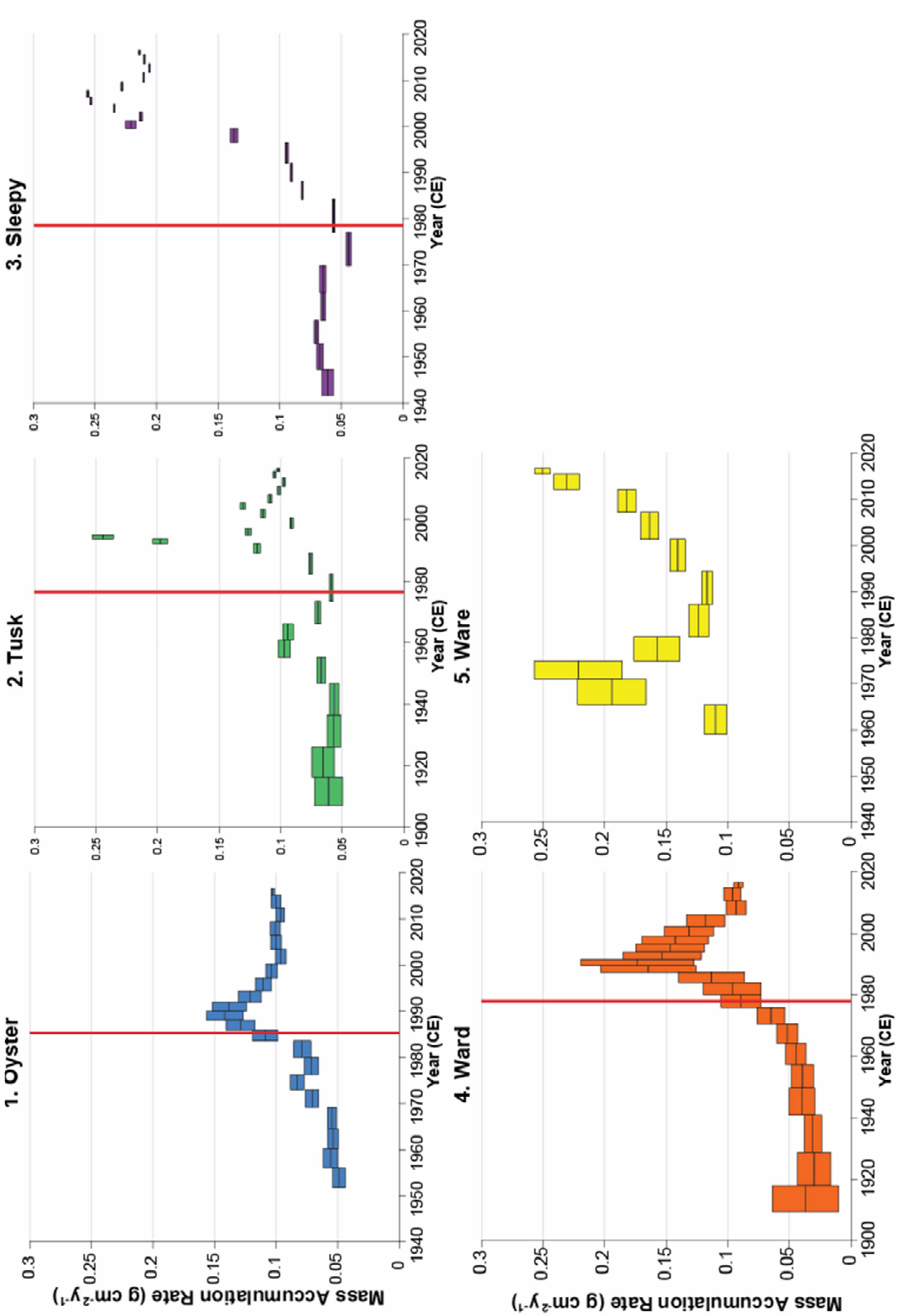

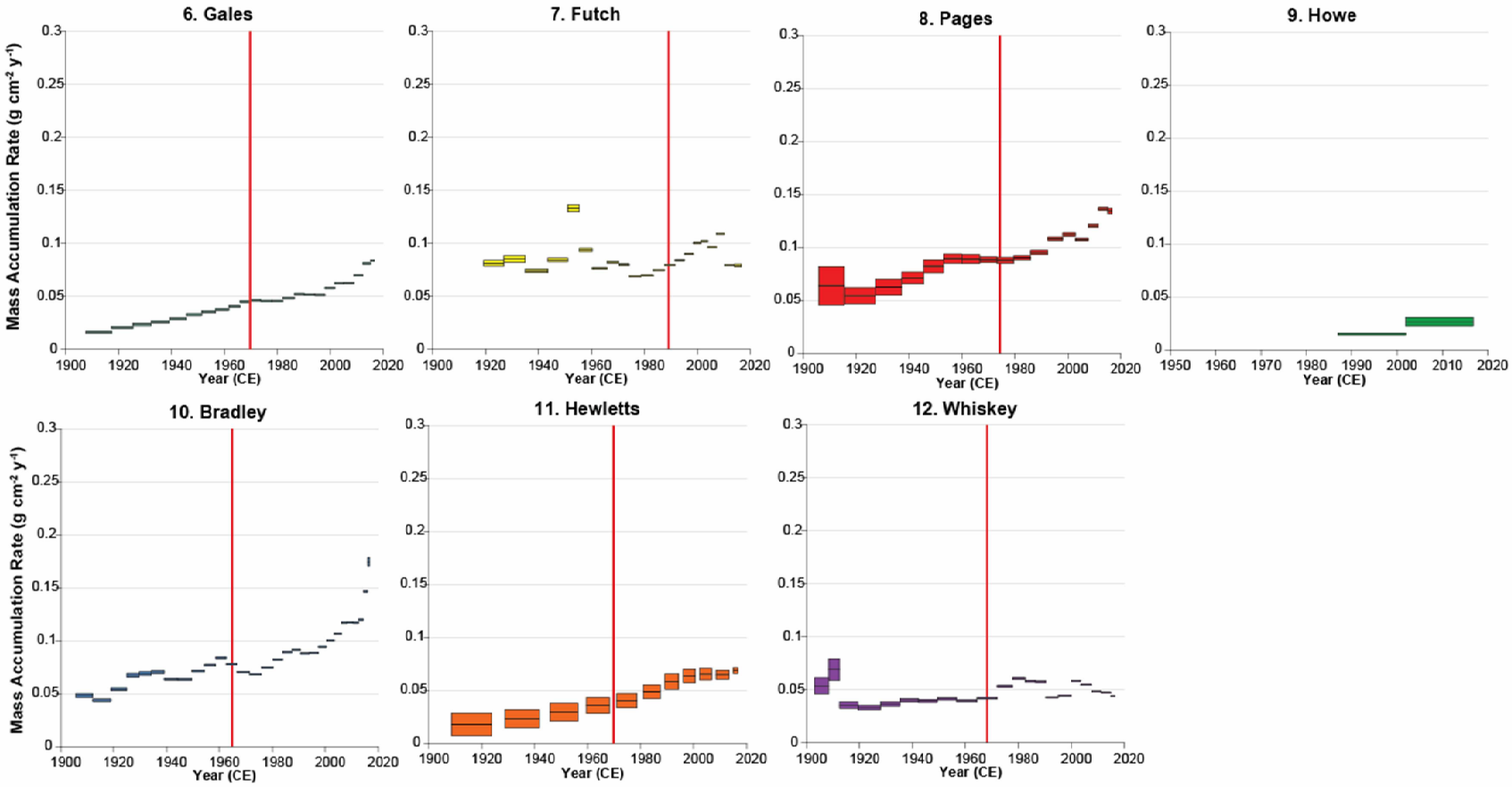
6. Gales
7. Futch
8. Pages
9. Howe
10. Bradley
11. Hewletts
12. Whiskey
Mass Accumulation Rate (g cm-2 y-1)
Year (CE)